LOCKHEED MARTIN ENERGY RESEARCH LIBRARIES

3 4456 0515293 7

ORNL-4823
(ENDF-178)

cy. 4

A TEST OF NEUTRON TOTAL CROSS-SECTION EVALUATIONS FROM 0.2 TO 20 MeV FOR C, O, Al, Si, Ca, Fe, AND SiO_2

F. G. Perey
T. A. Love
W. E. Kinney

ORNL TECHNICAL INFORMATION DIVISION
Y-12 TECHNICAL LIBRARY
Document Reference Section
LOAN COPY ONLY

Do NOT transfer this document to any other person. If you want others to see it, attach their names, return the document, and the Library will arrange the loan as requested.

UCN-1624
(3 5-60)

OAK RIDGE NATIONAL LABORATORY
OPERATED BY UNION CARBIDE CORPORATION • FOR THE U.S. ATOMIC ENERGY COMMISSION

Printed in the United States of America. Available from
National Technical Information Service
U.S. Department of Commerce
5285 Port Royal Road, Springfield, Virginia 22151
Price: Printed Copy $3.00; Microfiche $0.95

This report was prepared as an account of work sponsored by the United States Government. Neither the United States nor the United States Atomic Energy Commission, nor any of their employees, nor any of their contractors, subcontractors, or their employees, makes any warranty, express or implied, or assumes any legal liability or responsibility for the accuracy, completeness or usefulness of any information, apparatus, product or process disclosed, or represents that its use would not infringe privately owned rights.

ORNL-4823
(ENDF-178)

Contract No. W-7405-eng-26

NEUTRON PHYSICS DIVISION

A TEST OF NEUTRON TOTAL CROSS-SECTION EVALUATIONS FROM 0.2 TO 20 MeV FOR C, O, Al, Si, Ca, Fe, AND SiO_2

F. G. Perey, T. A. Love and W. E. Kinney

DECEMBER 1972

NOTE: THIS WORK FUNDED BY DEFENSE NUCLEAR AGENCY UNDER SUBTASK No. PE075

OAK RIDGE NATIONAL LABORATORY
Oak Ridge, Tennessee 37830
operated by
UNION CARBIDE CORPORATION
for the
U. S. ATOMIC ENERGY COMMISSION

LOCKHEED MARTIN ENERGY RESEARCH LIBRARIES

3 4456 0515293 7

CONTENTS

Page No.

I. Introduction 1

II. Experimental Technique and Data Reduction 3

General Description 3

Neutron Detector 4

Electronics 5

Data Acquisition Method 7

Data Reduction 9

III. Results and Comparison with the Evaluations 16

Carbon 18

Oxygen 20

Aluminum 21

Silicon 21

Calcium 21

Iron 22

Silicon Dioxide 23

IV. Conclusions 23

V. Acknowledgments 23a

Figure Index 25

A TEST OF NEUTRON TOTAL CROSS-SECTION EVALUATIONS FROM 0.2 TO 20 MeV FOR C, O, Al, Si, Ca, Fe, AND SiO_2

F. G. Perey, T. A. Love and W. E. Kinney

ABSTRACT

Neutron transmission measurements from 0.2 to 20.0 MeV have been made for the shielding materials carbon, oxygen, aluminum, silicon, calcium, iron and the compound silicon dioxide. The measurements were performed at the ORELA Shield Test Station with a resolution of about 0.12 nsec/meter on sample thicknesses varying from 0.65 to 0.9 atoms/barn. The transmission measurements were compared with the predictions obtained from the Defense Nuclear Agency evaluated cross-section library. Since the total cross-section files for these elements are also the ones present in the ENDF/B-III library, we are also checking its total cross-section files for all of the elements with the exception of oxygen. There are serious discrepancies between our data and the predictions based on the evaluated files. These discrepancies are often large in the energy region from 0.2 to 0.6 MeV.

I. INTRODUCTION

In this report we present some results of neutron uncollided flux measurements which were performed at the ORELA Shield Test Station. These measurements were undertaken to provide a test of the neutron total cross-section files, from 0.2 to 20 MeV, of a few important shielding materials in the DNA cross-section library[1] for moderately deep transport applications, i.e. for between 0.5 and 1 atom per barn of material. The neutron transmission data obtained for carbon, oxygen, aluminum, silicon, calcium, iron and the compound silicon dioxide at a resolution of about 0.12 nsec/m, are compared with predictions based on the total cross-section files of the DNA shielding cross-section library as of July 1972. Since the total cross-section files for these elements are also the ones used in the ENDF/B Version III library data set, our data also provide a test for the ENDF/B III evaluations.

These transmission checks are necessary because the total cross-section evaluations are based on measurements from various sources using different techniques covering different energy regions and often with inadequate energy resolution to resolve all of the structure in the cross sections. This situation results in two major sources of errors in the file affecting the cross-section magnitude and its energy scale. The energy scale differences in the data may often be solved, for a given element, at the time the evaluation is made when there is sufficient energy overlap between the various data sets. However, for practical shielding applications involving several elements, it is difficult to insure that the energy scale of the different evaluations is consistent unless a high degree of absolute accuracy is achieved in each evaluation. The finite energy resolution of the transmission data, upon which the total cross section's evaluation is based, may cause very serious errors when all of the structure is not resolved. This is so because the average transmission obtained at a given energy for a specific sample thickness cannot be converted to an average cross section which would be valid for other energy resolutions and/or sample thickness. Above 0.5 MeV neutron energy, total cross sections are usually obtained from transmission measurements using time-of-flight with a "white neutron source" and recoil proton detectors for sample thicknesses between 0.2 and 0.3 atoms per barn. Our measurements which were obtained with similar techniques will, therefore, test the adequacy of these data with sample thicknesses 3 to 4 times larger. From 0.2 to 0.5 MeV the data situation varies very much from nuclei to nuclei, and often the evaluations are based on very fragmentary data from diverse sources. It is very difficult to estimate

a priori the adequacy of the evaluations in this energy region, but typically we may expect errors to be as large as 30 to 40%.

In Section II we shall describe the experimental technique used and the data reduction method. In Section III we shall present the experimental results and the comparison with the predictions of the evaluations.

II. EXPERIMENTAL TECHNIQUE AND DATA REDUCTION

General Description

The data were acquired using ORELA as the neutron source. Neutrons were produced by photonuclear processes due to bremstrahlung from electron impact on a water-cooled beryllium clad tantalum target. For this experiment the electron energy was about 125 MeV, with a repetition rate of 1000 pulses per second. The electron pulse width was 5 nsec and a total electron beam power of 11 kW was used.

Measurements were performed using the ORELA Shield Test Station 47 meter flight path. About 40 m of the flight path was under vacuum in order to reduce the structure in the neutron flux due to scattering resonances in air. Because of the very high neutron flux available with the above accelerator conditions, a set of neutron filters was placed in the neutron beam 6 m from the linac target. In the first part of the run where measurements were performed for C, Ca, and Si, the filters consisted of 12.7 cm of depleted uranium preceeded by 1.9 cm of ^{10}B. The boron filter removed "all" neutrons of less than 1 keV energy, preventing overlap between neutrons of adjacent accelerator pulses. In the second part of the run for the measurement on Fe, Al, O and SiO^2, the depleted uranium filter thickness was increased to 14 cm. The neutron beam at the sample

was defined by a collimator in the flight path which was 7.6 cm in diameter and located 28 m from the linac target. It consisted of 30 cm of borated polyethylene followed by 30 cm of lead. The transmission samples, 10-cm diameter cylinders, were placed about 1.5 m behind this collimator. Two precollimators were also used, one on each side of the neutron filters at about 4 and 4.5 m from the linac target, and were each 8.5 cm in diameter. The neutron flux intensity was measured at 47.35 m from the linac target, in the center of the shield test station.

The neutron beam was dumped in a concrete beam catcher located 5 m behind the neutron detector.

Two independent neutron flux monitors were used. The primary neutron flux monitor was a 6 x 6 mm NE-110 plastic recoil proton detector located in the edge of the neutron beam after the collimator and operated in the "time-of-flight" mode. The second neutron monitor, used as a check on the proper operation of the time-of-flight neutron monitor, was located in the ORELA target room[2] and gave a count rate proportional to the total neutron output of the tantalum linac target.

Neutron Detector

The neutron detector used for the transmission measurement was a 4.4 x 4.4 cm right cylinder NE-110 plastic scintillator[3] viewed by an RCA 8575 photomultiplier. It was located 47.35 m from the linac target. The distance, established by standard surveying techniques, should be accurate to better than 0.5 cm. The NE-110 plastic recoil proton scintillator was used because its high optical transmission characteristics allow the detection of much lower energy recoil protons than do other commonly used recoil proton detectors such as NE-213 or NE-102. At about 1 MeV

recoil proton energy, its light output is comparable to that of NE-102, but at approximately 150 keV its light output is about 3 times higher than for NE-102.[4] This very important property of NE-110 makes possible the measurement of the transmission down into the keV region with a single detector.

Electronics

The electronics consisted of two independent time-of-flight systems, one for the neutron flux monitor and the other for the transmission detector. Data acquisition was performed using a PDP-9 computer which recorded both time-of-flight spectra and various scalers and also controlled the sample changer located about 29.5 m from the linac target.

Monitor Electronics. - The monitor time-of-flight spectrum was obtained using a time-to-amplitude converter started by a fiducial signal based on the linac gamma flash. This fiducial signal is obtained from a bare photo tube which views the linac target directly. The stop signal for the time-to-amplitude converter is derived from the anode signal of the monitor detector photomultiplier. A tunnel diode discriminator rejects all anode pulses below its bias level. The output of the tunnel diode discriminator goes through a gate opened 300 nsec after the gamma flash for 4 μsec. The bias level of the tunnel diode discriminator was adjusted by observing a linear signal derived from a photomultiplier dynode in coincidence with the discriminator output. The bias level was frequently monitored during the runs and no significant drifts were observed. The counting rate in the monitor detector, within the time gate period, was only about 0.017 counts per neutron burst for the 12.7-cm depleted uranium filter and 0.011 counts per neutron burst for the 14-cm-thick filter. Deadtime losses

were therefore very small for the monitor detector. The ORELA target room monitor output was scaled on a fast scaler; its counting rate was about 0.2 counts per neutron burst. The ratio of the two monitor counting rates was checked throughout the experiment and found to be always within two standard deviations.

Detector Electronics. - The time-of-flight spectrum for the main detector was obtained using an EGG model TDC 100 digital clock operated in a mode which allowed a single stop per start pulse. The time channel widths were set at 2 nsec per channel. The start signal for the clock was the fiducial signal based on the linac gamma flash. The anode signal from the detector photomultiplier went through a "timing filter" amplifier (ORTEC-454) to a "constant fraction" discriminator (ORTEC-463). After suitable shaping the constant fraction discrimination output was used to stop the clock. Time delays between the clock start and stop signals were adjusted so that the gamma flash peak was recorded in the spectrum. A gamma flash signal was detected for approximately 5% of the neutron bursts for the 12.7-cm-thick depleted uranium filter and for only about 2% of the time with the 14-cm-thick filter. As for the monitor detector, the fast discriminator bias level was set and monitored periodically during the runs by observing in coincidence with its output the amplified linear signal from a photomultiplier dynode. The discriminator setting was at 0.01 light units[5] which should correspond to about 50 keV recoil proton energy. During the whole run the linear gains of the system varied by less than 1.5% and no shifts in bias setting were detected. The total counting rate for the sample-out condition at the output of the "constant fraction" discriminator was approximately 3 per neutron burst for the 12.7-cm-thick depleted uranium filter and 2 with the 14-cm-thick filter.

Data Acquisition Method

The PDP-9 data acquisition computer stored time-of-flight spectra of 4096-channels for the main detector and 256-channels for the monitor. The discriminator outputs were scaled as well as clock valid stops, the number of gamma flashes and the ORELA target room monitor pulses. The data acquisition program recorded the time-of-flight spectra and scaler readings for a preset beam-on-target time and alternated sample-in and sample-out measurements via remote control of the sample changer at the 30 meter station of the flight path. Each spectrum and scaler reading was recorded on tape to be processed off-line. A rate meter, activated by the gamma flash signal, detected when the beam was off target and data acquisition resumed only 30 seconds after the beam was on target again to avoid fluctuations in power levels during data taking.

Samples

All samples were right cylinders approximately 10 cm in diameter. The sample thicknesses, expressed in atoms/barn, were determined from their masses and diameters.

Carbon. - Two transmission samples were machined from the same block of purified Union Carbide C-18 graphite. (Purity greater than 99.9% carbon.) The density of the two cylinders was found to differ by slightly under 1%. The two samples were used alternatively for the sample-in measurements. The average density was 1.750 g/cm^3 and the average thickness 0.8916 atoms/barn.

Calcium. - The calcium samples were machined out of two ingots cast by the ORNL Metals and Ceramics Division. The calcium was analyzed and contained negligible impurities except for 0.2% strontium and 0.2% magnesium.

The two pieces were found to have the same density, 1.534 g/cm^3 to better than 0.1%. Each freshly machined cylinder was inserted in a stainless steel jacket, both ends being sealed by a welded stainless steel sheet with a 0.0152 cm thickness. The two cylinders, 15.24 cm in length, were x-rayed for voids; none could be detected. Both samples were used for the transmission measurements giving 0.7028 atoms/barn. For the sample-out measurements, one empty stainless steel jacket closed by two 0.0304-cm-thick stainless steel sheets was used.

Silicon. - The silicon sample was made up of discs of various thicknesses of amorphous silicon purchased from Texas Instruments (purity 99.999% silicon). The density of each piece was measured and all were found to be within 0.2% of the average value 2.328 g/cm^3. The total thickness used for the sample in the measurement was 0.6660 atoms/barn.

Silicon Dioxide. - Fused quartz discs were obtained from two sources: Apache Chemicals Inc. (Rockford, Ill.) and Corning Glass Works (Corning, N.Y.) (purity greater than 99.9% of SiO^2). The density being 2.201 g/cm^3. The total thickness used was 0.3247 molecules of SiO^2 per barn. To perform the oxygen transmission measurements, the "sample-out" measurements were made with a silicon disc stack of 0.3226 atoms/barn. The oxygen measurements were therefore made for a sample of 0.6494 atoms/barn thick.

Aluminum. - The aluminum sample was machined from an ingot cast by the ORNL Metals and Ceramics Division (purity of the material is 99.99% aluminum). The density of the sample was 2.692 g/cm^3; the total thickness used was 0.7638 atoms/barn.

Iron. - The iron sample was fabricated out of Armco iron which was analyzed for impurities (0.05% Ni, 0.033% Mn, 0.03% Cu, 0.02% Si and

0.01% Mo). The density was 7.848 g/cm^3 and the total thickness 0.8581 atoms/barn.

Table I gives a summary of the sample thicknesses used, in atoms/barn, and the estimated uncertainties.

Data Reduction

The data reduction for transmission measurements is straightforward. Both sample-in and sample-out spectra are corrected for background contributions and for deadtime losses. The spectra are then normalized to the same neutron source intensity using the neutron monitor readings. The average transmission in a given time channel is given by the ratio of the corrected counts for sample-in to those for the sample-out measurements. The neutron energy to which each channel corresponds is obtained from a relativistic calculation knowing the flight path distance, the time of arrival of the gamma flash and the time interval for each channel.

Once the average transmission is obtained for each channel, with the knowledge of the sample thickness, it may be converted to a total cross section. As explained previously this total cross section is only meaningful as a microscopic quantity when it is known that the energy resolution was adequate to resolve all of the structure in the cross section. Because of our broad-energy resolution, ~ 0.12 nsec/meter, it is more meaningful for us to compare our measured transmission data to the predicted transmission data using the evaluated total cross-section files and "smearing" the prediction with a resolution of ~ 0.12 nsec/meter. We shall now estimate the various uncertainties in our transmission data.

Table I. Sample Thicknesses Used and Their Estimated Uncertainties

Element	Atoms/barn
C	0.8916 ± 1%
O	0.6494 ± 0.5%
Al	0.7638 ± 0.5%
Si	0.6660 ± 0.5%
Ca	0.7028 ± 1%
Fe	0.8581 ± 0.5%
SiO_2	0.3247 ± 0.5%

Background Corrections. - The so called "background contributions" in transmission measurements come mostly from two sources: 1. time-independent background due to radioactivity in the room and to cosmic rays, and 2. time-dependent background due to leakage, streaming and scattering in the flight path and the room where the detector is placed. The first source of background is easily measured with a neutron beam stop in the flight path or with the accelerator shut down. Because of the short time of observation following the gamma flash and the high counting rate in this interval of time, this contribution to the background was found to be a fraction of a count per channel, a negligible contribution to the statistical error in the data for each channel. The time correlated background due to streaming, leakage in the flight path and injection of the neutron burst in the flight station cannot be observed directly in the same conditions as for the measurement of the transmission data. However, its importance can be estimated for the sample-in condition when there are large resonances in the total cross section. If the cross section is sufficiently large at the resonance, only a very small fraction of the neutrons may reach the detector uncollided through the sample at the energy of the resonance. Therefore at these energies the background contributions are relatively more important. In our raw data we observed several "peak-to-valley ratios" in "transmission dips" as high as 450 indicating small contribution of the background near these energies. In order to estimate quantitatively the possible magnitude of this background in the transmission data, we give in Table II some observed values of the transmission together with the calculated values based on the total cross-section

values in the evaluations except for Fe where we estimated it on the assumption that it was an isolated S-wave resonance. The experimental transmission data were averaged over several channels to improve the statistical accuracy. On the basis of the comparisons, we estimate that the background contribution in the data below 1 MeV could be as high as 0.002 as seen from the comparison with the oxygen and iron resonance, but it is more likely of the order of 0.001 to 0.0005 from the other resonances.

Deadtime Corrections. - Since we accepted only one event per pulse, the deadtime correction was very straightforward to perform. For carbon, calcium and silicon the sample-out measurements (the fast-discriminator output) had a counting rate of approximately 3 per pulse. The deadtime correction for the low-energy neutrons was therefore quite large. Even though in these cases the deadtime correction factor is large (up to a factor of 30), its statistical accuracy is very good and does not contribute appreciably (less than 10% of error) to the statistical error in the data. Serious systematic errors may be introduced in the data when the deadtime correction factor is large, if there are fluctuations in the counting rate during data acquisition. This is so because deadtime corrections are then a sensitive function of the counting rate. Deadtime corrections were made assuming a constant average rate, and we have investigated the uncertainties in the data due to counting-rate variations in the experiment. Each time-of-flight spectrum was made up of several individual runs, each contributing from 5 to 15% of

Table II. Comparison of Some Observed Values of the Transmission With Corresponding Calculated Values

Element	E_n keV	Experimental	σ_{Total} Barns	Calculated
O	440	0.002 ± .0005	16.0	0.00003
Al	367	0.0013 ± .0001	7.2	0.0041
Al	785	0.0034 ± .00001	7.3	0.0037
Si	566	0.0012 ± .0001	10.5	0.00092
Fe	320	0.0027 ± .0003	8.0	0.0010

the data depending upon the element. For all the partial runs, the average counting rates were constant within ±2% except for calcium where one partial run (15% of the data) had an average counting rate 8% lower, and for silicon for one partial run it was 4% lower. These average counting rates were obtained from 0.5 to 1 hour of running time and do not reflect any dispersion in intensity which may exist from pulse to pulse. The dispersion in neutron intensity from pulse to pulse is difficult to measure directly. However, it is possible to perform such measurements for the intensity of the gamma flash and logical to assume corresponding fluctuations in the neutron intensity. A few such measurements have been made on ORELA[6] and revealed a normal distribution of intensity with a dispersion of 15%. Although no such measurements were performed at the time of our data acquisition, and the exact dependence of this dispersion on the accelerator conditions is not known, it is likely that during the runs there was some dispersion in the beam burst intensity of this order of magnitude. In order to estimate the errors in the data due to our assumption that we had constant average counting rates for calculating the deadtime correction, we have performed numerical experiments. Spectra were computed under various constant counting rates. These spectra were then summed and the deadtime correction performed based on the total average counting rate. These studies showed that at an average counting rate of 3 events per pulse, if the counting rate is 10% higher for 1/2 the time, the maximum error introduced in the data, when it is corrected on the basis of the total average counting rate, is 0.8%. If for 20% of the time the counting rate is changed by 20%, at most a 2% error is made. If the average counting rate is reduced to 2 per pulse, the corresponding numbers are 0.6% and 1%. In an independent test, we

performed the deadtime corrections on each individual partial run and compared the results with the corrected data obtained by adding all the partial runs and then performing the deadtime correction, maximum differences of the order of 0.2% were observed. On the basis of these studies, we estimate we may have as large as a 2% error in our transmission data due to dispersion in the intensity in the neutron burst. This error would be systematic and tend to make our transmission data too large at low energy.

Flux Normalization. - The time-of-flight spectra for sample-in and sample-out have to be normalized to the same incident neutron flux to obtain the transmission. Our time-of-flight monitor was used to perform these normalizations. If the ORELA target room monitor had been used instead, a systematic error of at most 0.4% would have been made based on the observed ratios for these two different monitors.

Energy Calibration. - The greatest uncertainty in the energy calibration results from the uncertainty in the position of the gamma flash peak. Over a 7-day period the position of the gamma flash peak was observed to drift by 0.4 channel. This drift was monotonic and probably associated with the fiducial timing circuit. Any slow drift of this magnitude should not affect the peak position of any given element by more than 0.1 channel. Uncertainties in the flight path, 0.02%, and the integral linearity of the digital clock, 0.001%, should be negligible.

Summary of Error Estimates. - On the basis of the above discussion, we assign the following estimated systematic errors in our transmission data.

Background	$\Delta T = +0.001, -0.000$
Deadtime Corrections	+ 1% above 1 MeV, + 2% below 1 MeV
Flux Normalization	+ 1%

The uncertainty in the energy scale should be that introduced by an error of $\pm$ 0.1 channel in the position of the gamma flash peak.

When comparing our transmission data with an evaluation or when our resolution is adequate and it is meaningful to extract a cross section from our data, the errors given in Table I should be used for the sample thicknesses. The energy resolution of our data is approximately a Gaussian function of full width at half maximum of about [illegible]

III. RESULTS AND COMPARISON WITH THE EVALUATIONS

The results of our transmission measurements consist of approximately 3500 data points per element or altogether more than 24,000 data points. It is not practical to tabulate these numerical values in a report. The numerical values of our transmission data are available upon request from the Radiation Shielding Information Center (ORNL) on magnetic tapes. In this report we shall only present our data in graphical form together with the comparison with predictions based on the evaluations.

Predicted transmissions from the evaluations were calculated using the sample thicknesses given in Table I. The calculation for each element was performed in two steps. First the transmission corresponding to neutron energy intervals equal to each one of our time-of-flight channels was computed by adding the contributions due to energy intervals equal to 1/5 of each channel width. This calculated transmission spectrum A_i, with i the channel number, had therefore an "energy resolution" equivalent to a time-of-flight spectrum having a rectangular time resoltuion function of 2 nsec. In order to convert the spectrum A_i to one T_i, having a resolution function comparable to our experimental one, we used the following "smoothing" algorithm

$$T_i = \sum_{j=-2}^{2} a_j A_{i+j} ,$$

with $a_o = 3/8$, $a_{-1} = a_1 = 1/4$, $a_{-2} = a_2 = 1/16$. Since we did not measure accurately our time resolution function and its dependence upon neutron energy, any small departures between calculated and experimental results could be attributable to slight resolution differences. Several slightly different smoothing algorithms were tried and found to have no effect on the remarks we wish to make on the basis of the graphical comparisons.

We shall now proceed with a brief discussion, for each element, of the salient features of the comparisons, usually emphasizing only areas of major disagreement. We shall not attempt to analyze or explain in detail the areas of major disagreement (usually due to poor or no data available at the time the evaluations were performed), nor discuss the relative merits of the various data sets upon which the evaluations are based. The graphical comparisons given here, together with the comments, are intended to provide assistance to the users of the evaluated data files in pointing out areas of possible differences in the total cross sections. Evaluators planning to revise the total cross-section files should also find the data useful in testing their modifications for adequacy in predicting neutron transmission through such sample thicknesses.

In the graphical representation of our data, the transmission measured in each of our time-of-flight channels is represented by a closed circle with only the statistical accuracy indicated. In certain energy regions, when neither our data nor the evaluations indicated structure consistent to our statistical errors and energy resolution, we have averaged our transmission data over several time-of-flight channels. This is indicated

on the graphs by showing only the statistical accuracy without the central point. This situation often prevailed for neutron energies below 0.6 MeV and above 10 MeV.

Carbon

There is at present no carbon evaluation in the DNA cross-section library. The ENDF/B-III evaluation is MAT = 1165. For E_n < 2.0 MeV the carbon total cross section has no known resonances and has been recently evaluated by two independent groups. The work at KAPL[7] resulted in a total cross-section set believed by its authors to be good to 0.5% and is the one used in MAT = 1165. The work at JAERI[8] resulted in a set whose authors believe is accurate to 2%. In view of the lack of resonances, for E_n < 2 MeV, we have extracted cross-section values from our transmission data. Table III gives our results, every 0.1 MeV from 0.2 to 2.0 MeV, together with the KAPL[7] and JAERI[8] recommendations. In this table we have shown only our statistical errors obtained by averaging the data over several channels to improve on the statistical accuracy. Our measurements appear to be slightly over 1% higher than the KAPL recommendations and in somewhat better agreement with the JAERI values. However, if we take into consideration our estimate of the possible systematic errors in our data, approximately between 1.5 and 2.0%, we cannot conclude with our data which of the two sets might be preferable. We only conclude that the agreement shown in Table III is satisfactory and appears to substantiate, to some unknown degree, the estimate we made for the possible systematic errors in our data.

For E_n > 2.0 MeV the transmission data are shown on pages 26-28. There are two major areas of discrepancy: from 2.08 to 3.5 MeV and from

Table III. Comparison of Carbon Total Cross-Section Results (ORNL) from 0.2 to 2.0 MeV with the KAPL and JAERI Recommendations. The Errors indicated in the ORNL Data are Statistical Errors Only.

E_n MeV	σ_T ORNL Barns	$\Delta\sigma_T$ ORNL Barns	σ_T KAPL Barns	σ_T JAERI Barns	% Difference ORNL-KAPL	% Difference ORNL-JAERI
.2	4.040	.054	4.096	4.129	-1.4	-2.0
.3	3.871	.033	3.829	3.787	1.1	1.7
.4	3.646	.027	3.589	3.639	1.6	.2
.5	3.410	.017	3.372	3.422	1.1	- .3
.6	3.212	.015	3.178	3.223	1.1	- .3
.7	3.065	.011	3.000	3.041	2.2	.6
.8	2.862	.009	2.833	2.875	1.0	- .3
.9	2.728	.008	2.690	2.724	1.4	.1
1.0	2.602	.007	2.562	2.586	1.6	.6
1.1	2.457	.007	2.430	2.461	1.1	- .1
1.2	2.347	.006	2.312	2.347	1.5	0
1.3	2.235	.006	2.216	2.243	.9	- .2
1.4	2.142	.005	2.119	2.148	1.1	- .3
1.5	2.042	.005	2.037	2.061	.2	- .9
1.6	1.970	.005	1.946	1.979	1.2	- .4
1.7	1.881	.005	1.867	1.901	.7	-1.0
1.8	1.814	.005	1.806	1.826	.4	- .7
1.9	1.746	.005	1.739	1.752	.4	- .3
2.0	1.692	.006	1.677	1.677	.9	.9

7.25 to 8.5 MeV. The disagreements are fairly large but not surprising since the total cross sections in MAT 1165 have not been updated since 1965. However, the reevaluation of carbon cross sections currently in progress[9] should remedy this situation.

Oxygen

Because the silicon sample used for the sample-out measurement did not match exactly the silicon content of our quartz sample (a difference of 0.0021 atoms/barn out of 0.3247), a small correction had to be performed to obtain the transmission through the oxygen. This correction was established on the basis of the total cross sections measured with the 0.3247 atoms/barn silicon sample and was of the order of magnitude of the statistical error on the data. The contribution of this correction to the error on the transmission data for oxygen is, therefore, very small.

The DNA cross-section evaluation for oxygen is MAT 4134 mod 1 and is the same as the ENDF/B-III MAT 1134. The comparisons with our transmission data are shown on pages 29-35.

From 0.2 to 0.6 MeV, page 29, our sample was too thick to test the value of the cross sections in the 440 keV resonance. From 0.6 to 2.0 MeV, pages 30,31, the agreement is very satisfactory with a few minor exceptions. In the vicinity of the 2.34 MeV minima, our transmission data appear to be larger than the predictions by slightly more than our systematic error. Above 3 MeV, pages 33,34,35, the agreement is in general satisfactory although our data appear to be somewhat systematically higher, in particular at a few cross section minima (4.8 and 6.34 MeV for instance).

Aluminum

The DNA cross-section evaluation for aluminum is MAT 4135 mod 2 and is the same as ENDF/B III MAT 1135. The comparisons with our transmission data are shown on pages 36-45.

Below 0.5 MeV, pages 36 and 37, the disagreement is fairly large, in particular at the cross-section minima. Above 0.6 MeV the predictions resemble the data very closely with a few exceptions in both magnitude and resolution up to 3.0 MeV. From 3.0 to 10.0 MeV the resolution in our data appears much better than in the file and as a result transmission in the minima is being under predicted and the disagreements should become worse for thicker samples. From 10 to 20 MeV the agreement again becomes fairly good.

Silicon

The DNA cross-section evaluation for silicon is MAT 4151 mod 1 and is the same as ENDF/B III MAT 1151. The comparisons with our transmission data are shown on pages 46-52.

With the exception of the energy region from 1.8 to 3.0 MeV, pages 48 and 49, where the evaluation approximates fairly well our data but still slightly underestimates the transmission in the cross-section minima, the evaluation shows large discrepancies over the whole energy range covered by our measurements. The most serious discrepancies being in the energy ranges 1.0 to 1.8 MeV, page 48, and 3.0 to 6.0 MeV, page 50

Calcium

The DNA cross-section evaluation for calcium is MAT 4152 mod 2; the total cross-section file is the same as for ENDF/B-III MAT 1152. The comparisons with our transmission data are shown on pages 53-63.

From 0.2 to 0.5 MeV at the seven deep cross-section minima, the transmission is very seriously underestimated. The quality of the agreement improves very much above 0.5 MeV, and in particular is reasonably good in the deep cross-section minima around 0.55 MeV, page 55. In general, the cross-section minima do not appear to be deep enough in the evaluation, in particular from 2.0 to 3.0 MeV, page 60. The agreement is fairly good from 10 to 20 MeV, page 63.

Iron

The DNA cross-section evaluation for iron is MAT 4180, and it has the same total cross-section file as ENDF/B III MAT 1180. The comparisons with our data are shown on pages 64-74.

Below 0.45 MeV the evaluation is extremely deficient and in particular fails badly in the deep cross-section minima, pages 64, 65 and 66. Above 0.45 MeV the situation improves markedly although there is a tendency to predict too large a transmission up to 0.6 MeV, page 67. Above 0.6 MeV the agreement is very good except at a few isolated cross-section minima or maxima, for instance at 0.675 MeV (page 68) and at 1.1 MeV (page 70). There does not appear to be any large discrepancies between 2.0 and 3.0 MeV for this sample thickness.

As of September 1972 a new DNA cross-section evaluation for iron will be available with a designation MAT 4180 mod 1. This reevaluation is identified as MAT 6 in this report. The total cross-section file of MAT 6 is different from the one in MAT 4180 in two energy regions. Below 0.8 MeV recent preliminary data[10] in the deep minima, $\sigma_T < 0.8$ barns, became available and were used to improve the file. The evaluation was extended from 15 to 20 MeV. Comparisons with our data, in the energy

regions where MAT 6 differs from MAT 4180, are shown on pages 75 to 80. As expected there is a dramatic improvement in the agreement in the deep valleys below 0.8 MeV over MAT 4180. From 10 to 20 MeV the agreement is quite good.

Silicon Dioxide

On pages 81 to 87 we show the comparison of the prediction based on the DNA cross-section files with our transmission data on silicon dioxide obtained in conjunction with our oxygen transmission measurements.

All of the disagreement with the predictions from the files are due to the silicon cross-section file as we found very good agreement for the oxygen data file.

IV. CONCLUSIONS

For all the elements studied, with the exception of oxygen, serious discrepancies were found in some energy regions with the predictions from the evaluated data files. Since the sample thicknesses used are relatively thin for shielding materials, the disagreements observed are likely to be much more severe for thicker samples. With our moderate energy resolution, 0.12 nsec/meter, we are able to identify some of the energy regions where the evaluations would have to be improved in order to predict accurately neutron uncollided flux. The total cross-section file in the DNA and ENDF/B-III evaluations appear to have errors as large as 30% below 0.5 MeV and often as large as 10% above this energy.

V. ACKNOWLEDGMENTS

We wish to express our appreciation to J. K. Dickens, R. M. Freestone, J. W. McConnell, G. L. Morgan, H. Weaver (Neutron Physics Div.); Robert E. McDonald, Glynn Angel (Metals & Ceramics Div.); Jim Bentley (P&E Div.); and the craftsmen assigned to Bldg. 6010 for their contributions to this experimental program.

REFERENCES

1. Defense Nuclear Agency Working Cross Section Library, Radiation Shielding Information Center, Oak Ridge, Tennessee.

2. J. H. Todd, Instrumentation and Controls Div. Ann. Progr. Rept. Sept. 3, 1968, ORNL-4335, p. 17.

3. Nuclear Enterprises, Ltd., 550 Berry St., Winnipeg 21, Manitoba, Canada.

4. N. W. Hill, J. A. Harvey, G. G. Slaughter, and A. St. James, Physics Division Annual Progress Report, December 31, 1971, ORNL-4743, p. 137.

5. V. V. Verbinski, W. R. Burrus, T. A. Love, W. Zobel and N. W. Hill, Nucl. Instr. Meth. 65, 8 (1968).

6. R. W. Peelle, ORNL, private communication (1972).

7. N. C. Francis, C. R. Lubitz, J. T. Reynolds, C. J. Slavik, and G. R. Stieglitz, Proceedings of Neutron Standards and Flux Normalization, Argonne National Laboratory, October 1970, U. S. Atomic Energy Commission Division of Technical Information, AEC Symposium Series 23, p. 167.

8. K. Nishimura, S. Igarasi, T. Fuketa, and S. Tanaka, Evaluation of the Total Neutron Cross Section of Carbon up to 2 MeV, JAERI - 1218 (October 1971).

9. C. M. and F. G. Perey (ORNL).

10. J. A. Harvey, keV Neutron Total Cross-Section Measurements at ORELA, presented at the ANS National Topical Meeting, "New Developments in Reactor Physics and Shielding," Kiamesha Lake, N. Y. (September 12-15, 1972).

FIGURE INDEX

Element	Figure Nos.	Page Nos.
Carbon	1-3	26-28
Oxygen	4-10	29-35
Aluminum	11-20	36-45
Silicon	21-27	46-52
Calcium	28-38	53-63
Fe 1180	39-49	64-74
Fe 6	50-55	75-80
SiO_2	56-62	81-87

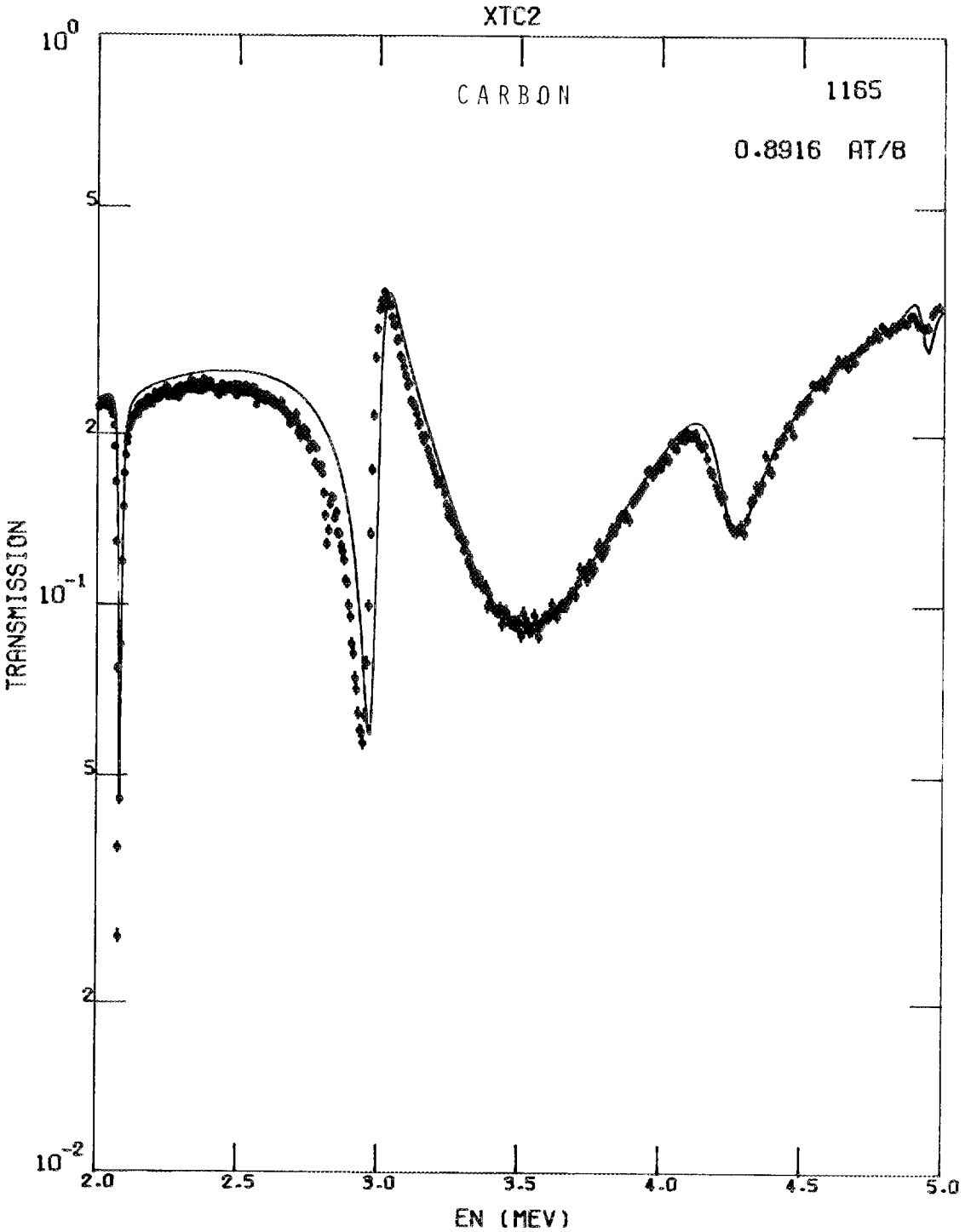
XTC2
CARBON
1165
0.8916 AT/B
TRANSMISSION
EN (MEV)
10^0
5
2
10^{-1}
5
2
10^{-2}
2.0
2.5
3.0
3.5
4.0
4.5
5.0

Figure 1

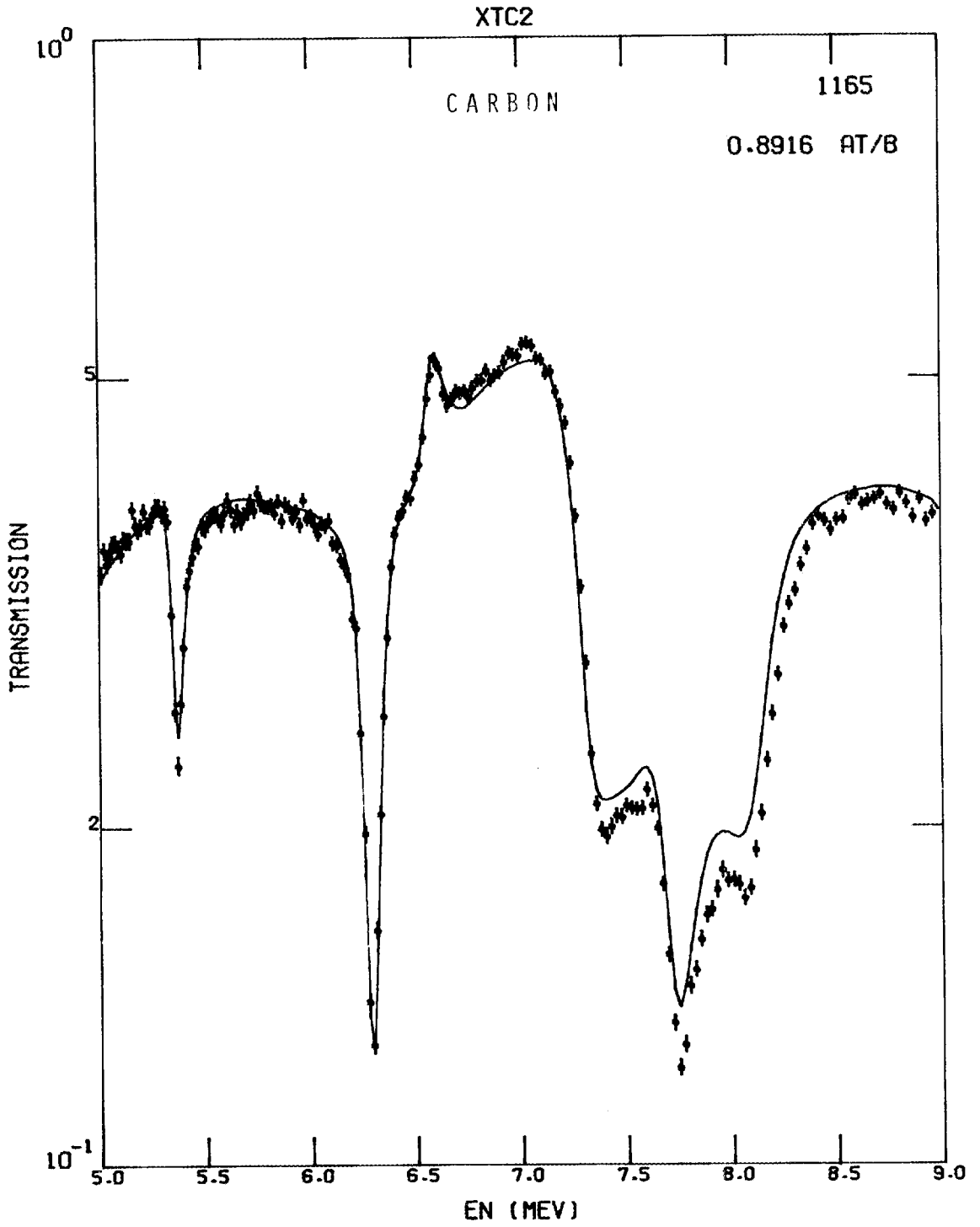
XTC2
CARBON
1165
0.8916 AT/B
TRANSMISSION
EN (MEV)
10^0
5
2
10^{-1}
5.0
5.5
6.0
6.5
7.0
7.5
8.0
8.5
9.0

Figure 2

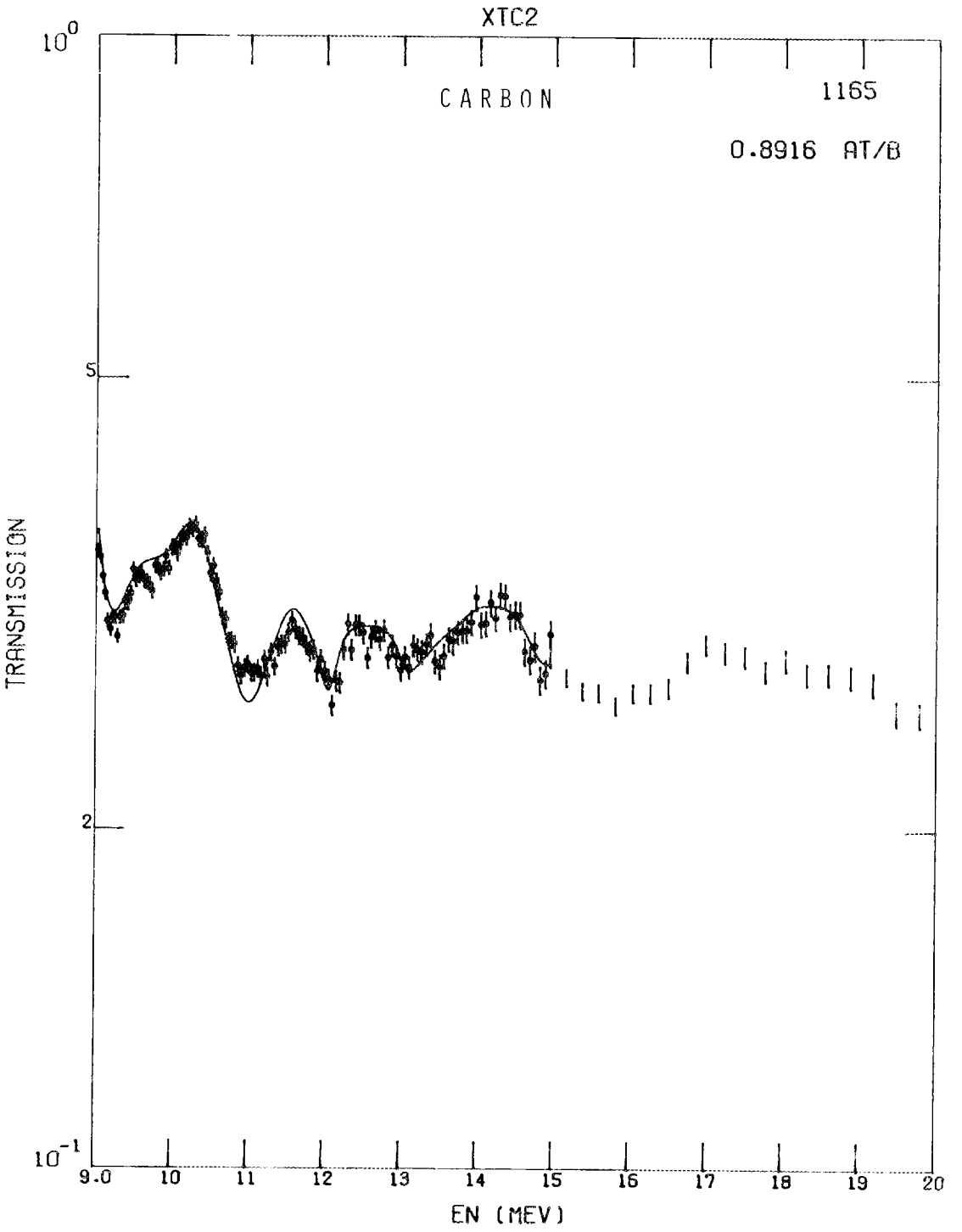
XTC2
CARBON
1165
0.8916 AT/B
TRANSMISSION
EN (MEV)
10^0
5
2
10^{-1}
9.0
10
11
12
13
14
15
16
17
18
19
20

Figure 3

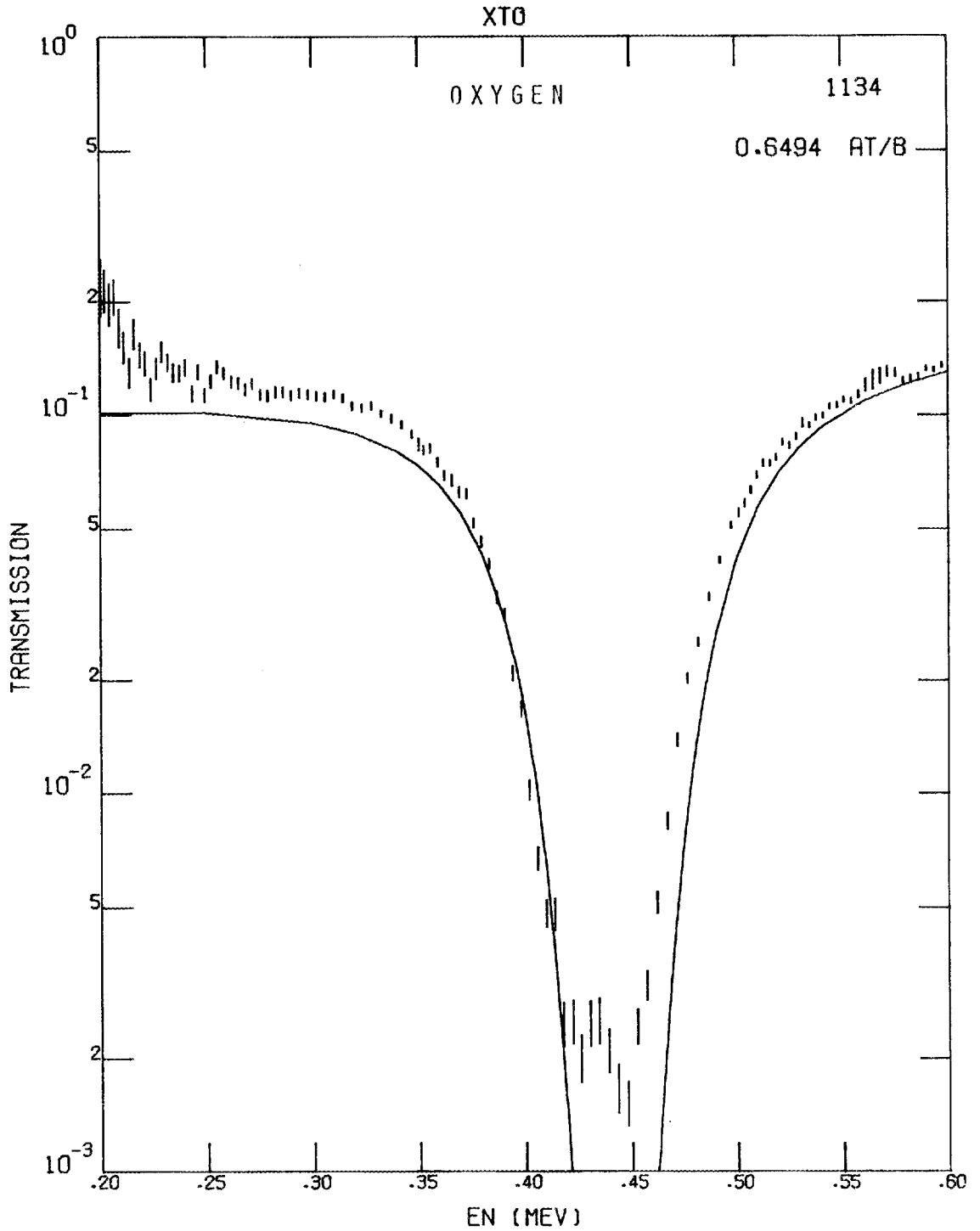
XTO
OXYGEN
1134
0.6494 AT/B
TRANSMISSION
EN (MEV)
10^0
5
2
10^{-1}
5
2
10^{-2}
5
2
10^{-3}
.20
.25
.30
.35
.40
.45
.50
.55
.60

Figure 4

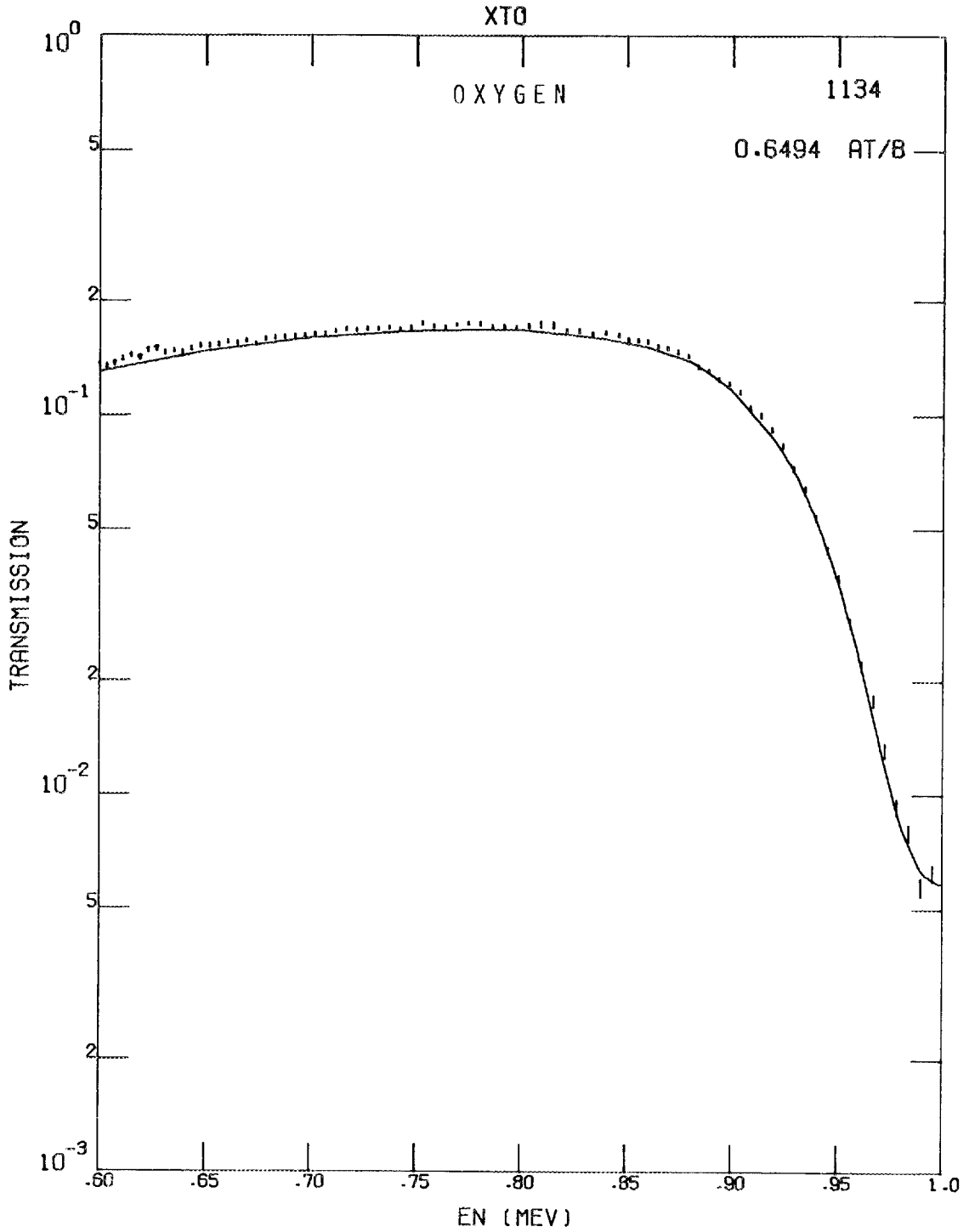
XTO
OXYGEN
1134
0.6494 AT/B
TRANSMISSION
EN (MEV)
10^0
5
2
10^{-1}
5
2
10^{-2}
5
2
10^{-3}
.60
.65
.70
.75
.80
.85
.90
.95
1.0

Figure 5

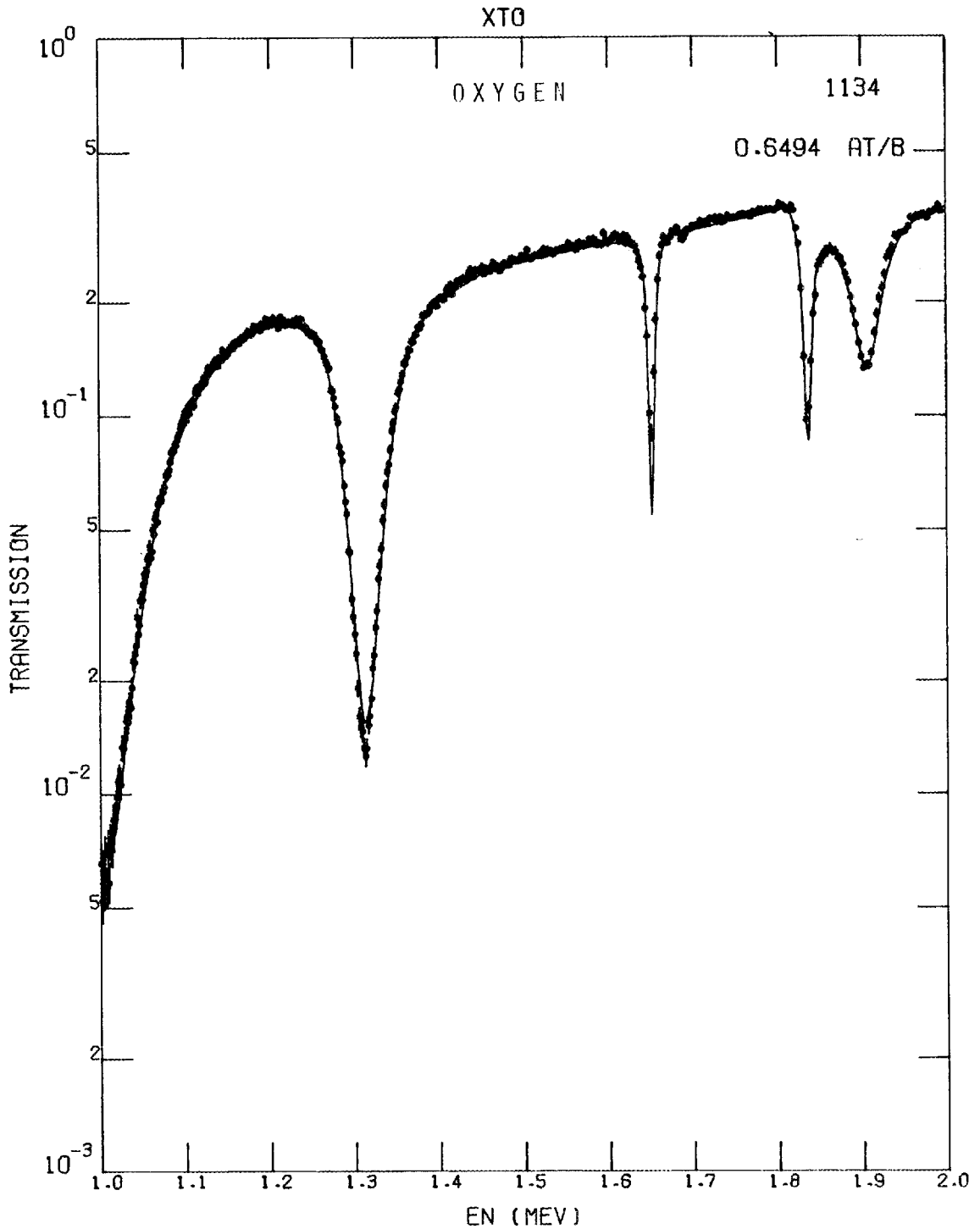
XTO
OXYGEN
1134
0.6494 AT/B
TRANSMISSION
EN (MEV)
10^0
5
2
10^{-1}
5
2
10^{-2}
5
2
10^{-3}
1.0
1.1
1.2
1.3
1.4
1.5
1.6
1.7
1.8
1.9
2.0

Figure 6

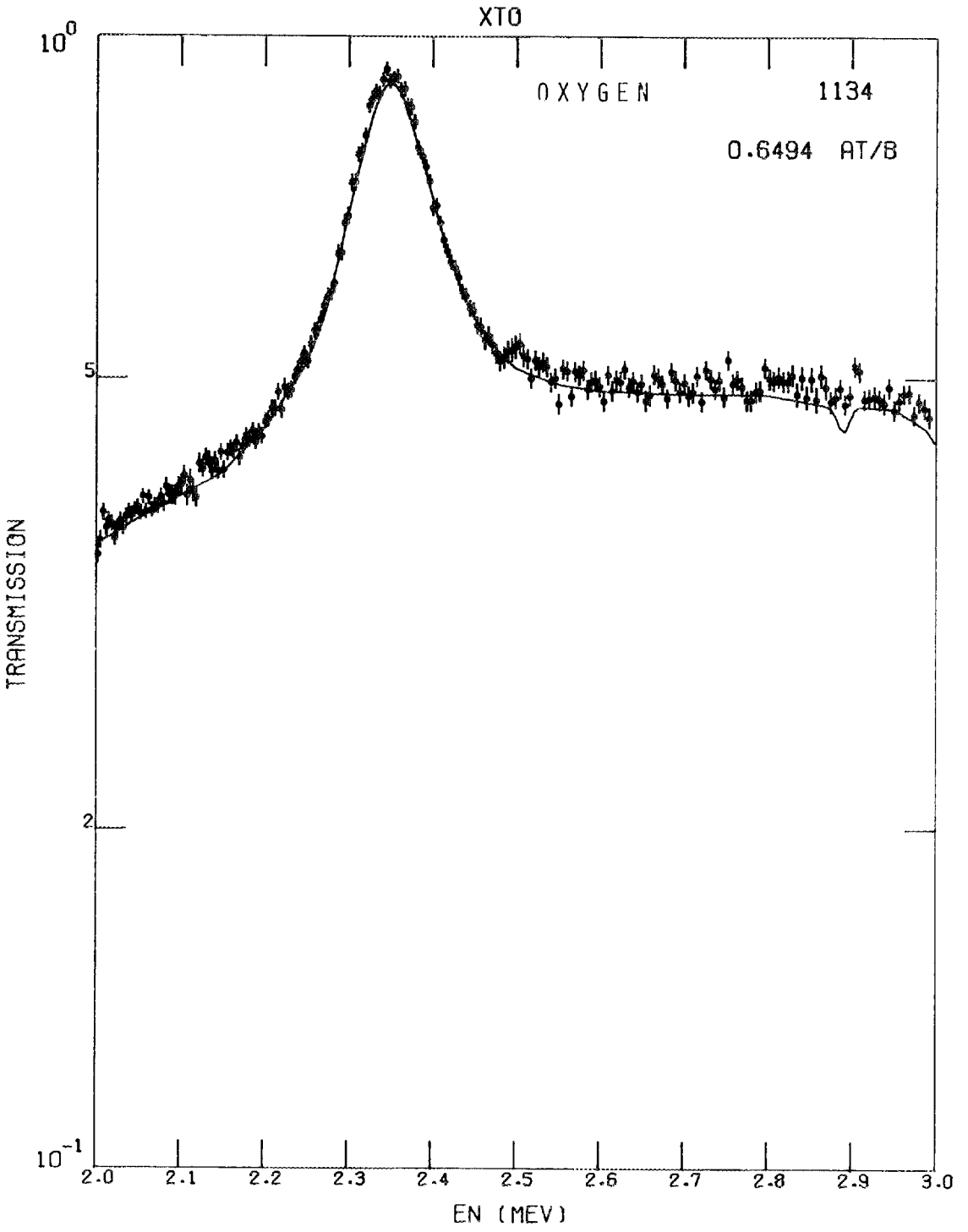
XTO
OXYGEN
1134
0.6494 AT/B
TRANSMISSION
10^0
5
2
10^-1
2.0
2.1
2.2
2.3
2.4
2.5
2.6
2.7
2.8
2.9
3.0
EN (MEV)

Figure 7

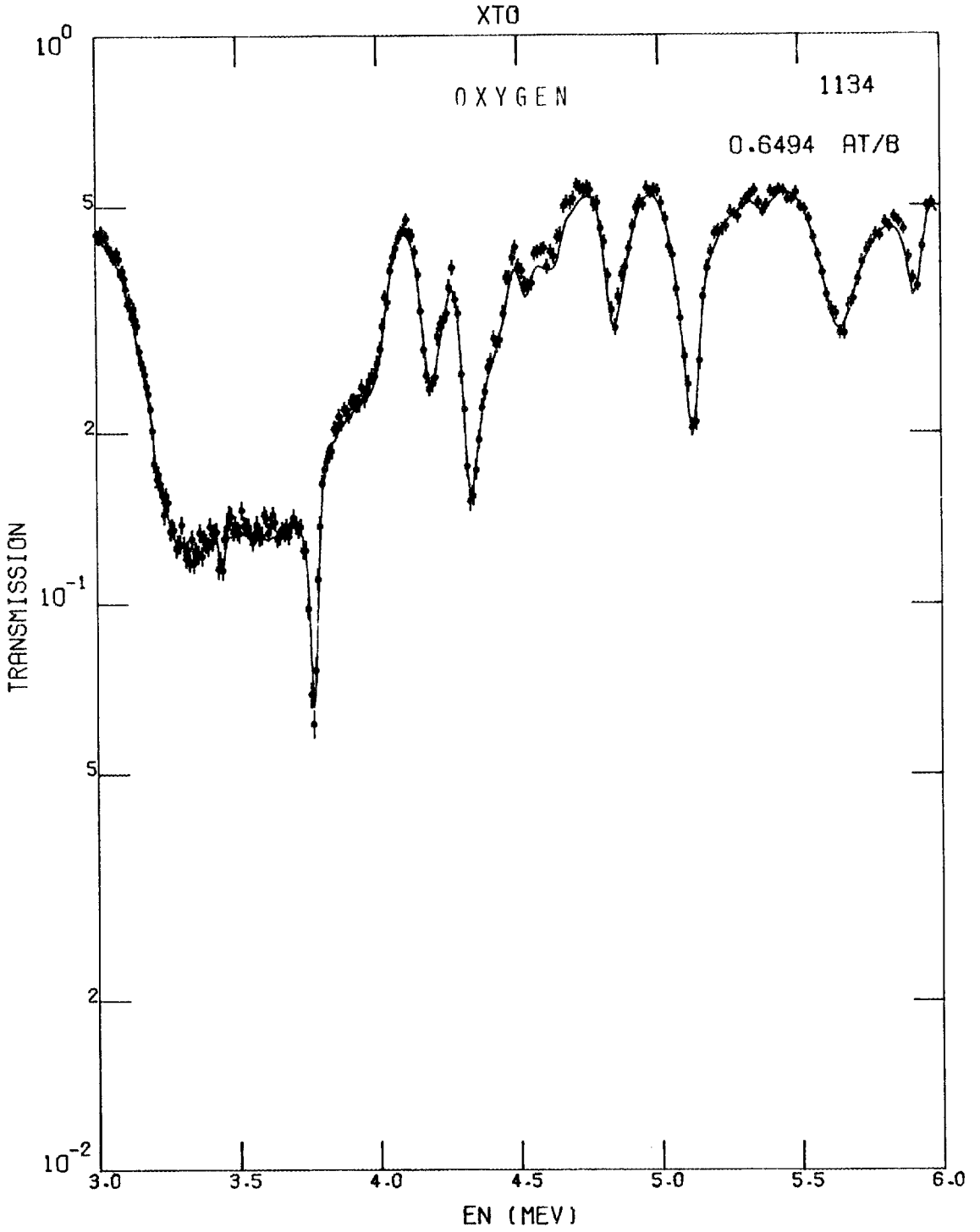
XTO
OXYGEN
1134
0.6494 AT/B
TRANSMISSION
EN (MEV)
10^0
5
2
10^{-1}
5
2
10^{-2}
3.0
3.5
4.0
4.5
5.0
5.5
6.0

Figure 8

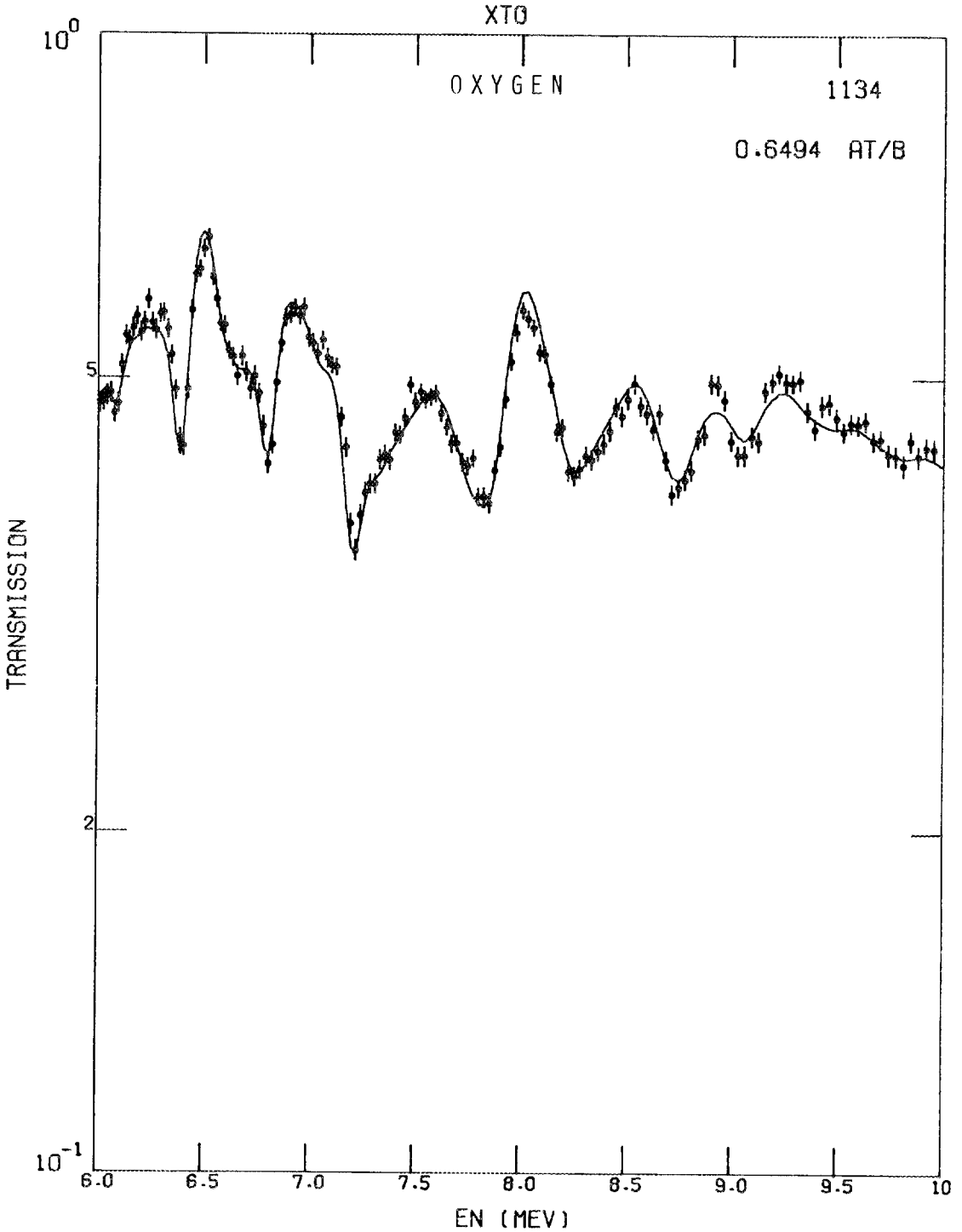
XTO
OXYGEN
1134
0.6494 AT/B
TRANSMISSION
10^0
5
2
10^{-1}
6.0
6.5
7.0
7.5
8.0
8.5
9.0
9.5
10
EN (MEV)

Figure 9

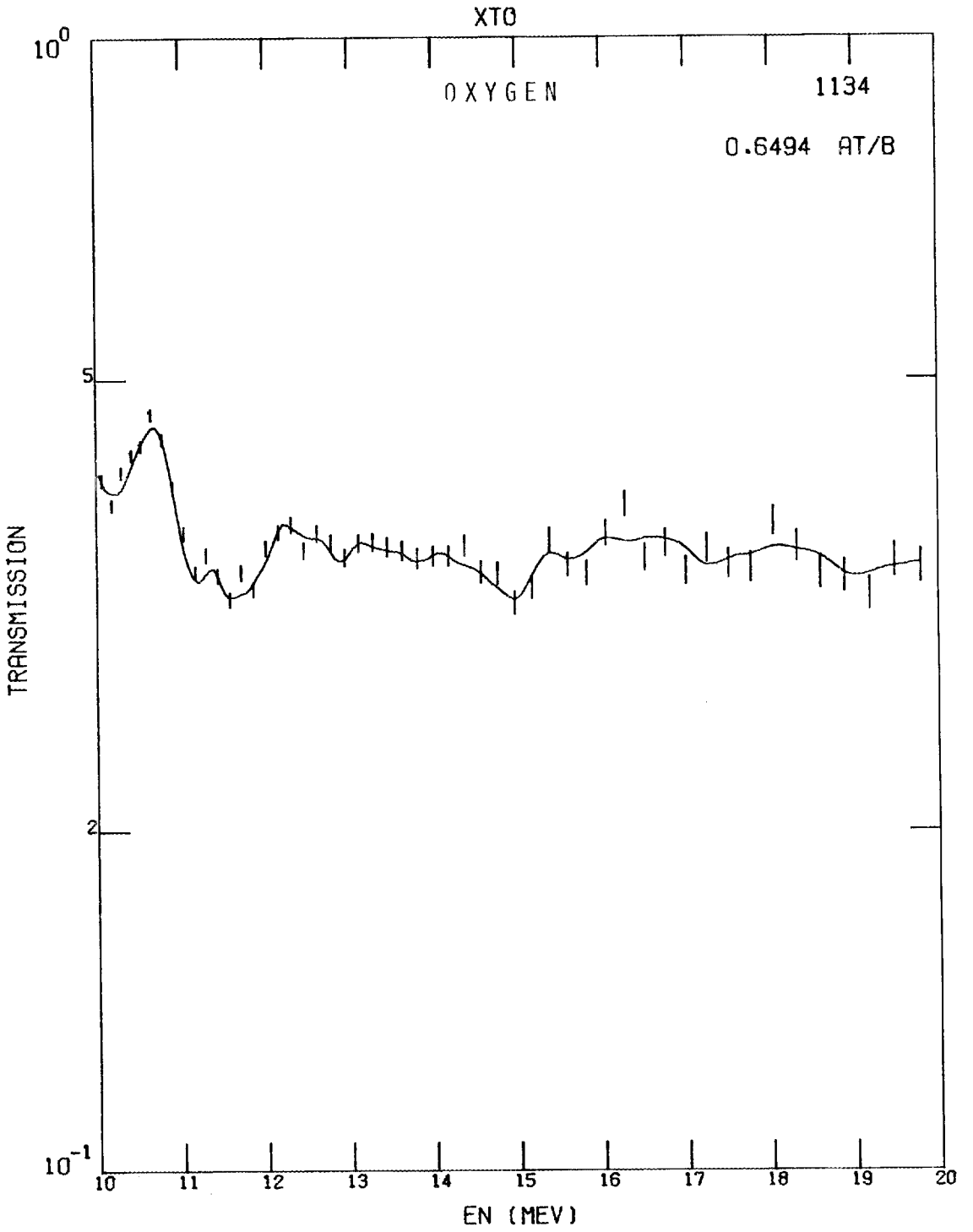
XTO
OXYGEN
1134
0.6494 AT/B
TRANSMISSION
EN (MEV)
10^0
5
2
10^{-1}
10
11
12
13
14
15
16
17
18
19
20

Figure 10

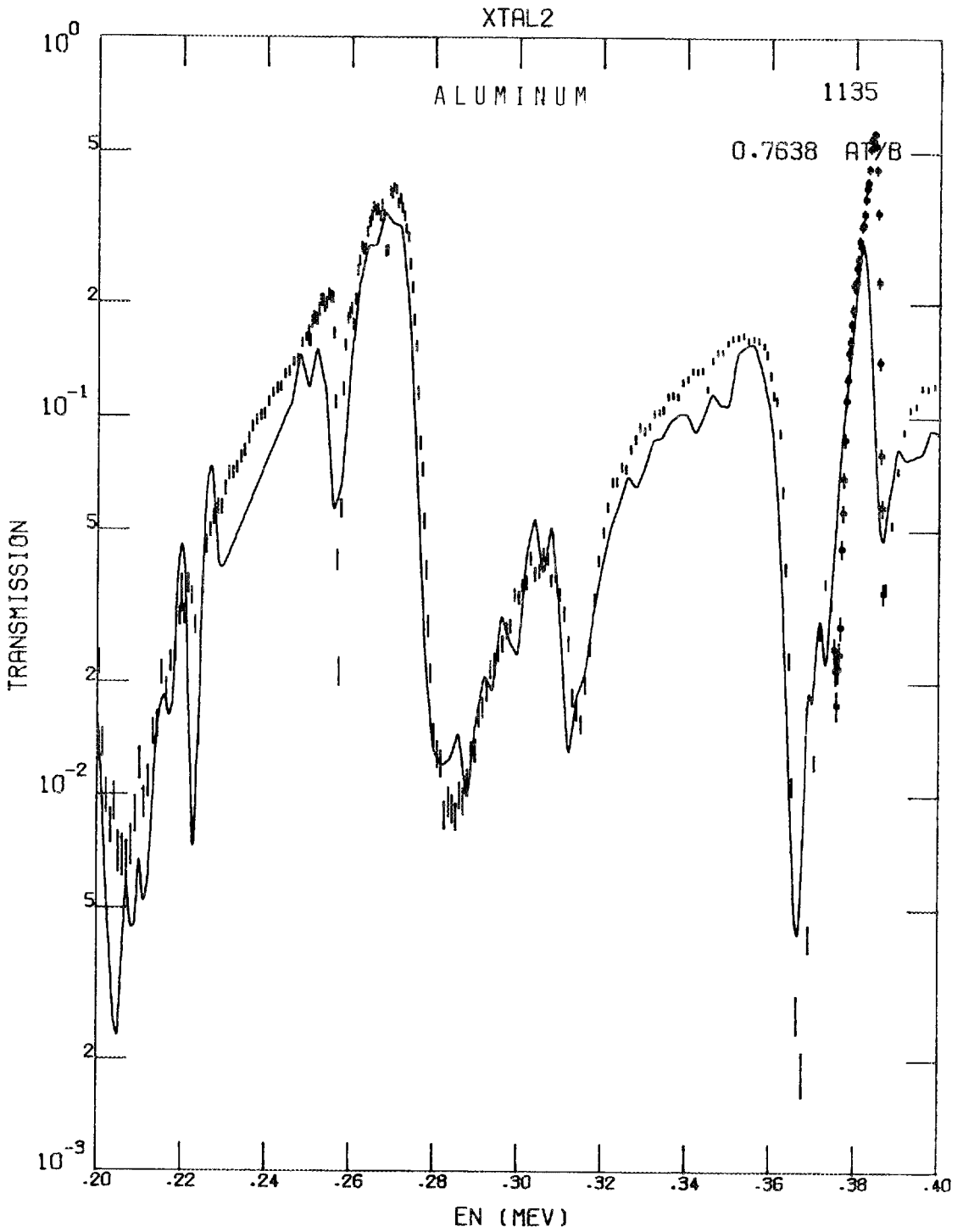
XTAL2
ALUMINUM
1135
0.7638 AT/B
TRANSMISSION
EN (MEV)
10^0
5
2
10^{-1}
5
2
10^{-2}
5
2
10^{-3}
.20
.22
.24
.26
.28
.30
.32
.34
.36
.38
.40

Figure 11

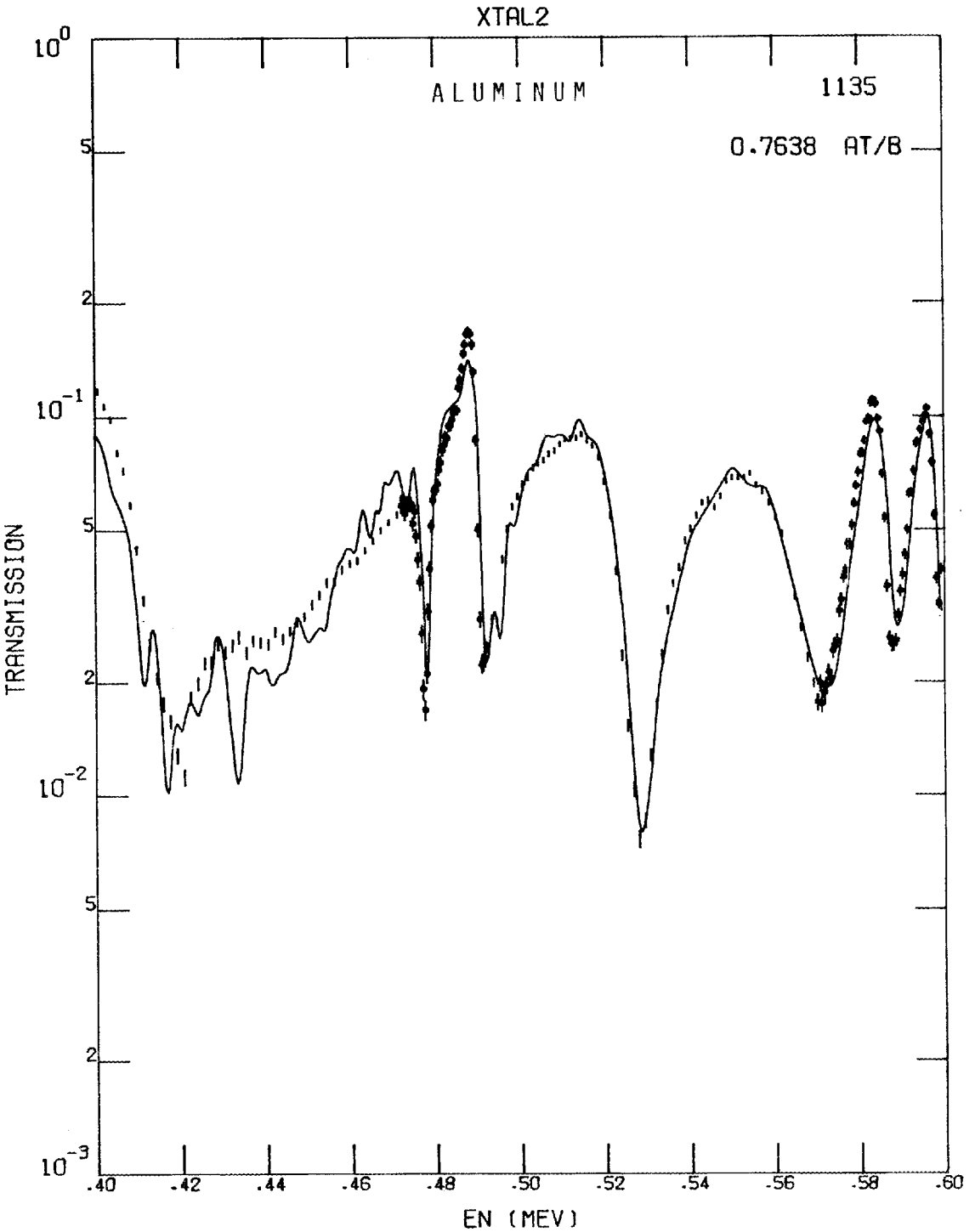
XTAL2
ALUMINUM
1135
0.7638 AT/B
TRANSMISSION
EN (MEV)
10^0
5
2
10^{-1}
5
2
10^{-2}
5
2
10^{-3}
.40
.42
.44
.46
.48
.50
.52
.54
.56
.58
.60

Figure 12

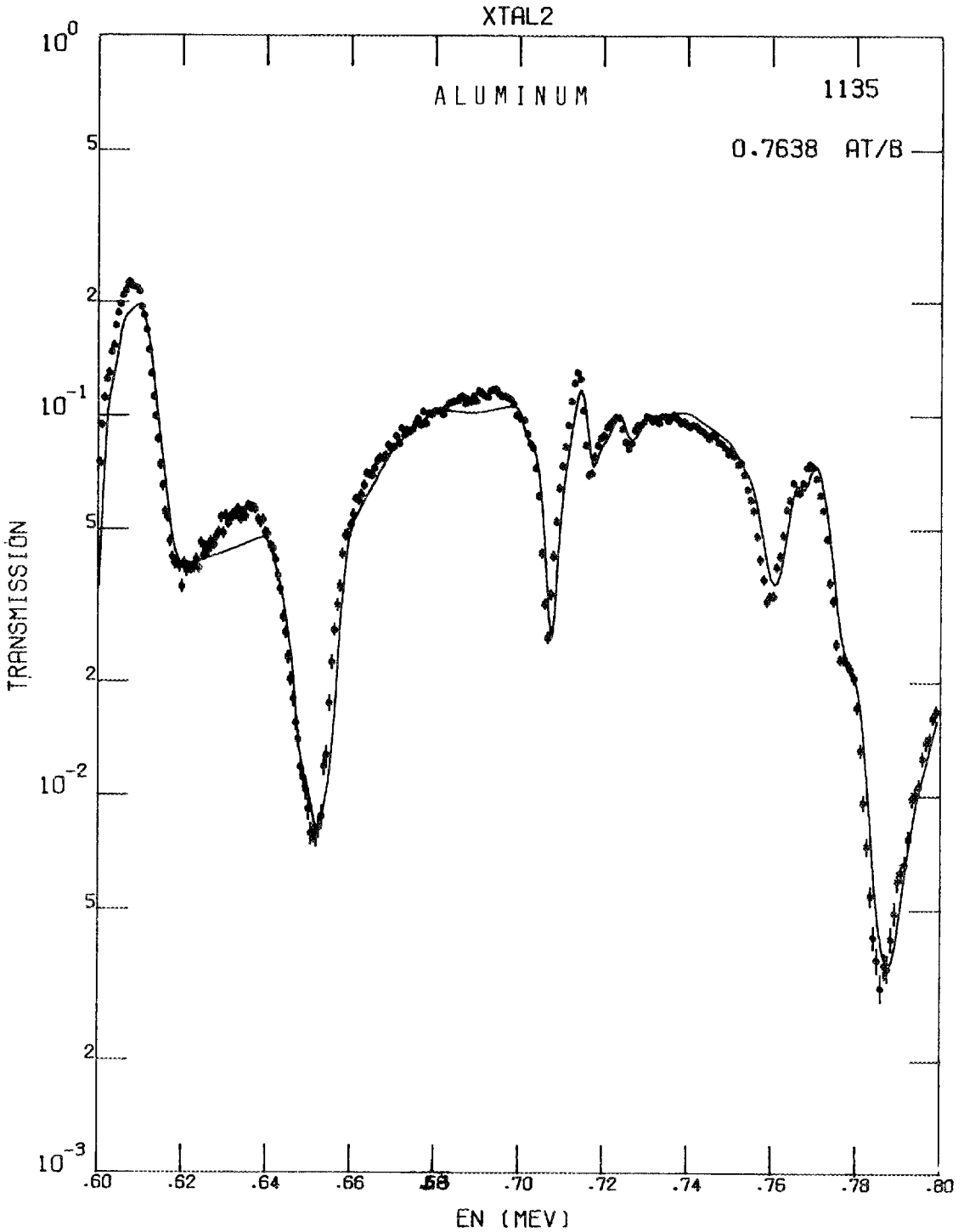
XTAL2
ALUMINUM
1135
0.7638 AT/B
TRANSMISSION
EN (MEV)
10^0
5
2
10^{-1}
5
2
10^{-2}
5
2
10^{-3}
.60
.62
.64
.66
.68
.70
.72
.74
.76
.78
.80

Figure 13

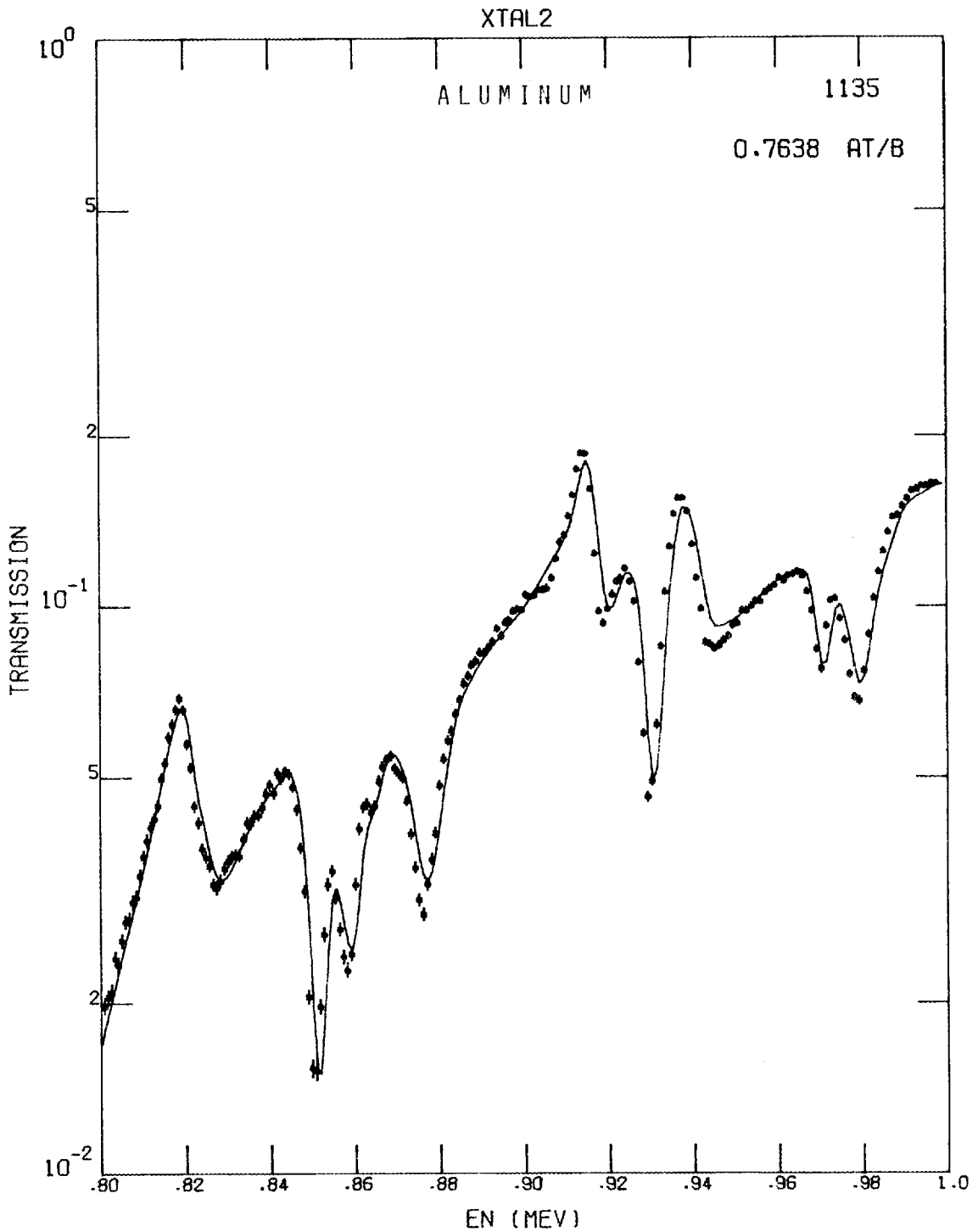
XTAL2
ALUMINUM
1135
0.7638 AT/B
TRANSMISSION
EN (MEV)
10^0
5
2
10^{-1}
5
2
10^{-2}
.80
.82
.84
.86
.88
.90
.92
.94
.96
.98
1.0

Figure 14

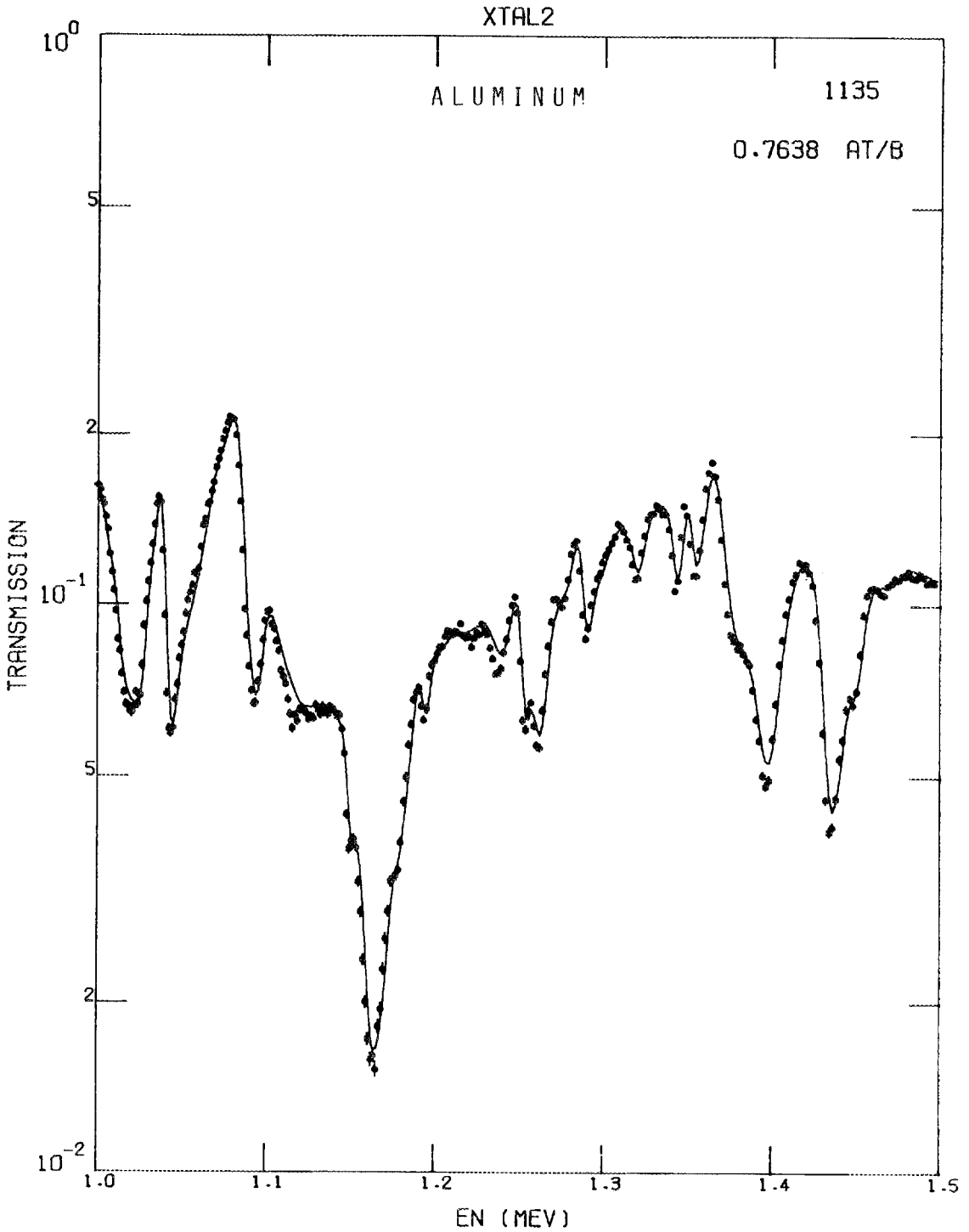
XTAL2
ALUMINUM
1135
0.7638 AT/B
TRANSMISSION
EN (MEV)
10^0
5
2
10^-1
5
2
10^-2
1.0
1.1
1.2
1.3
1.4
1.5

Figure 15

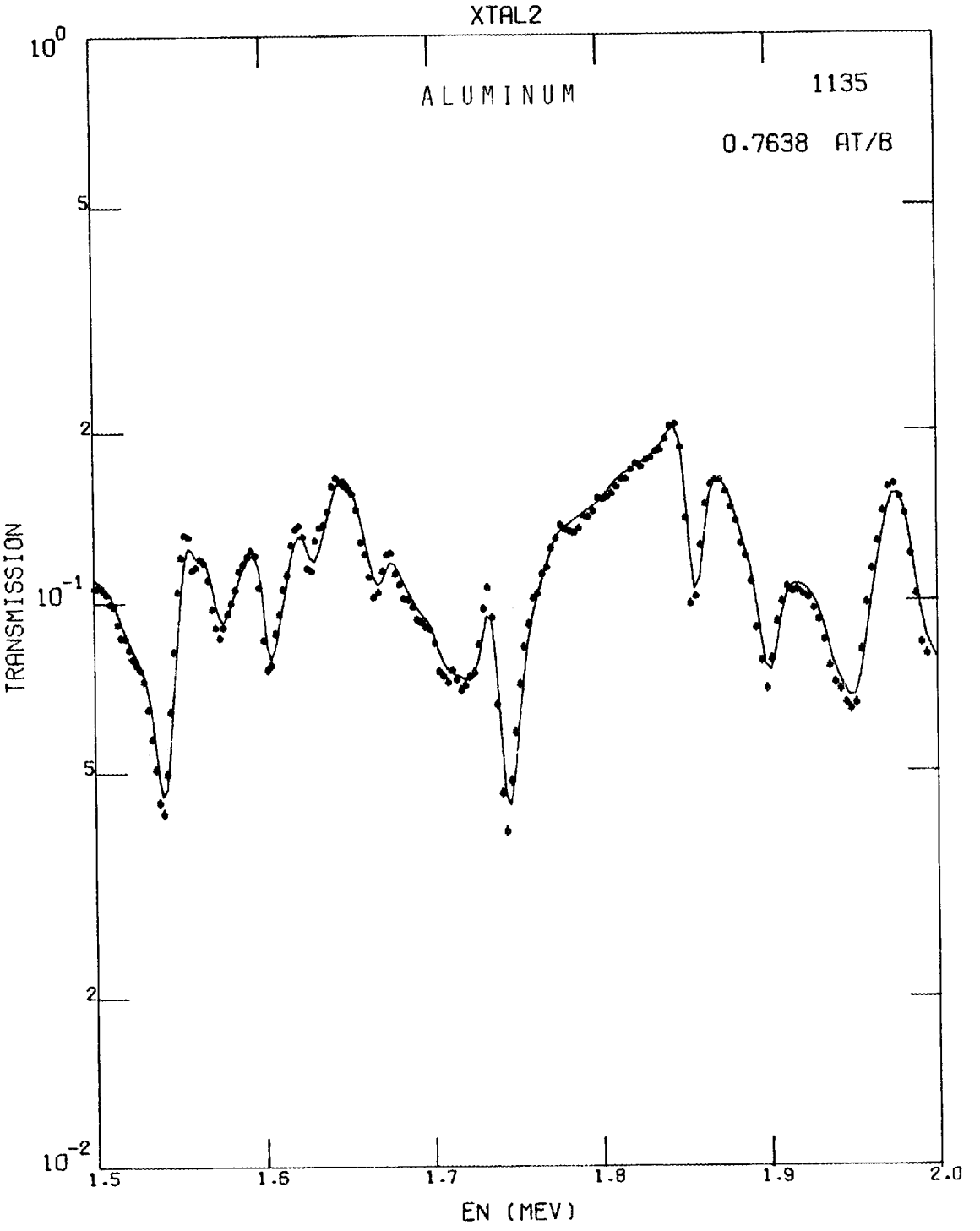
XTAL2
ALUMINUM
1135
0.7638 AT/B
TRANSMISSION
EN (MEV)
10^0
5
2
10^{-1}
5
2
10^{-2}
1.5
1.6
1.7
1.8
1.9
2.0

Figure 16

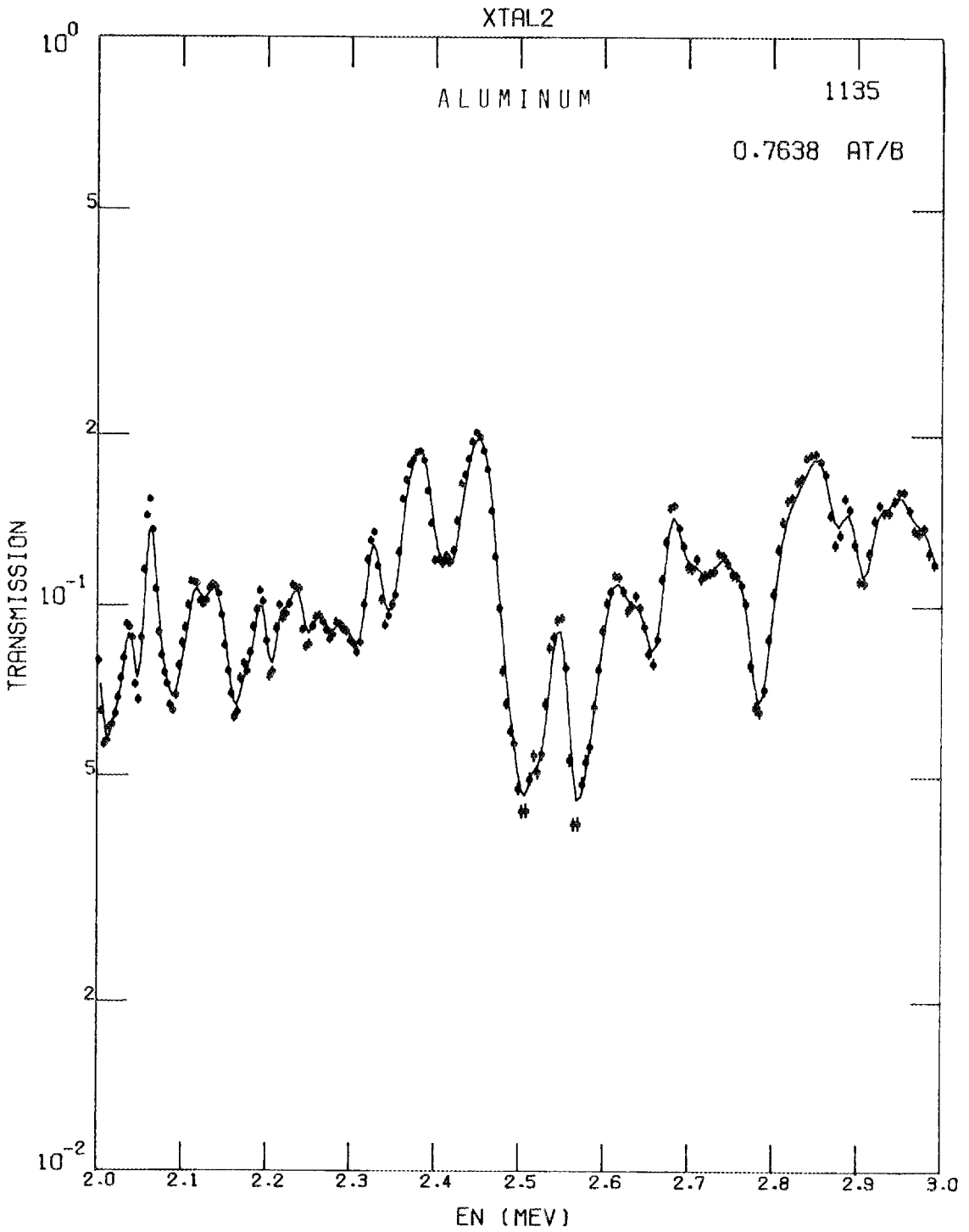
XTAL2
ALUMINUM
1135
0.7638 AT/B
TRANSMISSION
EN (MEV)
10^0
5
2
10^-1
5
2
10^-2
2.0
2.1
2.2
2.3
2.4
2.5
2.6
2.7
2.8
2.9
3.0

Figure 17

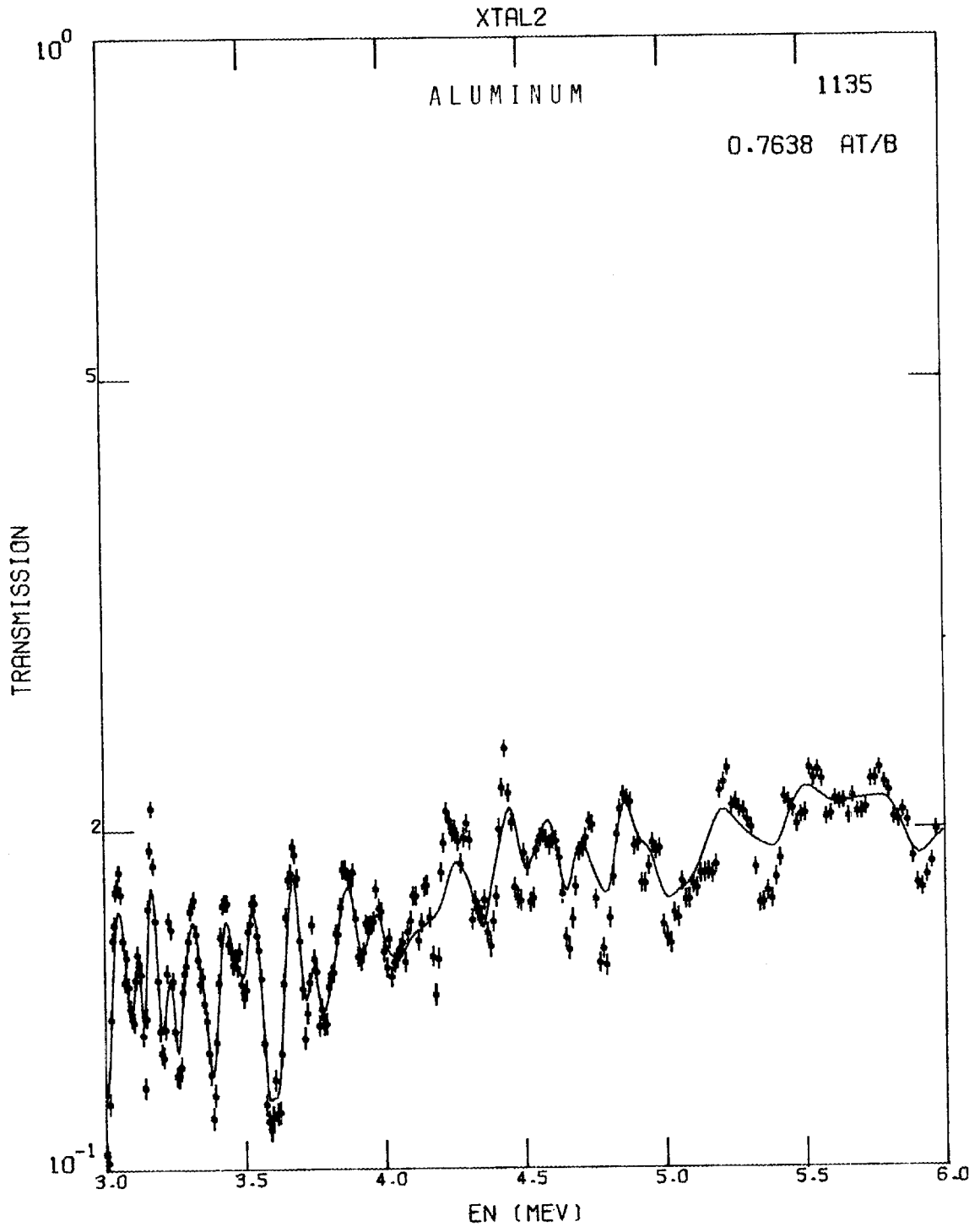
XTAL2
ALUMINUM
1135
0.7638 AT/B
TRANSMISSION
10^0
5
2
10^{-1}
3.0
3.5
4.0
4.5
5.0
5.5
6.0
EN (MEV)

Figure 18

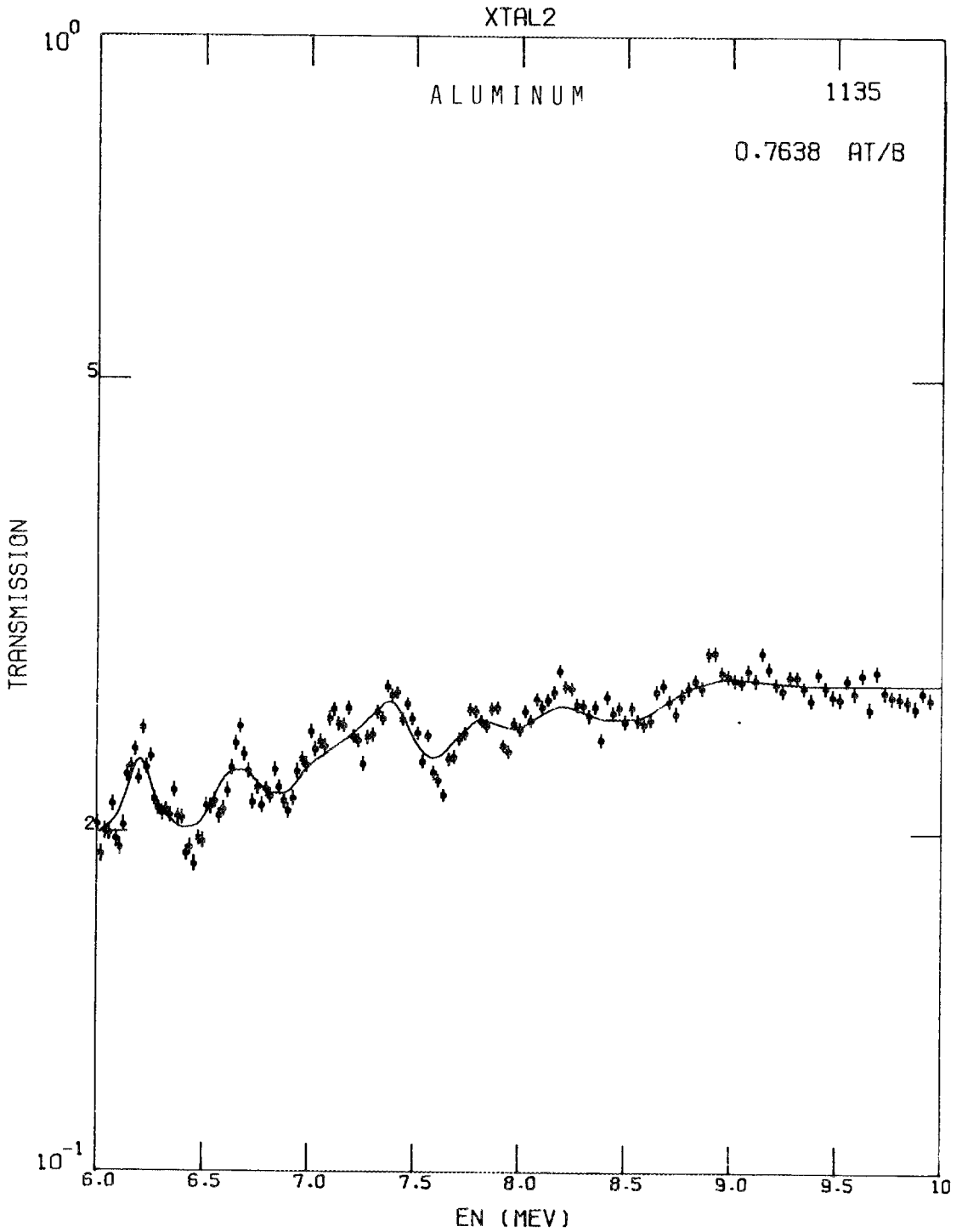
XTAL2
ALUMINUM
1135
0.7638 AT/B
TRANSMISSION
EN (MEV)
10^0
5
2
10^-1
6.0
6.5
7.0
7.5
8.0
8.5
9.0
9.5
10

Figure 19

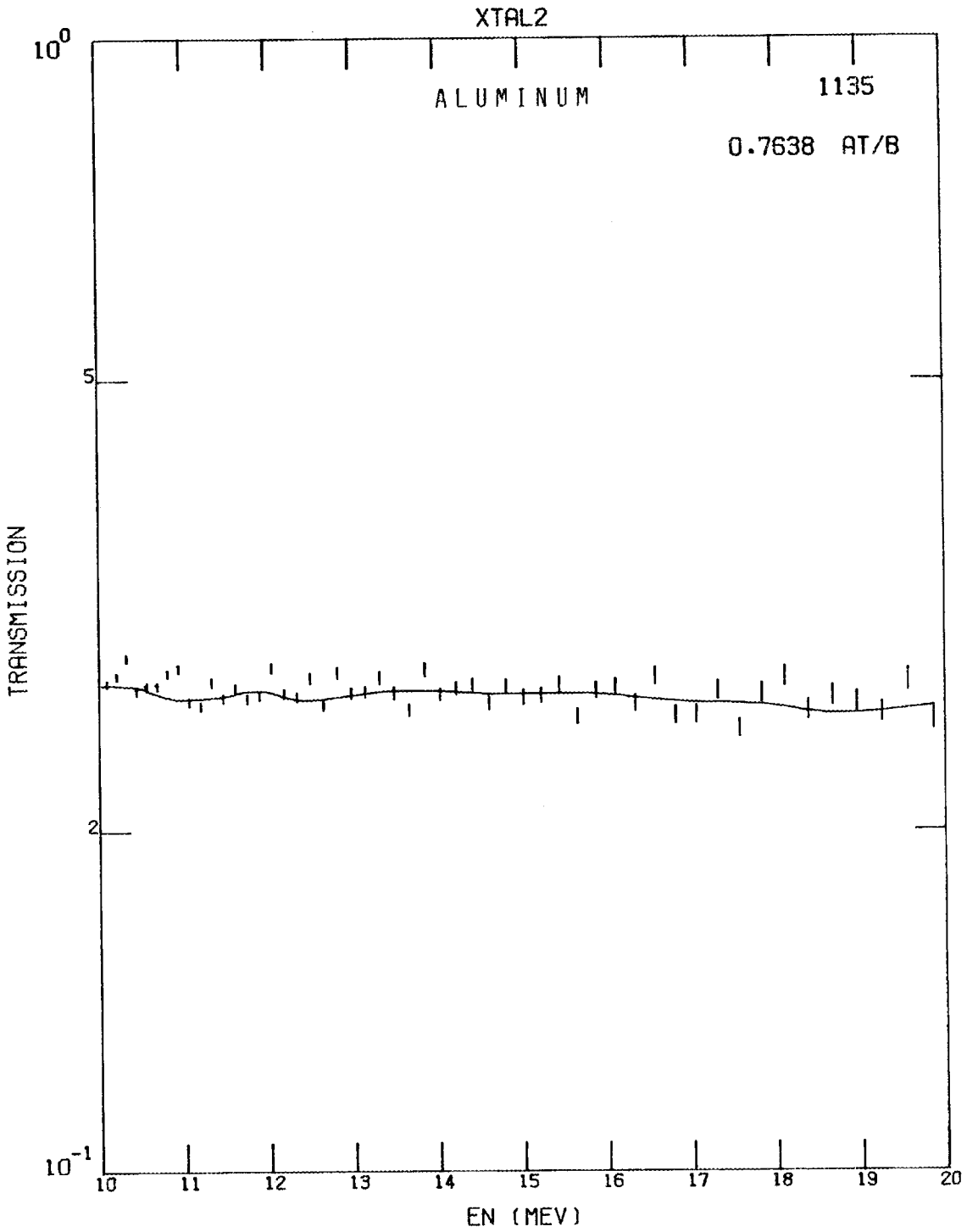
XTAL2
ALUMINUM
1135
0.7638 AT/B
TRANSMISSION
10^0
5
2
10^{-1}
10
11
12
13
14
15
16
17
18
19
20
EN (MEV)

Figure 20

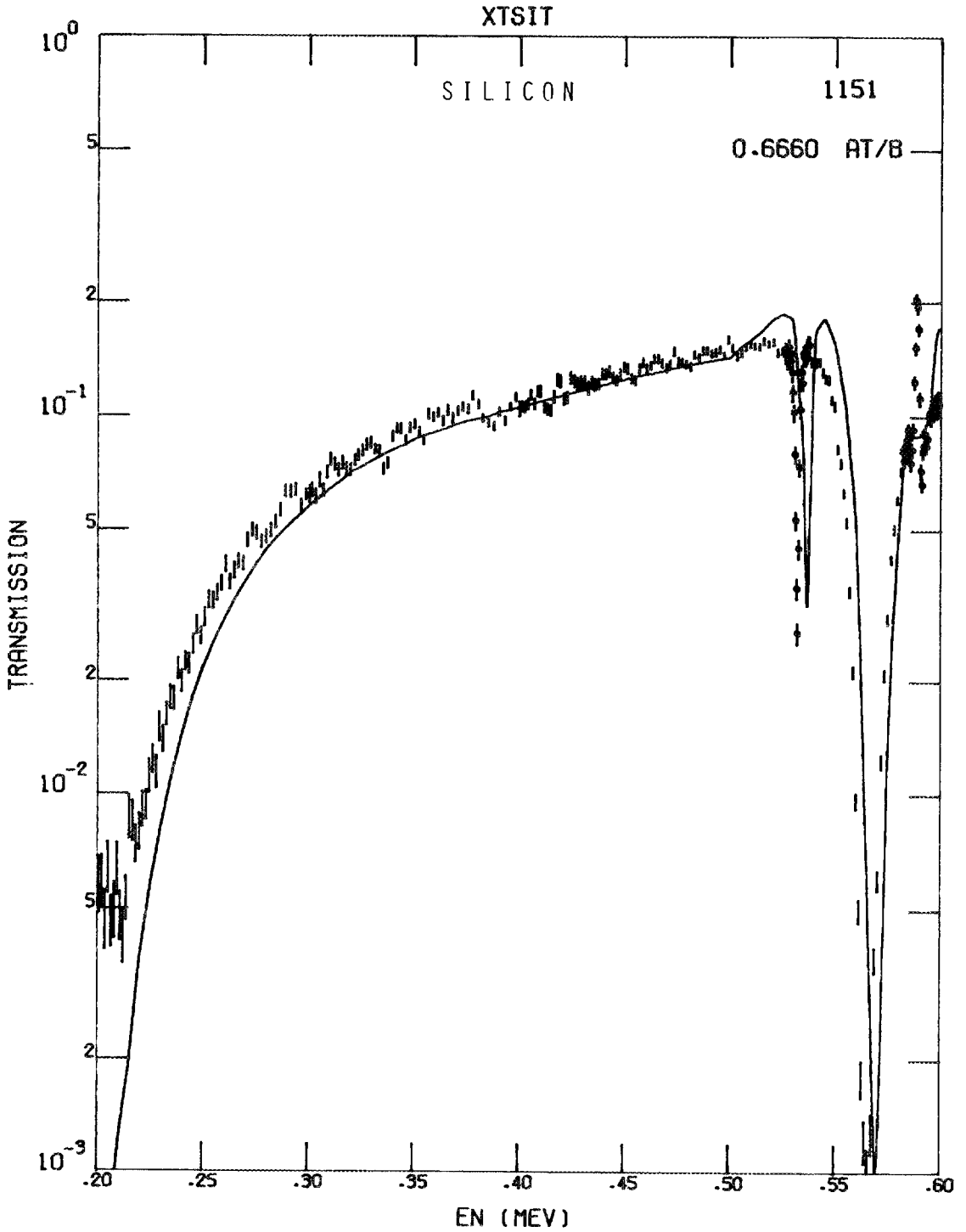
XTSIT
SILICON
1151
0.6660 AT/B
TRANSMISSION
EN (MEV)
10^0
5
2
10^{-1}
5
2
10^{-2}
5
2
10^{-3}
.20
.25
.30
.35
.40
.45
.50
.55
.60

Figure 21

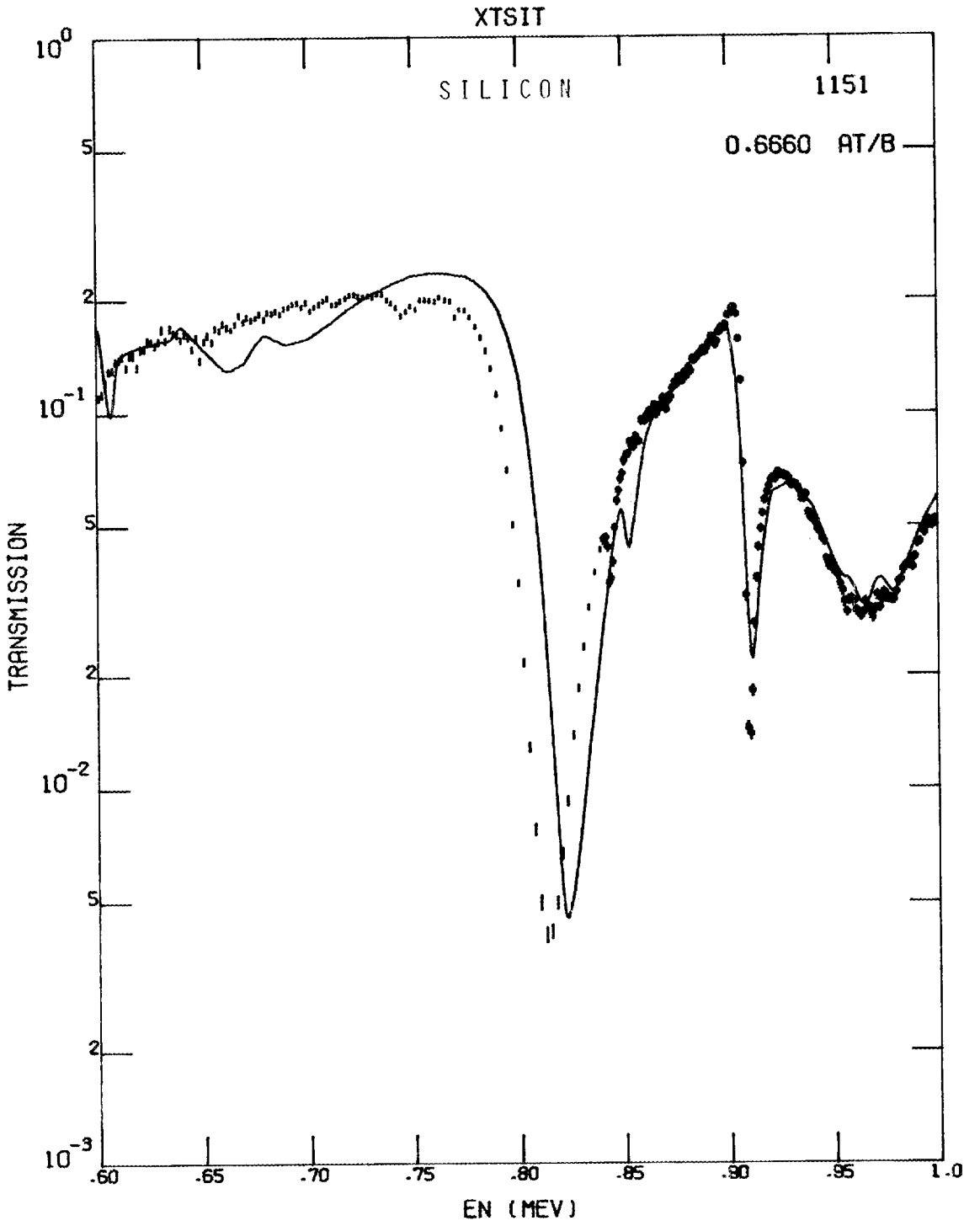
XTSIT
SILICON
1151
0.6660 AT/B
TRANSMISSION
EN (MEV)
10^0
5
2
10^{-1}
5
2
10^{-2}
5
2
10^{-3}
.60
.65
.70
.75
.80
.85
.90
.95
1.0

Figure 22

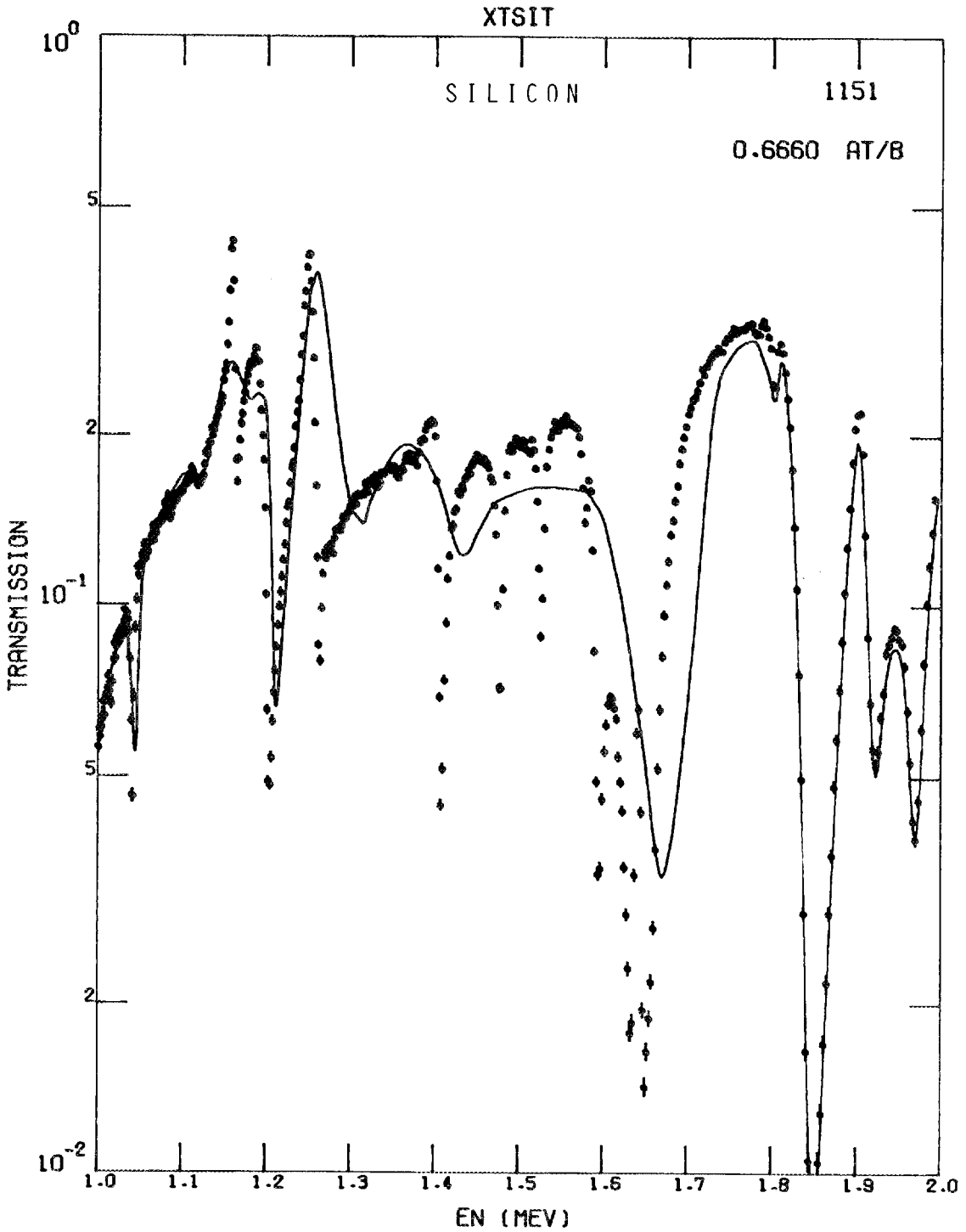
XTSIT
SILICON
1151
0.6660 AT/B
TRANSMISSION
EN (MEV)
10^0
5
2
10^-1
5
2
10^-2
1.0
1.1
1.2
1.3
1.4
1.5
1.6
1.7
1.8
1.9
2.0

Figure 23

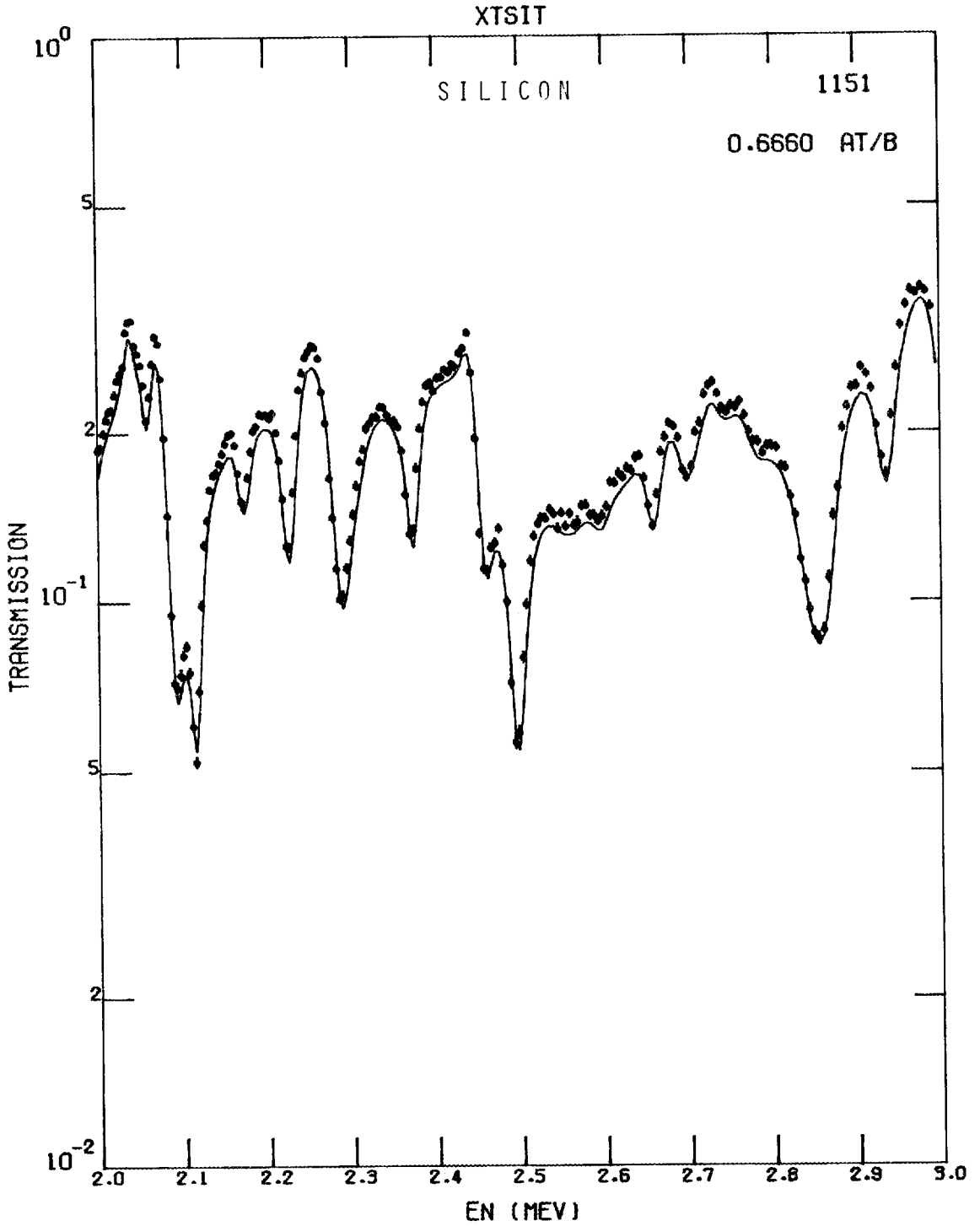
XTSIT
SILICON
1151
0.6660 AT/B
TRANSMISSION
EN (MEV)
10^0
5
2
10^{-1}
5
2
10^{-2}
2.0
2.1
2.2
2.3
2.4
2.5
2.6
2.7
2.8
2.9
3.0

Figure 24

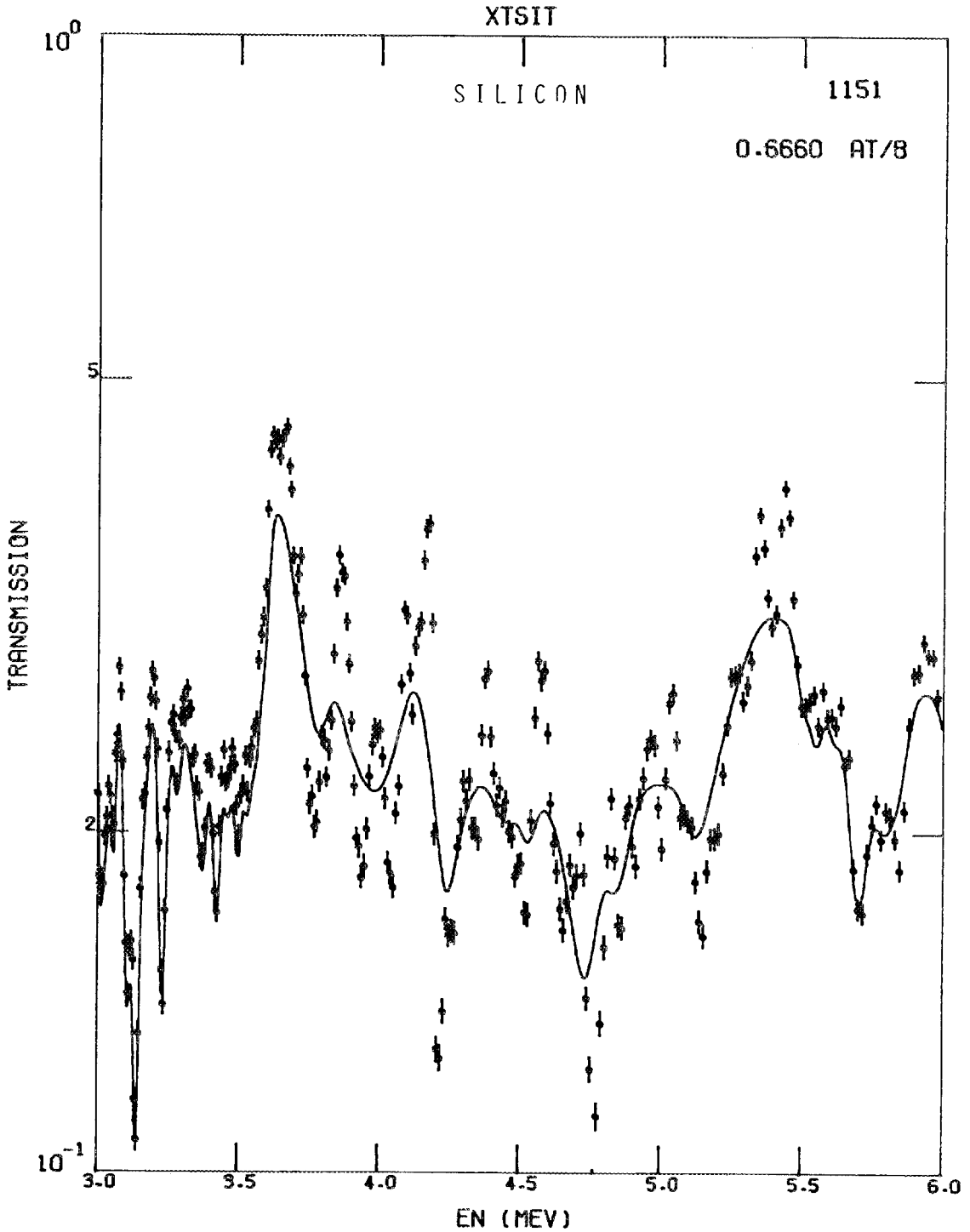
XTSIT
SILICON
1151
0.6660 AT/B
TRANSMISSION
EN (MEV)
10^0
5
2
10^{-1}
3.0
3.5
4.0
4.5
5.0
5.5
6.0

Figure 25

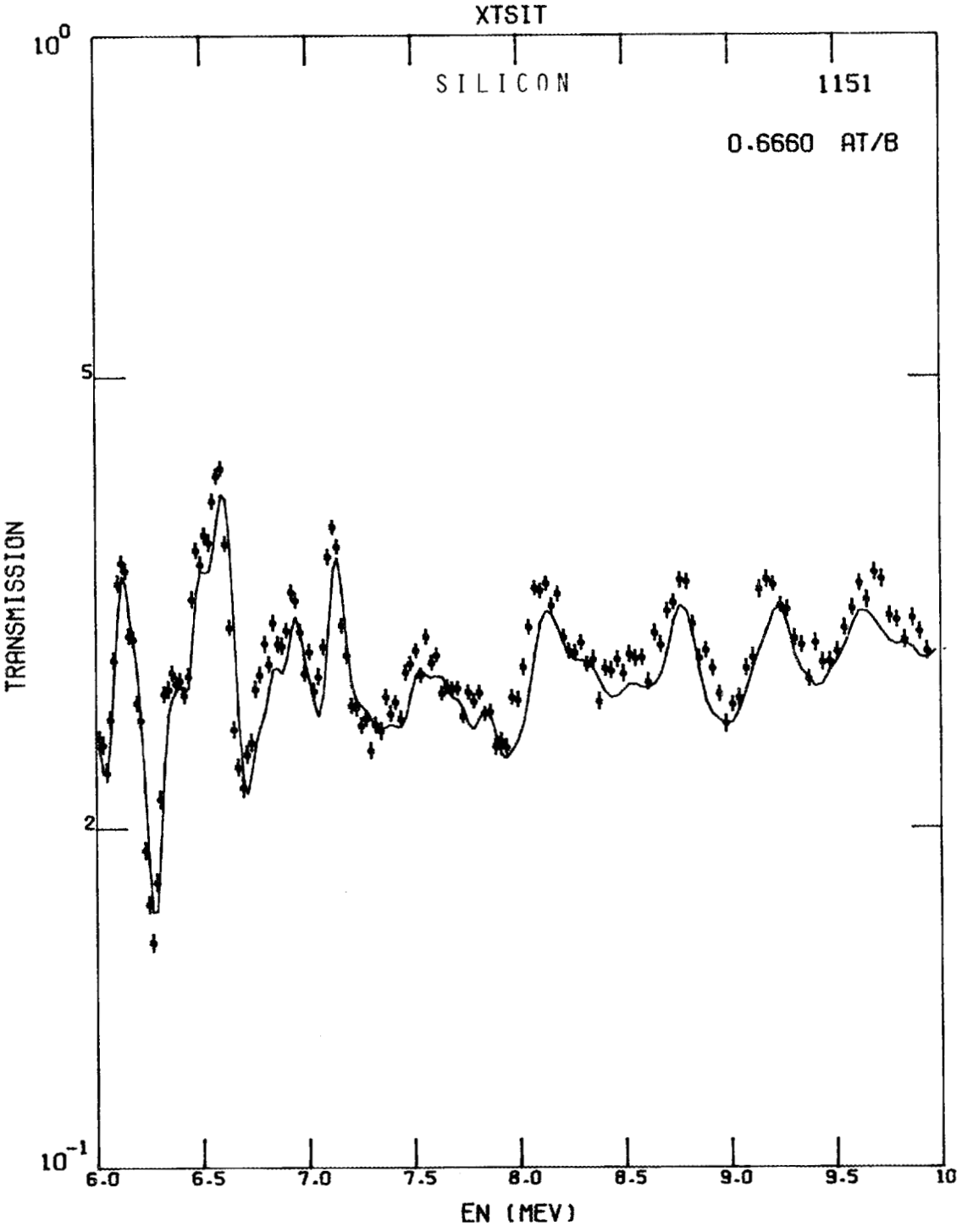
XTSIT
SILICON
1151
0.6660 AT/B
TRANSMISSION
EN (MEV)
10^0
5
2
10^{-1}
6.0
6.5
7.0
7.5
8.0
8.5
9.0
9.5
10

Figure 26

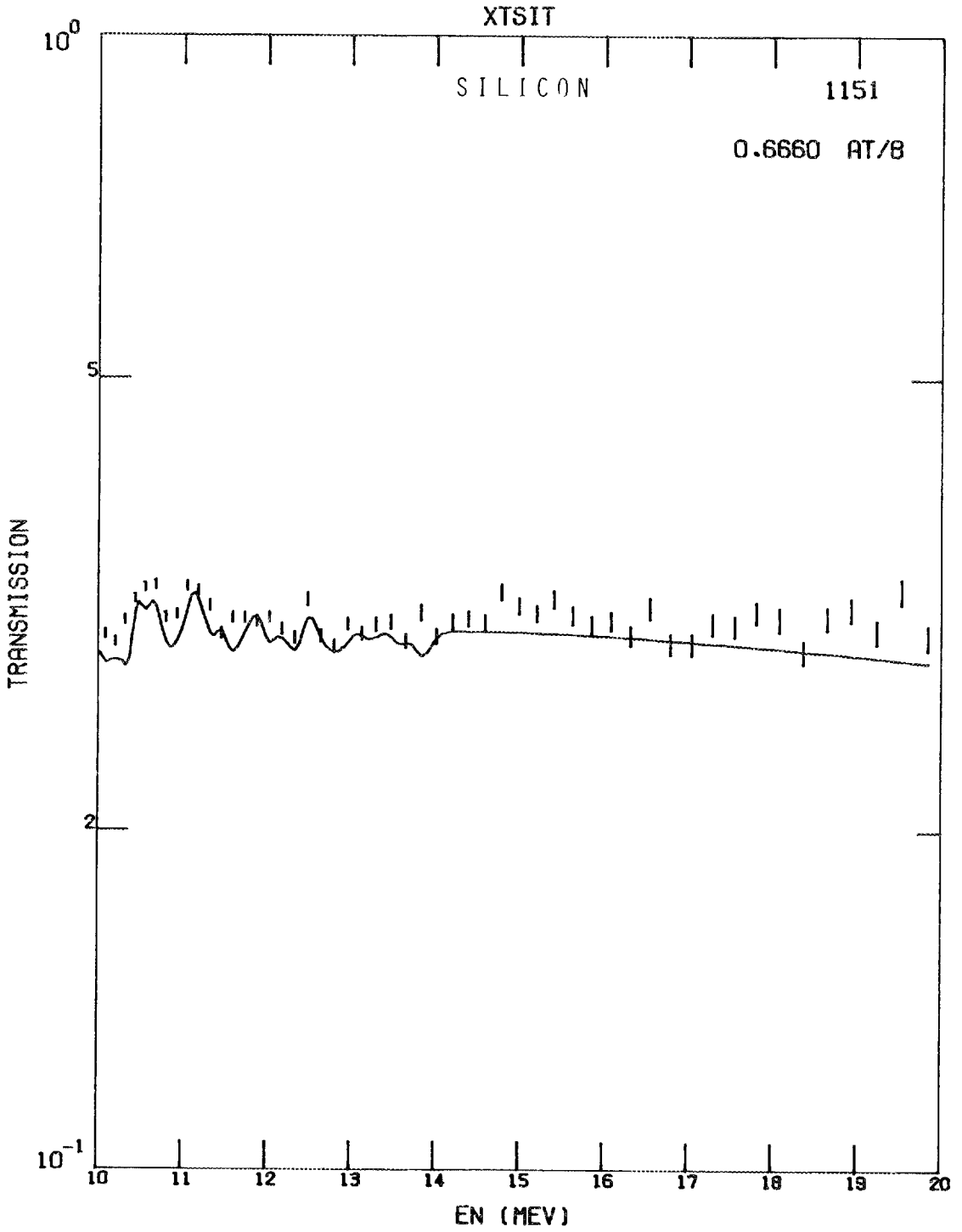
XTSIT
SILICON
1151
0.6660 AT/B
TRANSMISSION
EN (MEV)
10^0
5
2
10^-1
10
11
12
13
14
15
16
17
18
19
20

Figure 27

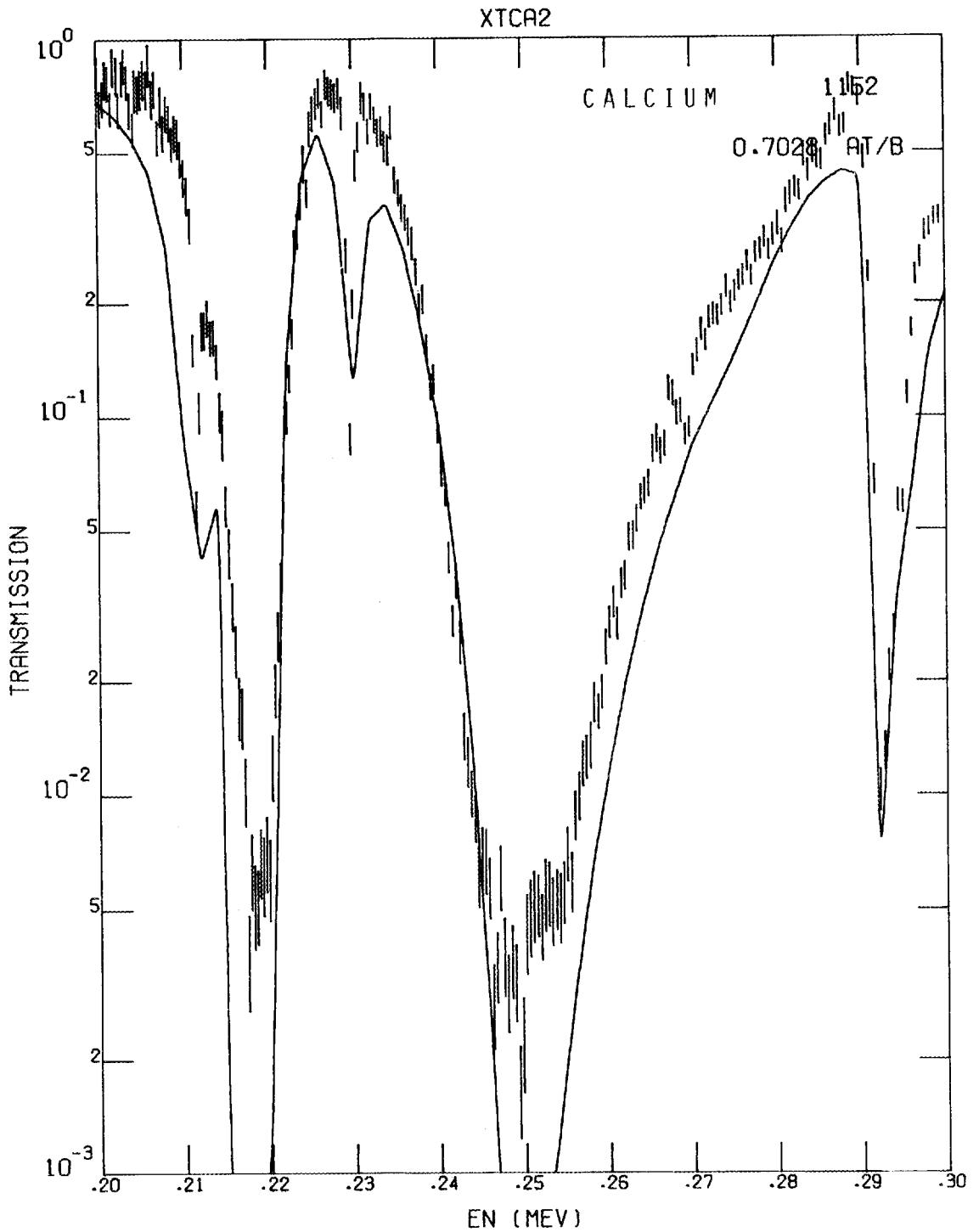
XTCA2
CALCIUM
1.152
0.7028 AT/B
TRANSMISSION
EN (MEV)
10^0
5
2
10^{-1}
5
2
10^{-2}
5
2
10^{-3}
.20
.21
.22
.23
.24
.25
.26
.27
.28
.29
.30

Figure 28

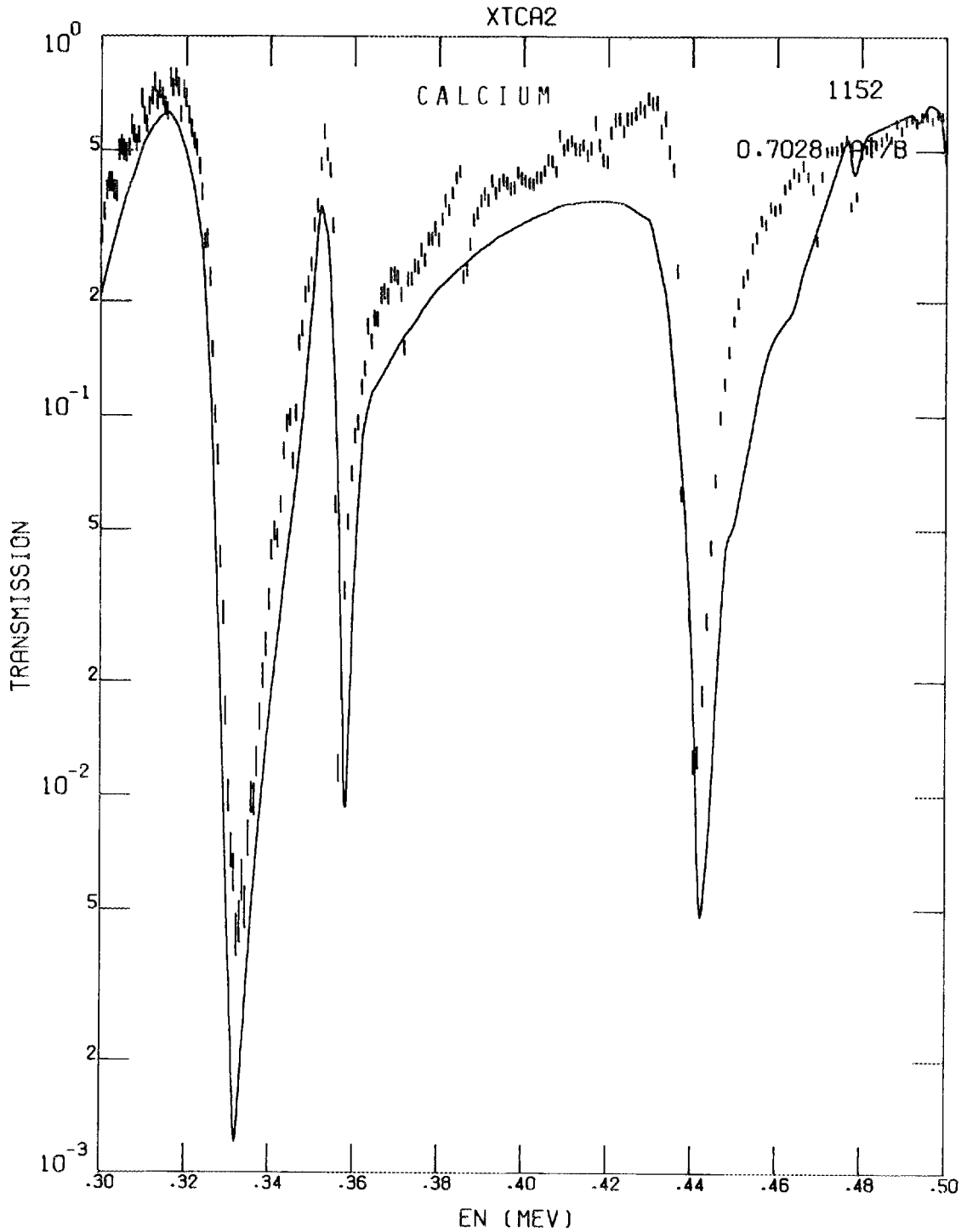
XTCA2
CALCIUM
1152
0.7028 AM/B
TRANSMISSION
EN (MEV)
10^0
5
2
10^{-1}
5
2
10^{-2}
5
2
10^{-3}
.30
.32
.34
.36
.38
.40
.42
.44
.46
.48
.50

Figure 29

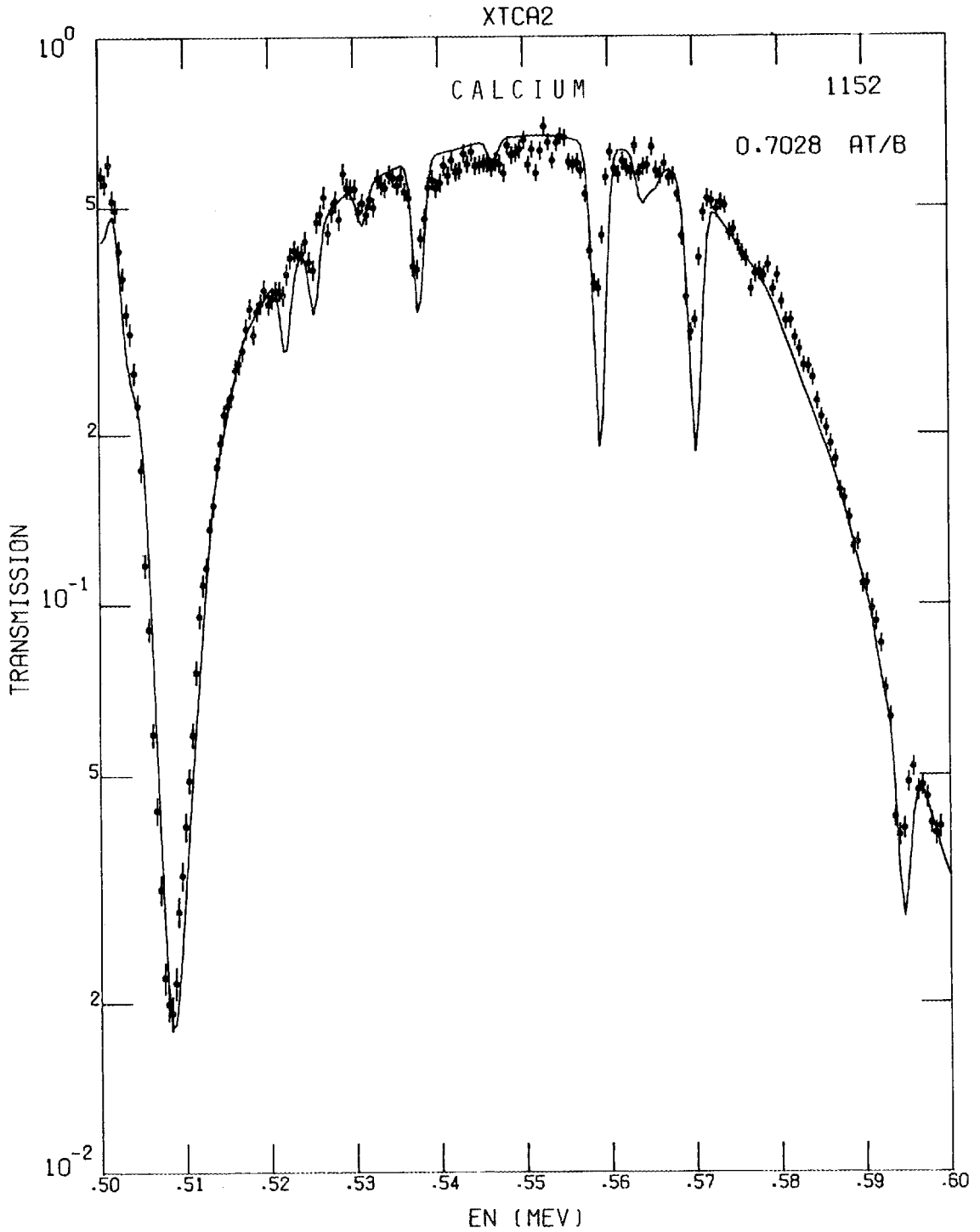
XTCA2
CALCIUM
1152
0.7028 AT/B
TRANSMISSION
EN (MEV)
10^0
5
2
10^{-1}
5
2
10^{-2}
.50
.51
.52
.53
.54
.55
.56
.57
.58
.59
.60

Figure 30

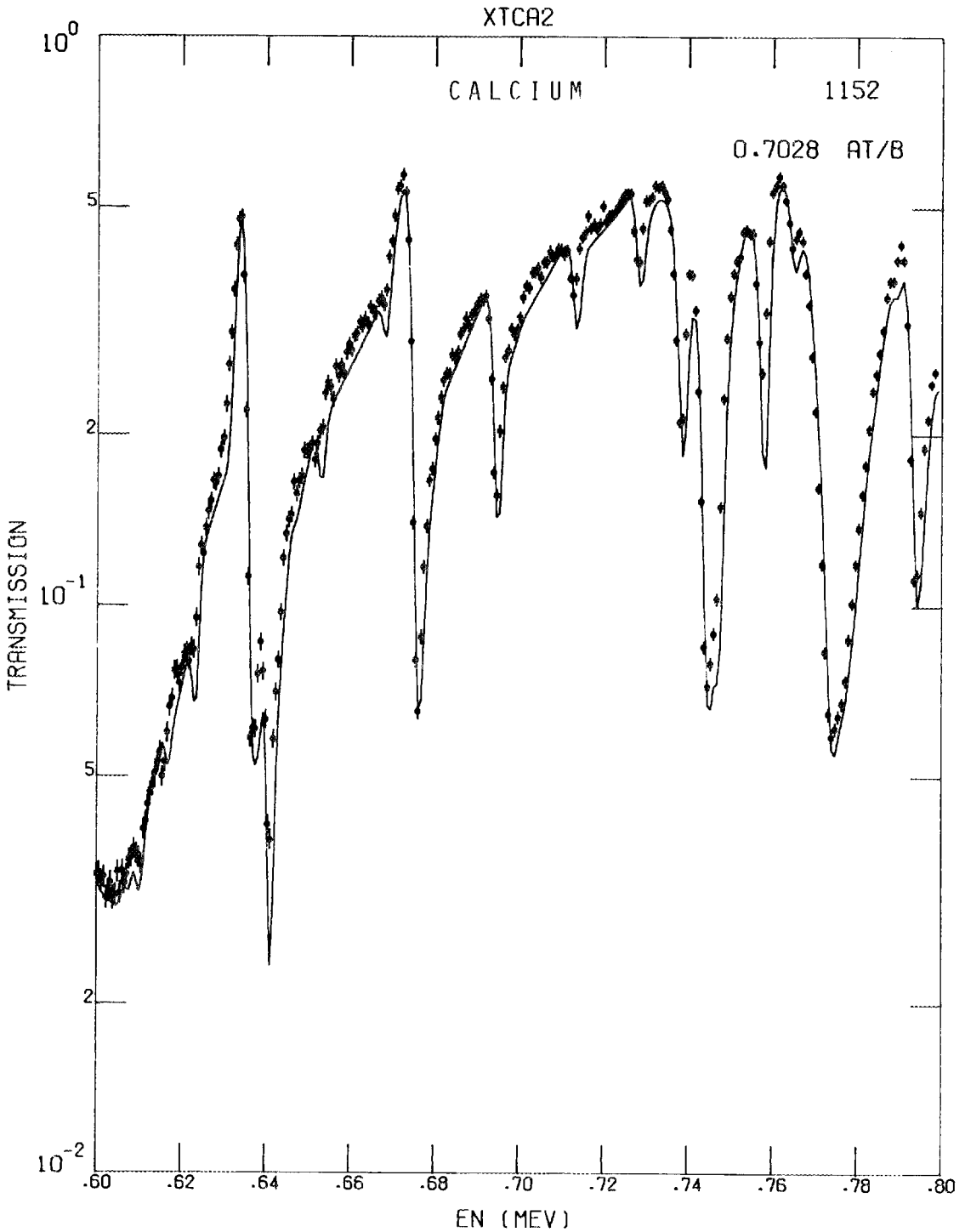
XTCA2
CALCIUM
1152
0.7028 AT/B
TRANSMISSION
EN (MEV)
10^0
5
2
10^{-1}
5
2
10^{-2}
.60
.62
.64
.66
.68
.70
.72
.74
.76
.78
.80

Figure 31

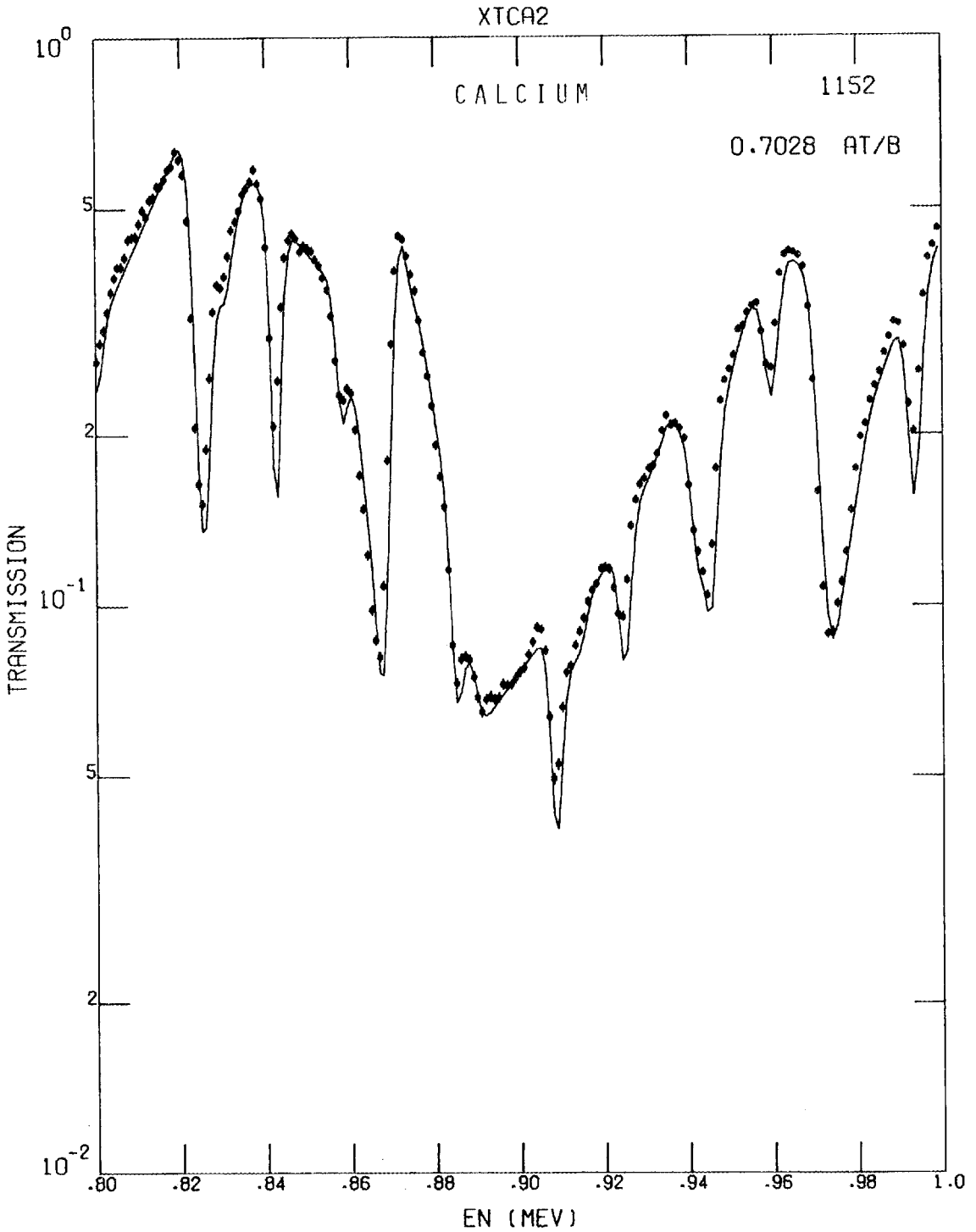
XTCA2
CALCIUM
1152
0.7028 AT/B
TRANSMISSION
EN (MEV)
10^0
5
2
10^{-1}
5
2
10^{-2}
.80
.82
.84
.86
.88
.90
.92
.94
.96
.98
1.0

Figure 32

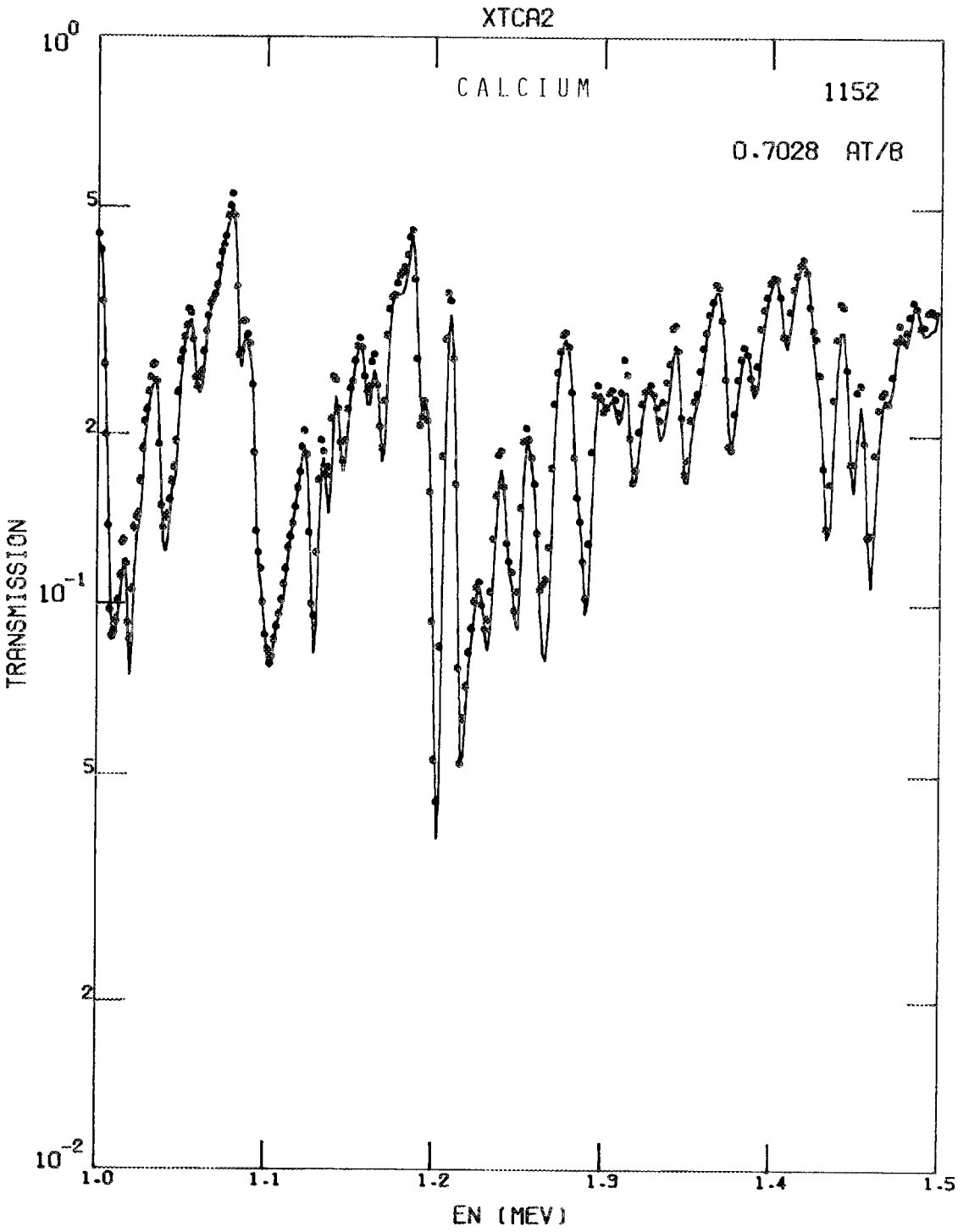
XTCA2
CALCIUM
1152
0.7028 AT/B
TRANSMISSION
EN (MEV)
10^0
5
2
10^{-1}
5
2
10^{-2}
1.0
1.1
1.2
1.3
1.4
1.5

Figure 33

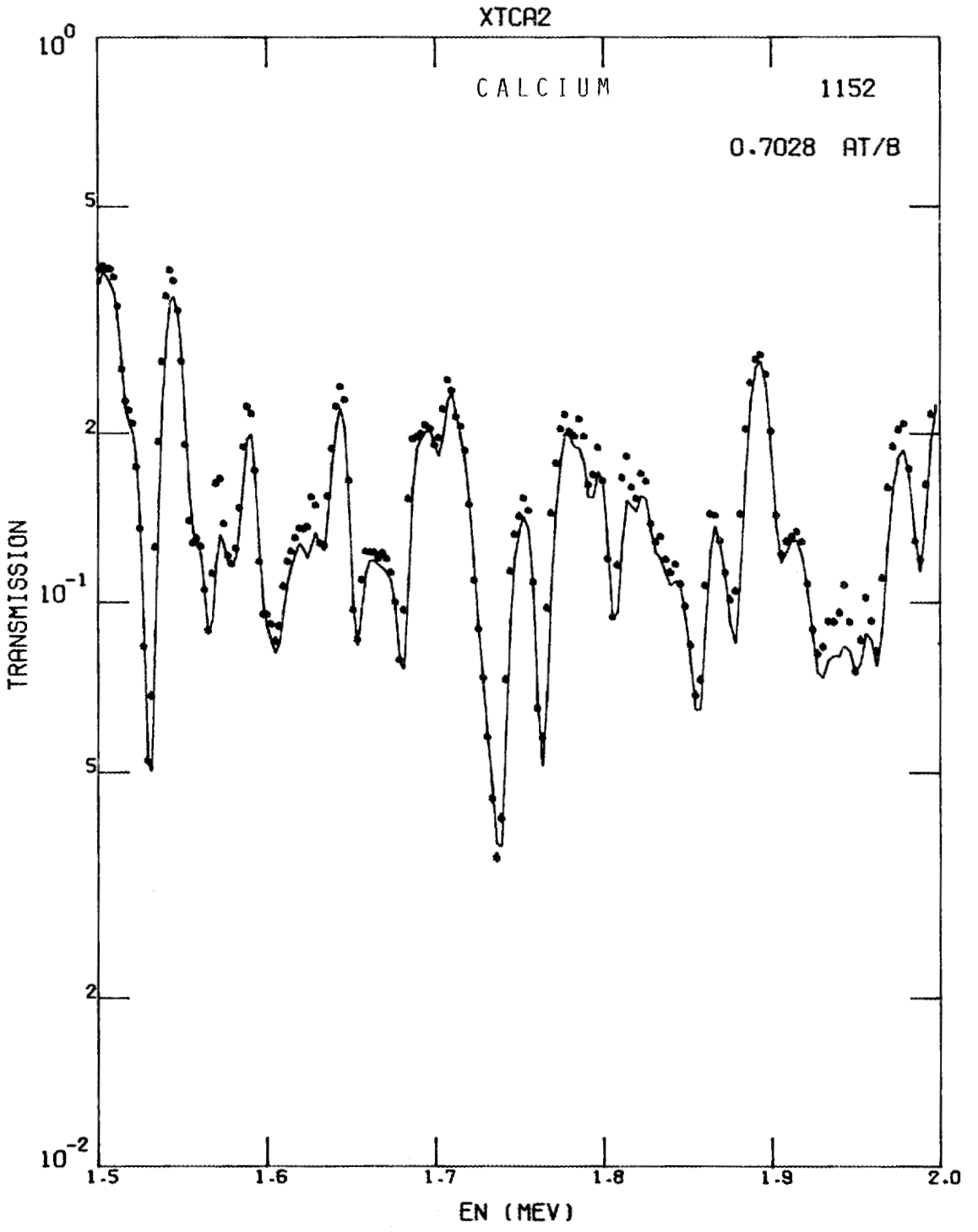
XTCA2
CALCIUM
1152
0.7028 AT/B
TRANSMISSION
EN (MEV)
10^0
5
2
10^{-1}
5
2
10^{-2}
1.5
1.6
1.7
1.8
1.9
2.0

Figure 34

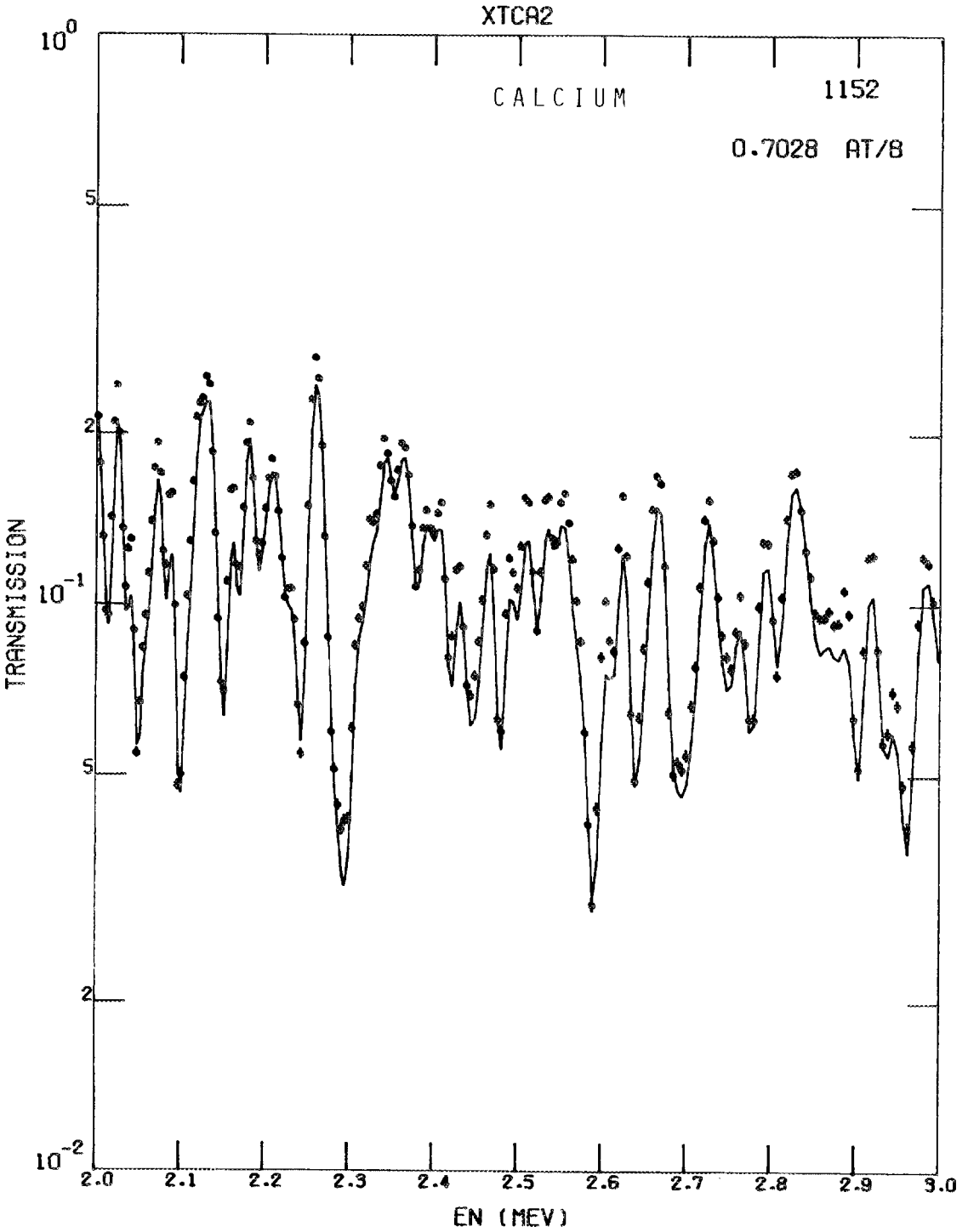
XTCA2
CALCIUM
1152
0.7028 AT/B
TRANSMISSION
EN (MEV)
10^0
5
2
10^{-1}
5
2
10^{-2}
2.0
2.1
2.2
2.3
2.4
2.5
2.6
2.7
2.8
2.9
3.0

Figure 35

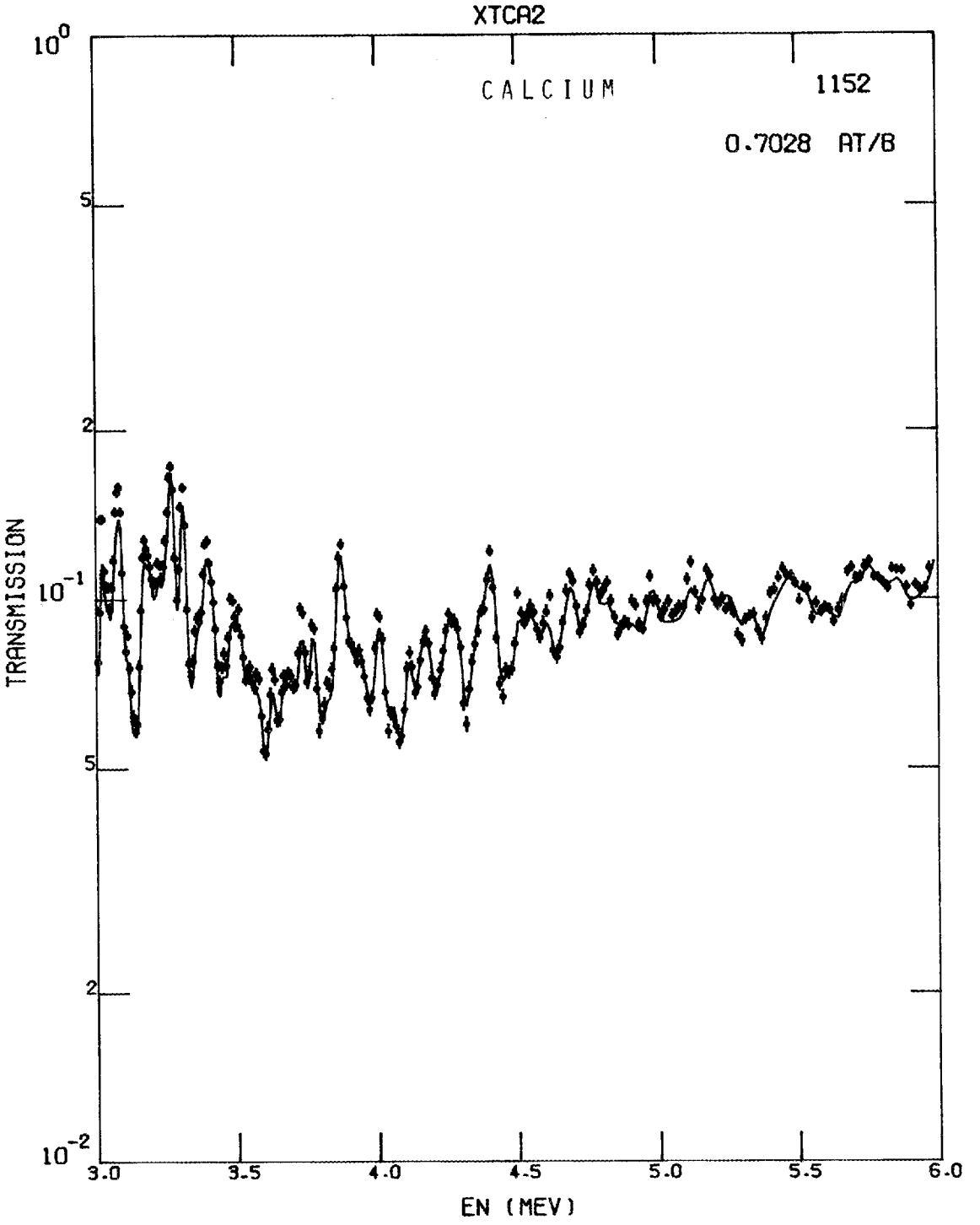
XTCA2
CALCIUM
1152
0.7028 AT/B
TRANSMISSION
EN (MEV)
10^0
5
2
10^{-1}
5
2
10^{-2}
3.0
3.5
4.0
4.5
5.0
5.5
6.0

Figure 36

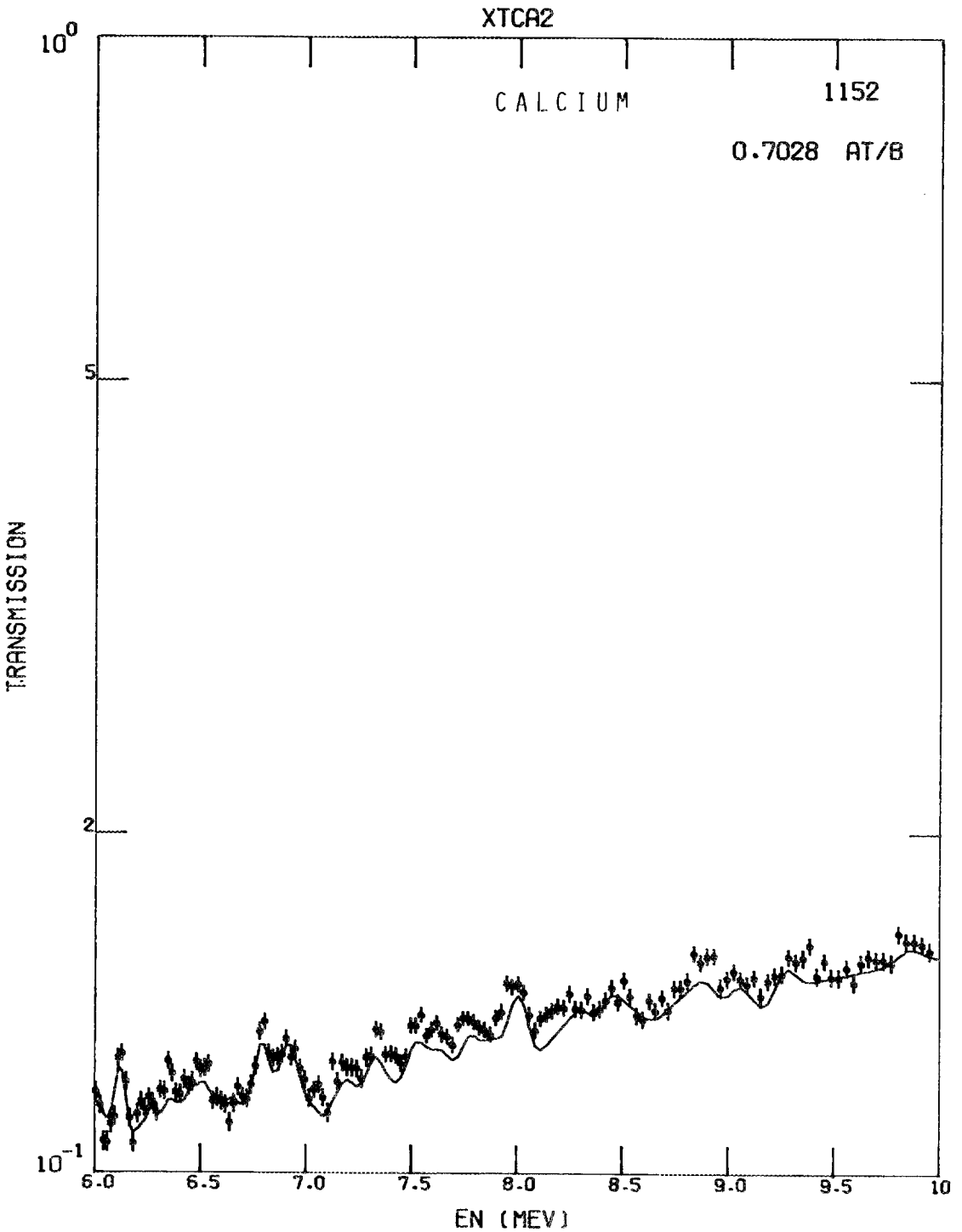
XTCA2
CALCIUM
1152
0.7028 AT/B
TRANSMISSION
EN (MEV)
10^0
5
2
10^-1
6.0
6.5
7.0
7.5
8.0
8.5
9.0
9.5
10

Figure 37

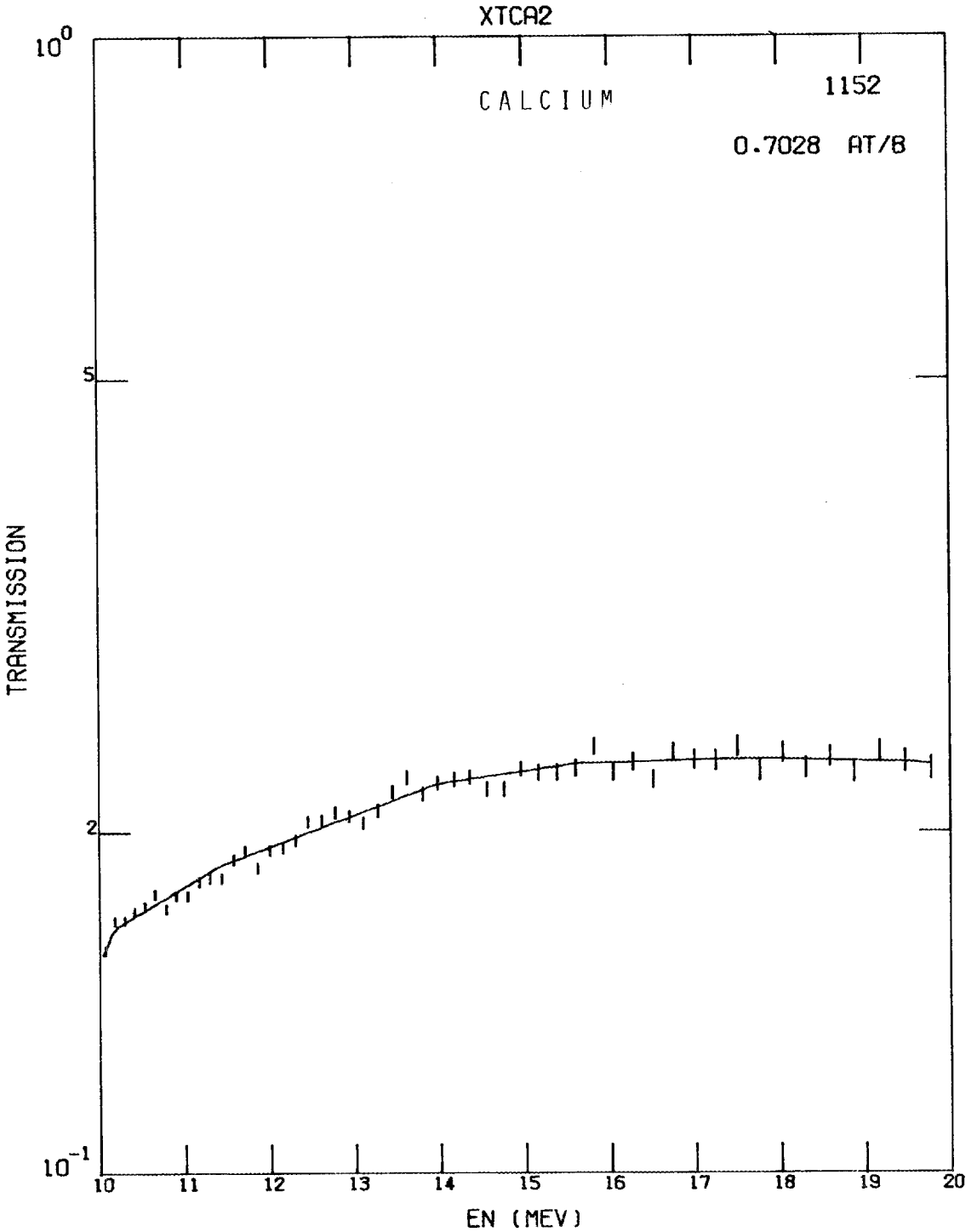
XTCA2
CALCIUM
1152
0.7028 AT/B
TRANSMISSION
EN (MEV)
10^0
5
2
10^-1
10
11
12
13
14
15
16
17
18
19
20

Figure 38

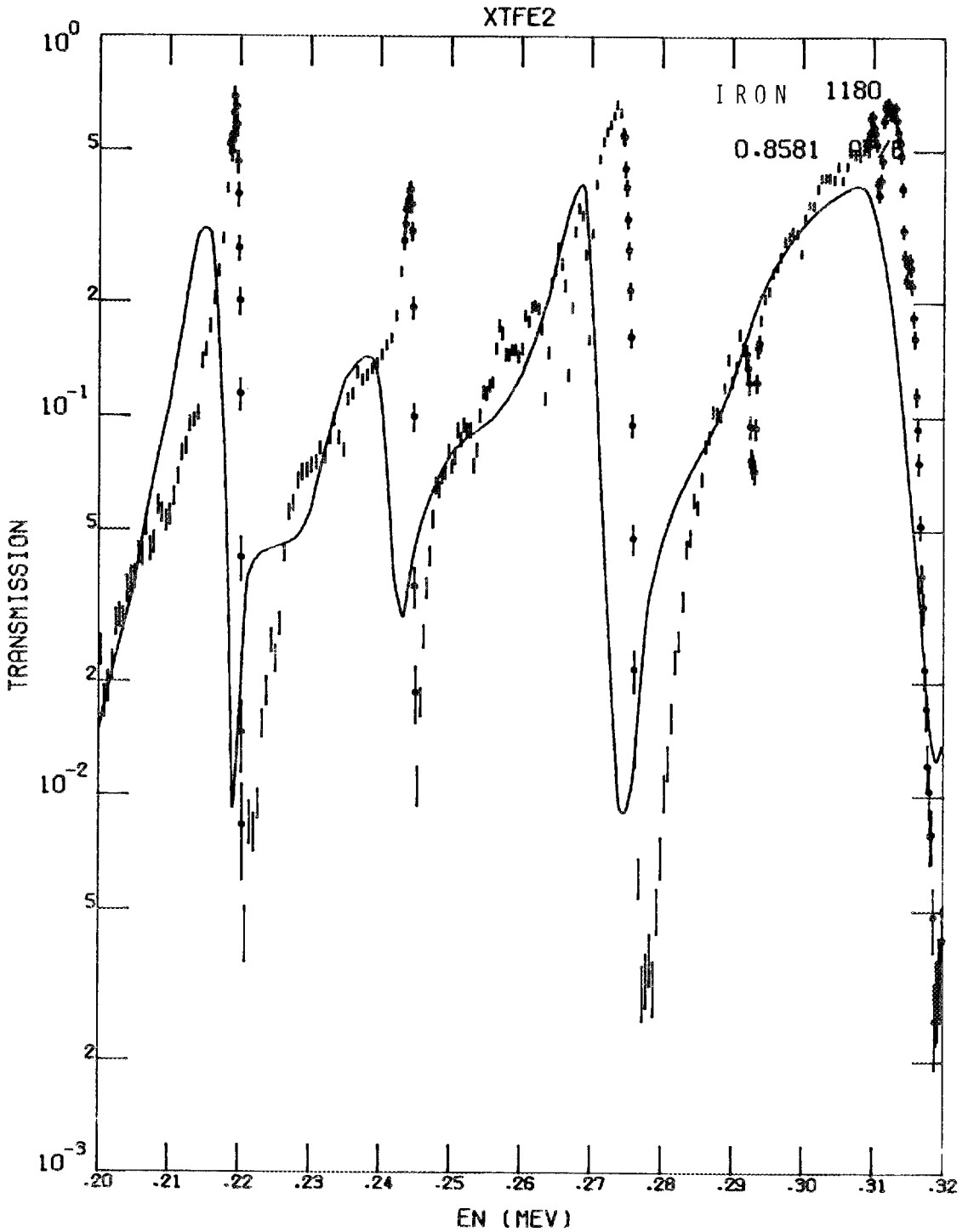
XTFE2
IRON 1180
0.8581 GM/C
TRANSMISSION
EN (MEV)
10^0
5
2
10^-1
5
2
10^-2
5
2
10^-3
.20
.21
.22
.23
.24
.25
.26
.27
.28
.29
.30
.31
.32

Figure 39

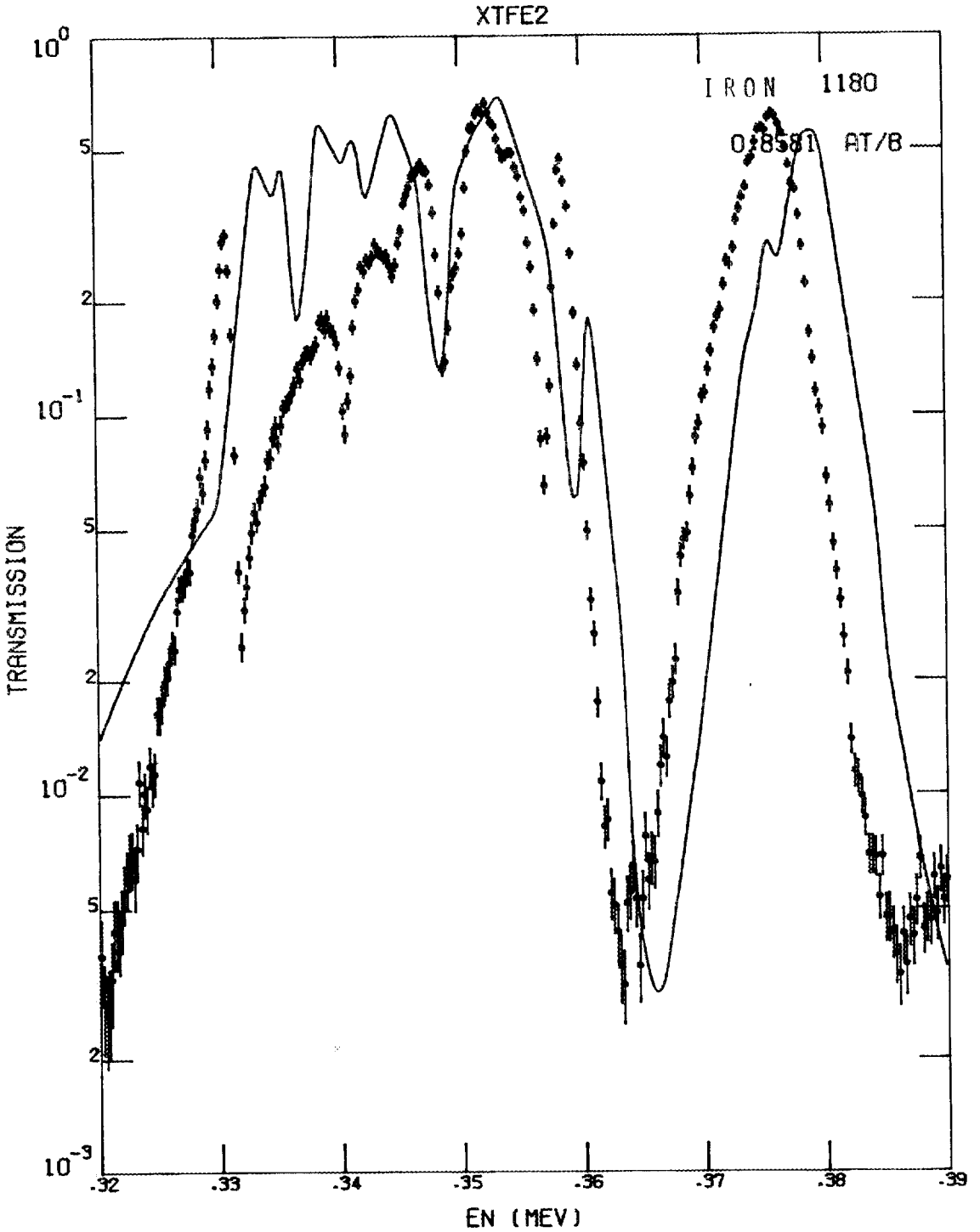
XTFE2
IRON 1180
0.8581 AT/B
TRANSMISSION
EN (MEV)
10^0
5
2
10^{-1}
5
2
10^{-2}
5
2
10^{-3}
.32
.33
.34
.35
.36
.37
.38
.39

Figure 40

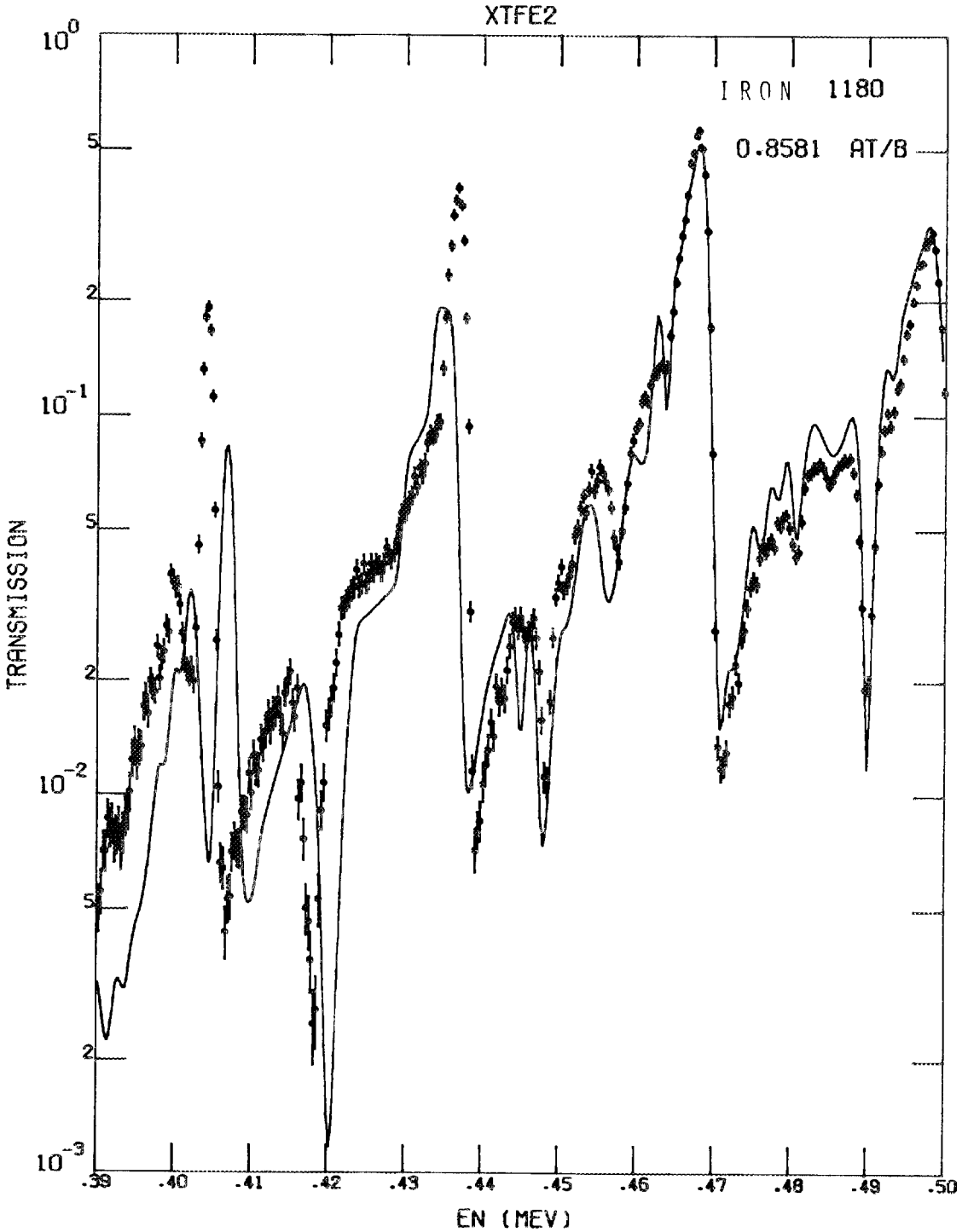
XTFE2
IRON 1180
0.8581 AT/B
TRANSMISSION
EN (MEV)
10^0
5
2
10^{-1}
5
2
10^{-2}
5
2
10^{-3}
.39
.40
.41
.42
.43
.44
.45
.46
.47
.48
.49
.50

Figure 41

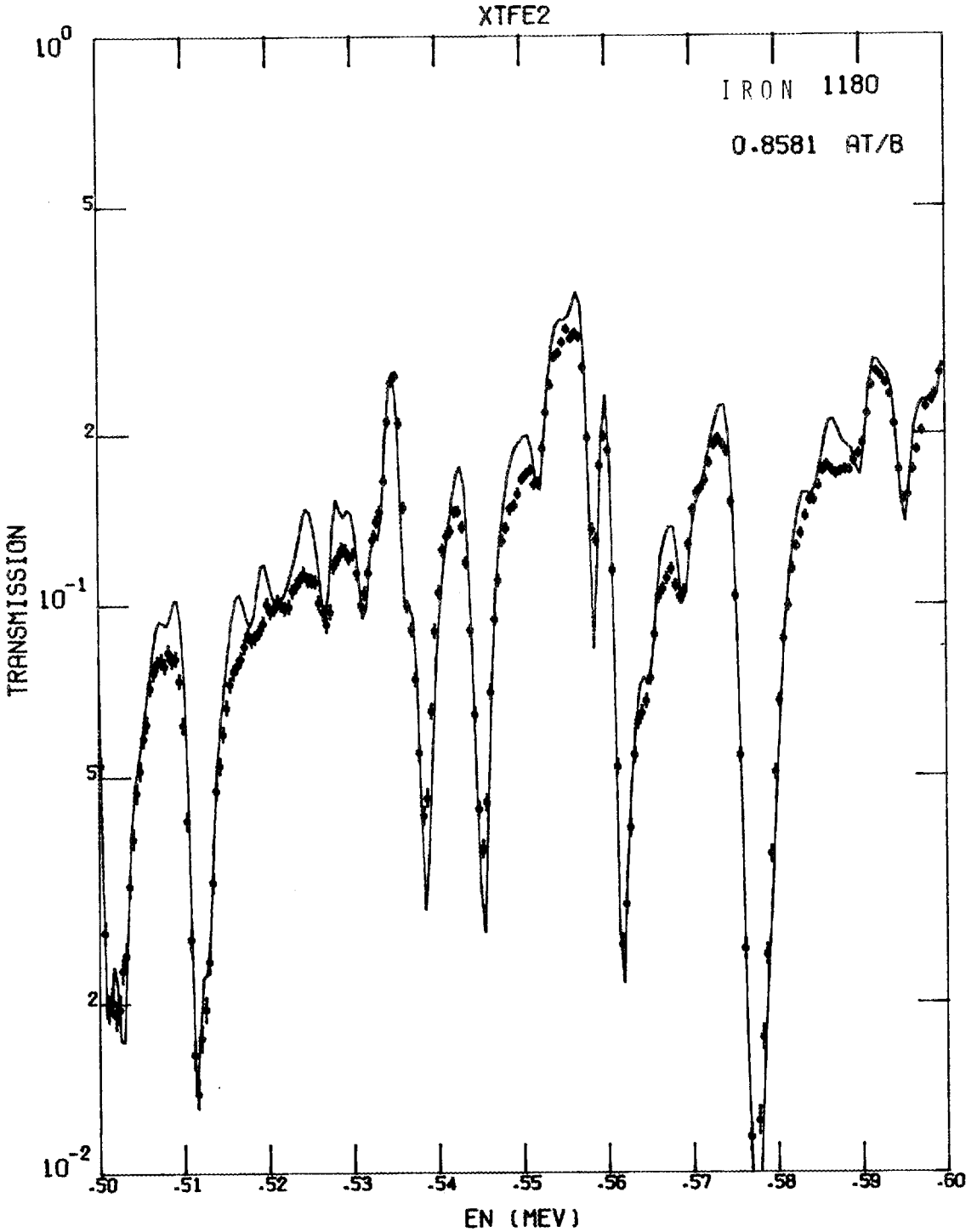
XTFE2
IRON 1180
0.8581 AT/B
TRANSMISSION
EN (MEV)
10^0
5
2
10^{-1}
5
2
10^{-2}
.50
.51
.52
.53
.54
.55
.56
.57
.58
.59
.60

Figure 42

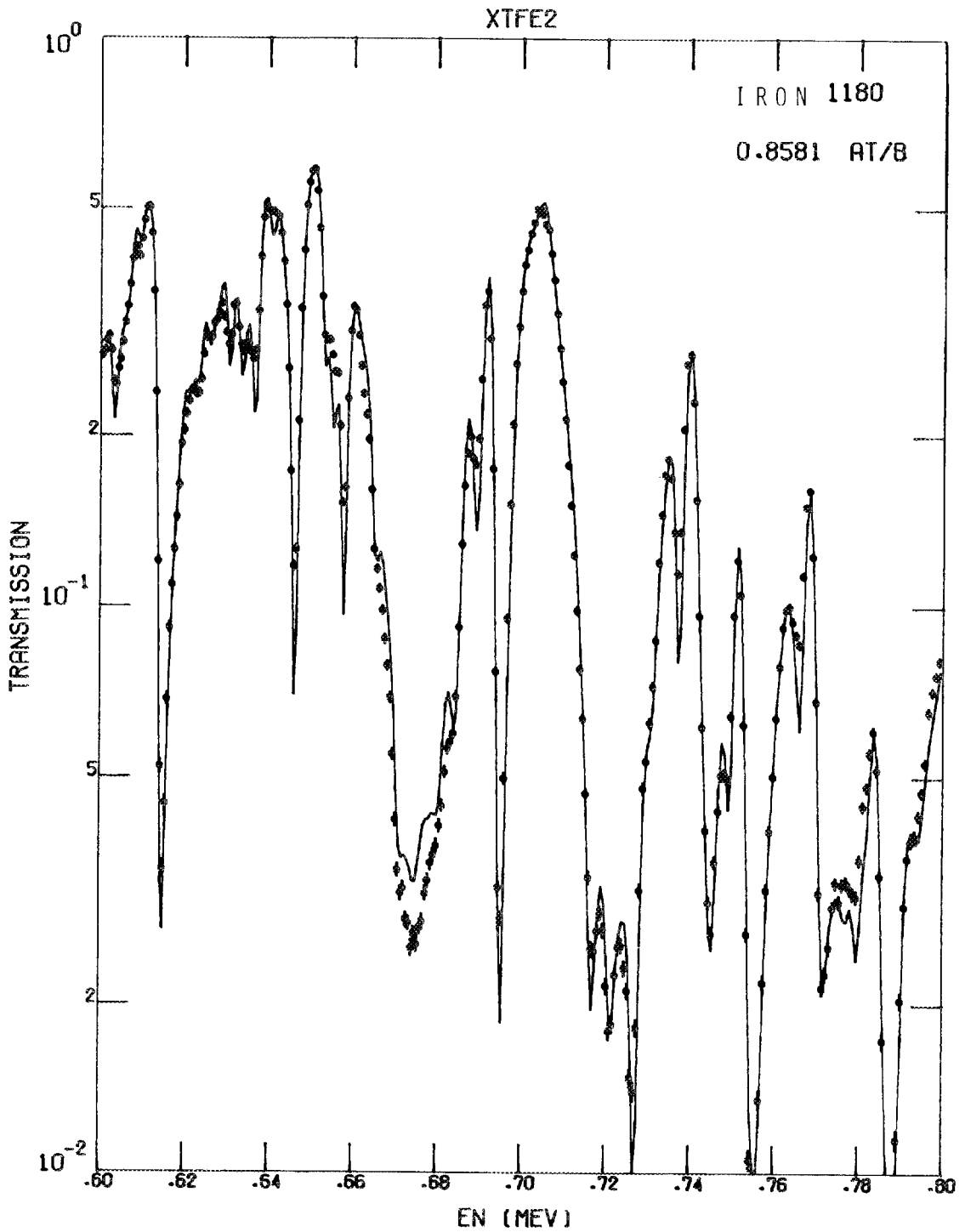
XTFE2
IRON 1180
0.8581 AT/B
TRANSMISSION
EN (MEV)
10^0
5
2
10^{-1}
5
2
10^{-2}
.60
.62
.64
.66
.68
.70
.72
.74
.76
.78
.80

Figure 43

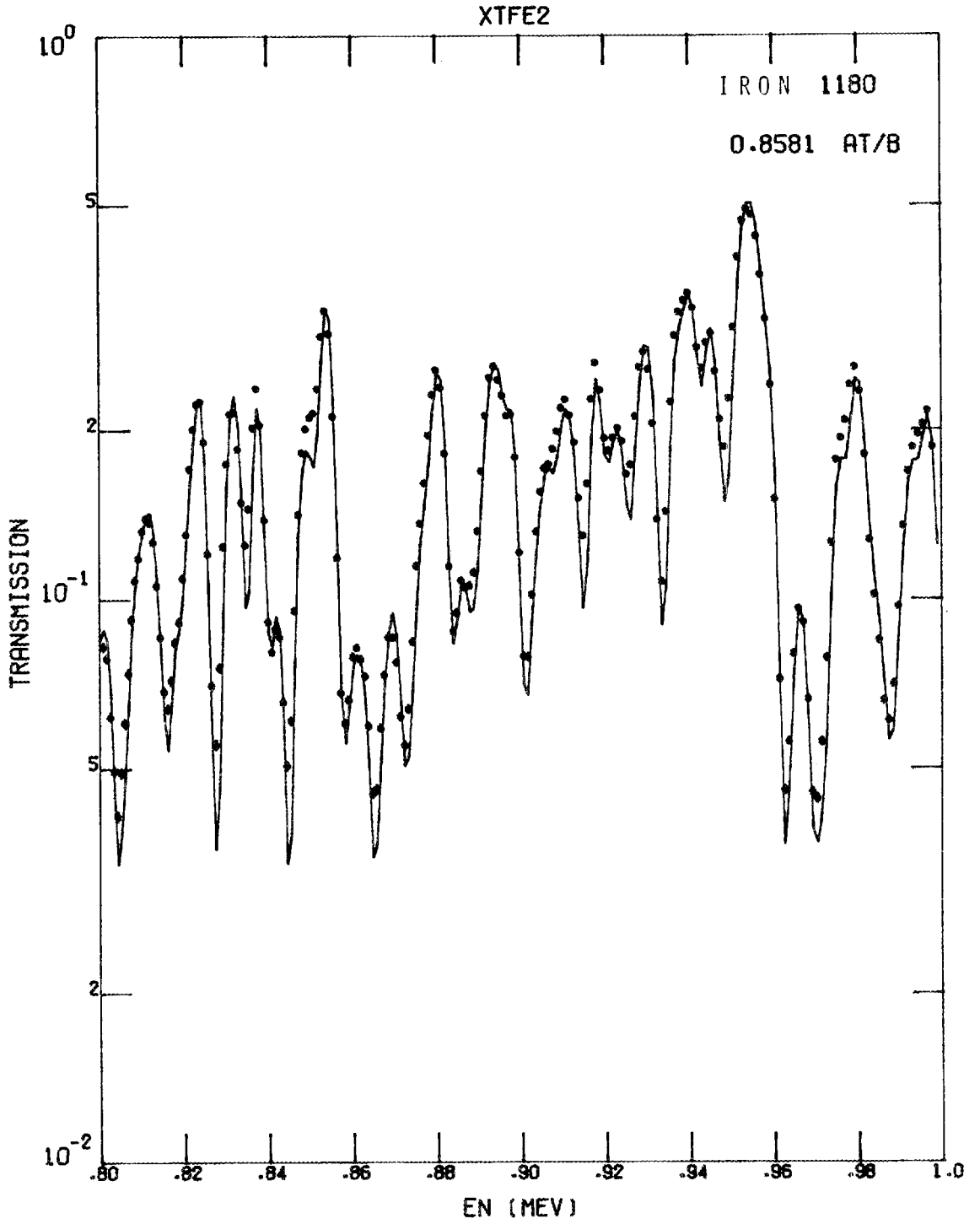
XTFE2
IRON 1180
0.8581 AT/B
TRANSMISSION
EN (MEV)
10^0
5
2
10^{-1}
5
2
10^{-2}
.80
.82
.84
.86
.88
.90
.92
.94
.96
.98
1.0

Figure 44

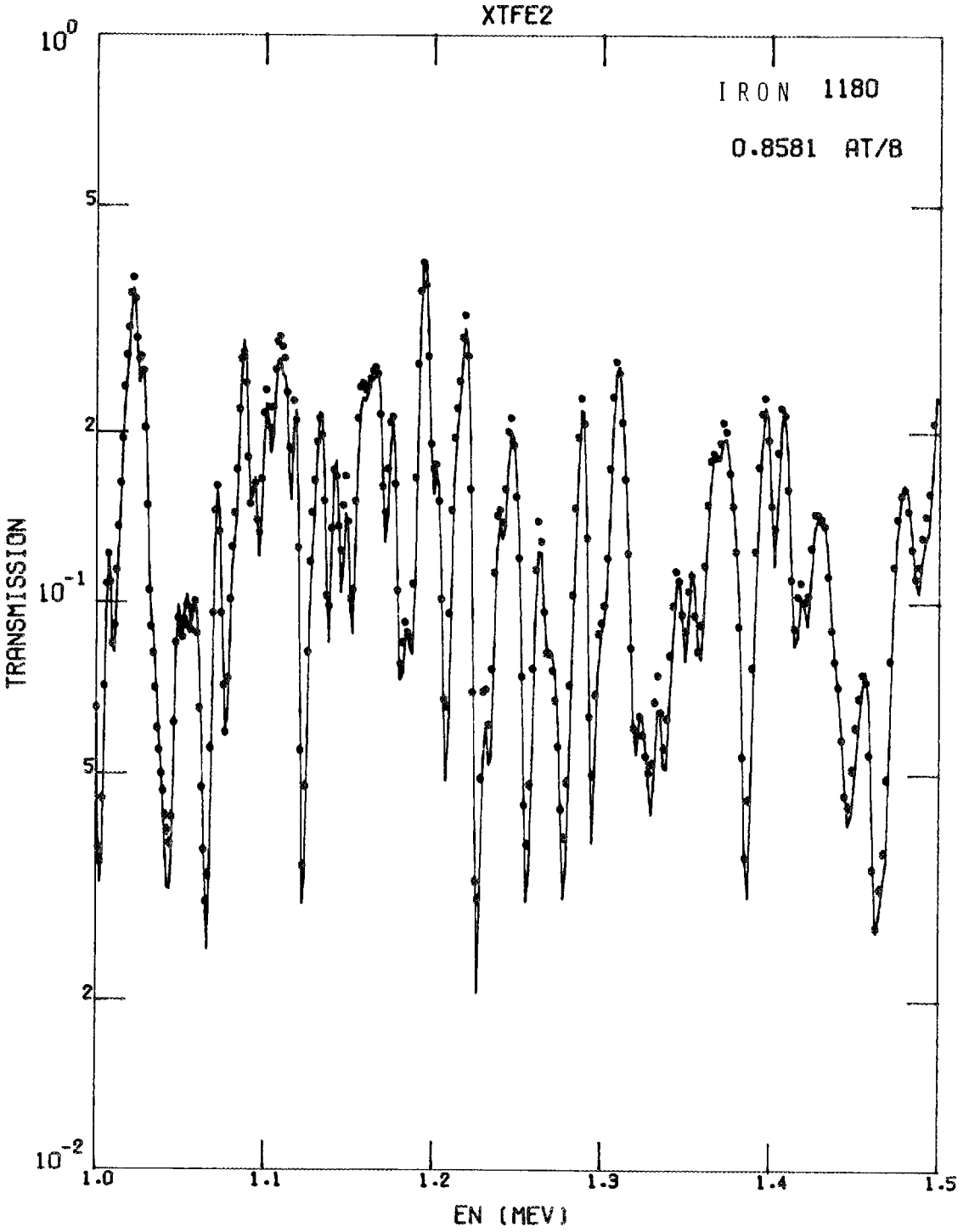
XTFE2
IRON 1180
0.8581 AT/B
TRANSMISSION
EN (MEV)
10^0
5
2
10^{-1}
5
2
10^{-2}
1.0
1.1
1.2
1.3
1.4
1.5

Figure 45

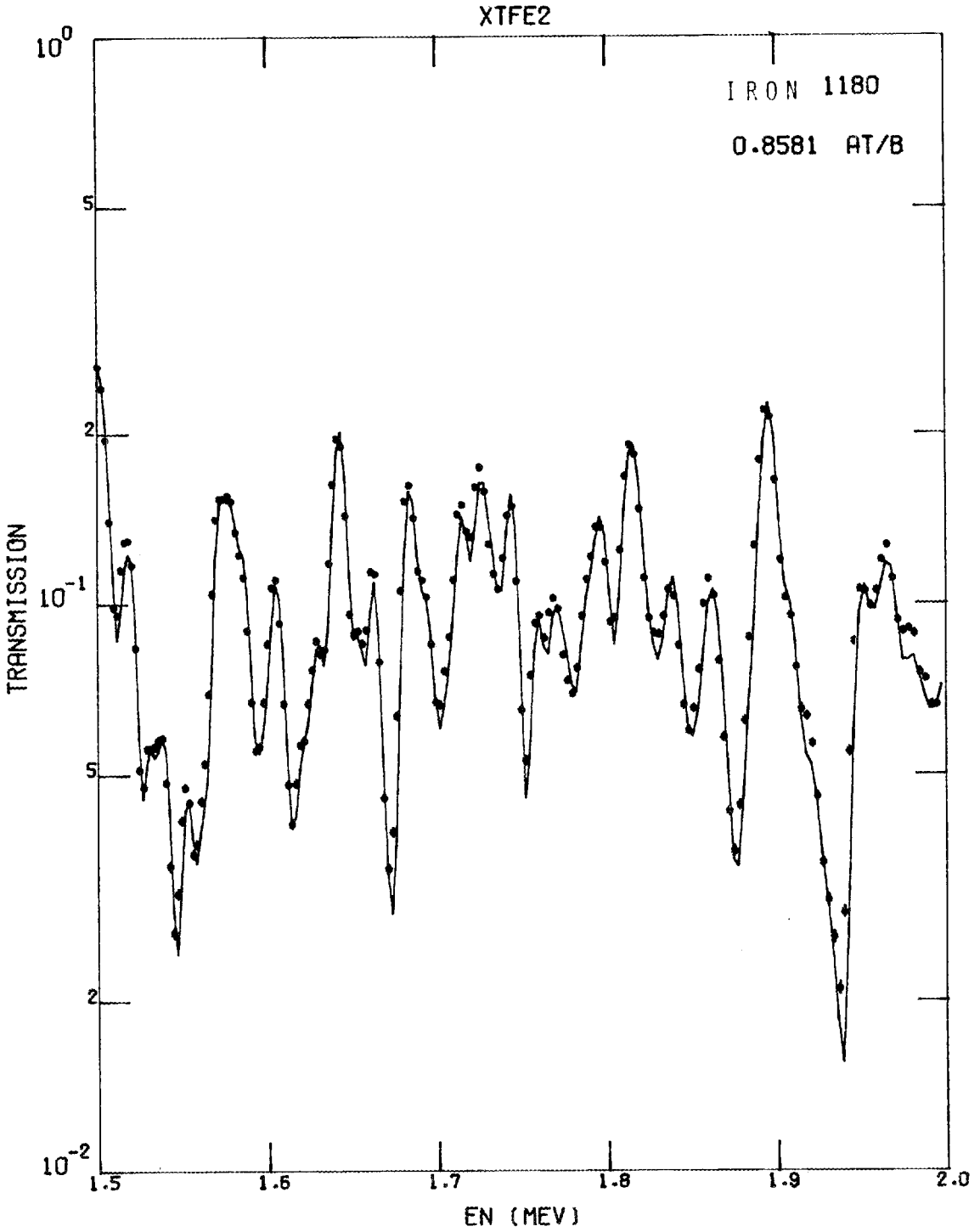
XTFE2
IRON 1180
0.8581 AT/B
TRANSMISSION
EN (MEV)
10^0
5
2
10^-1
5
2
10^-2
1.5
1.6
1.7
1.8
1.9
2.0

Figure 46

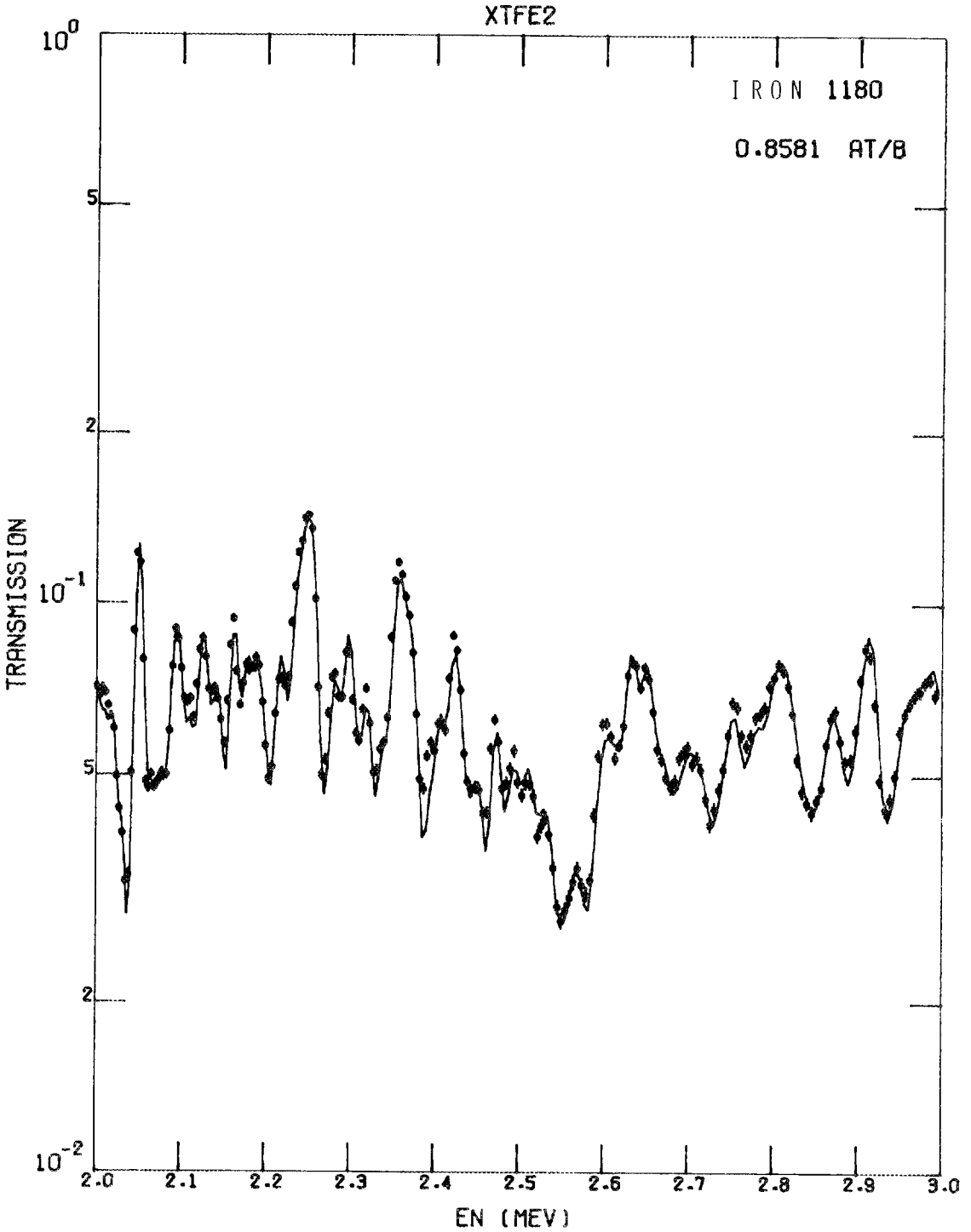
XTFE2
IRON 1180
0.8581 AT/B
TRANSMISSION
EN (MEV)
10^0
5
2
10^{-1}
5
2
10^{-2}
2.0
2.1
2.2
2.3
2.4
2.5
2.6
2.7
2.8
2.9
3.0

Figure 47

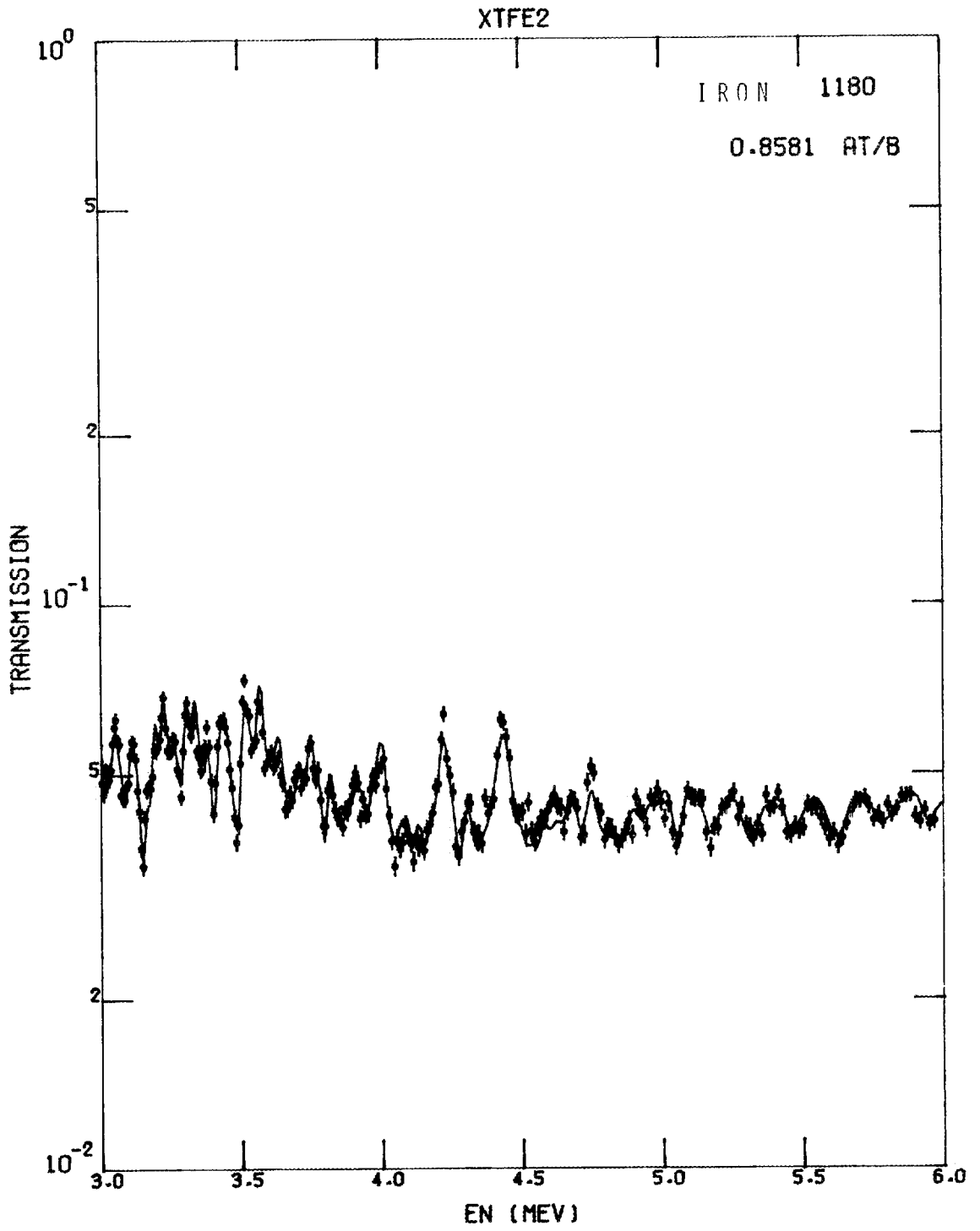
XTFE2
IRON 1180
0.8581 AT/B
TRANSMISSION
EN (MEV)
10^0
5
2
10^-1
5
2
10^-2
3.0
3.5
4.0
4.5
5.0
5.5
6.0

Figure 48

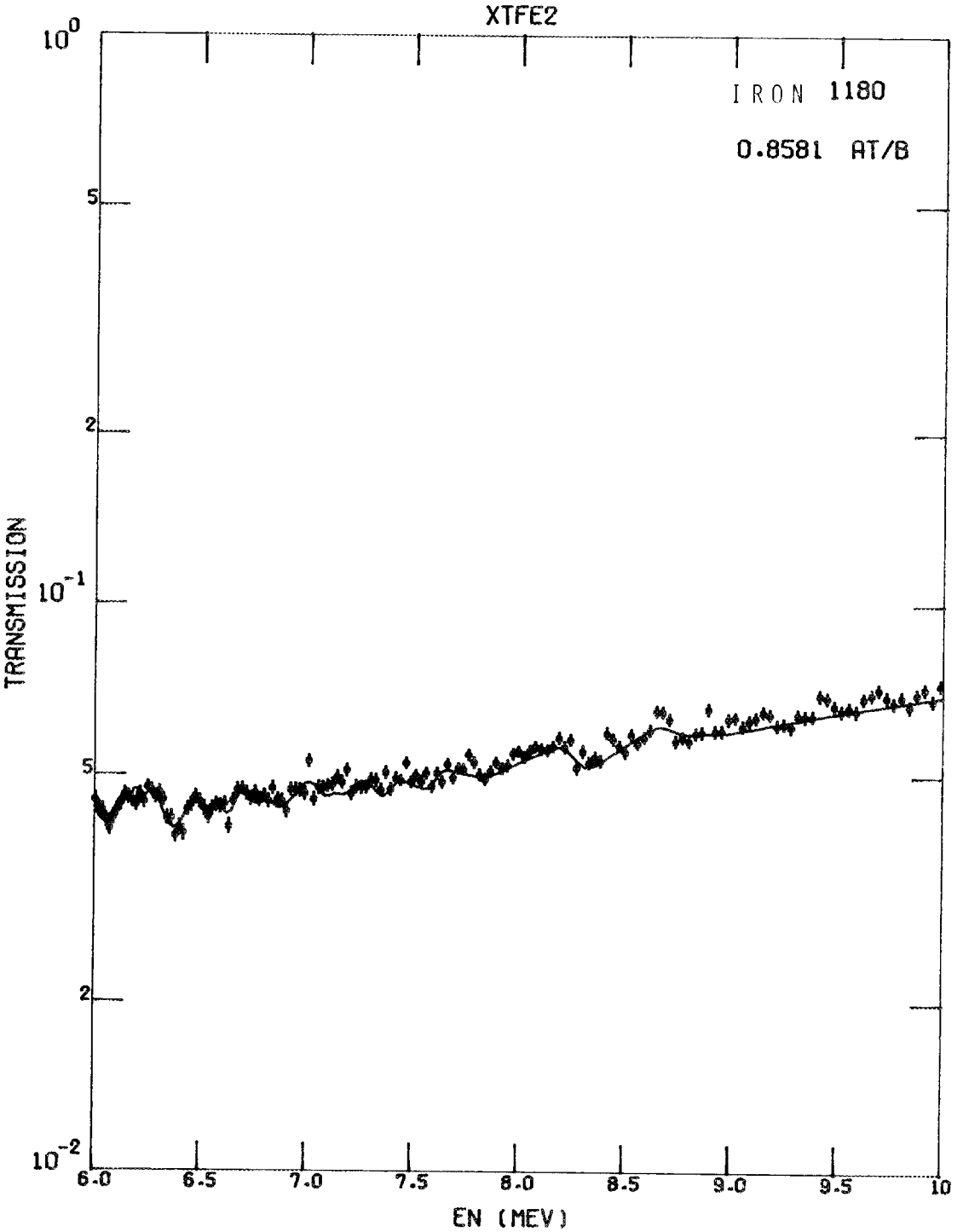
XTFE2
IRON 1180
0.8581 AT/B
TRANSMISSION
EN (MEV)
10^0
5
2
10^-1
5
2
10^-2
6.0
6.5
7.0
7.5
8.0
8.5
9.0
9.5
10

Figure 49

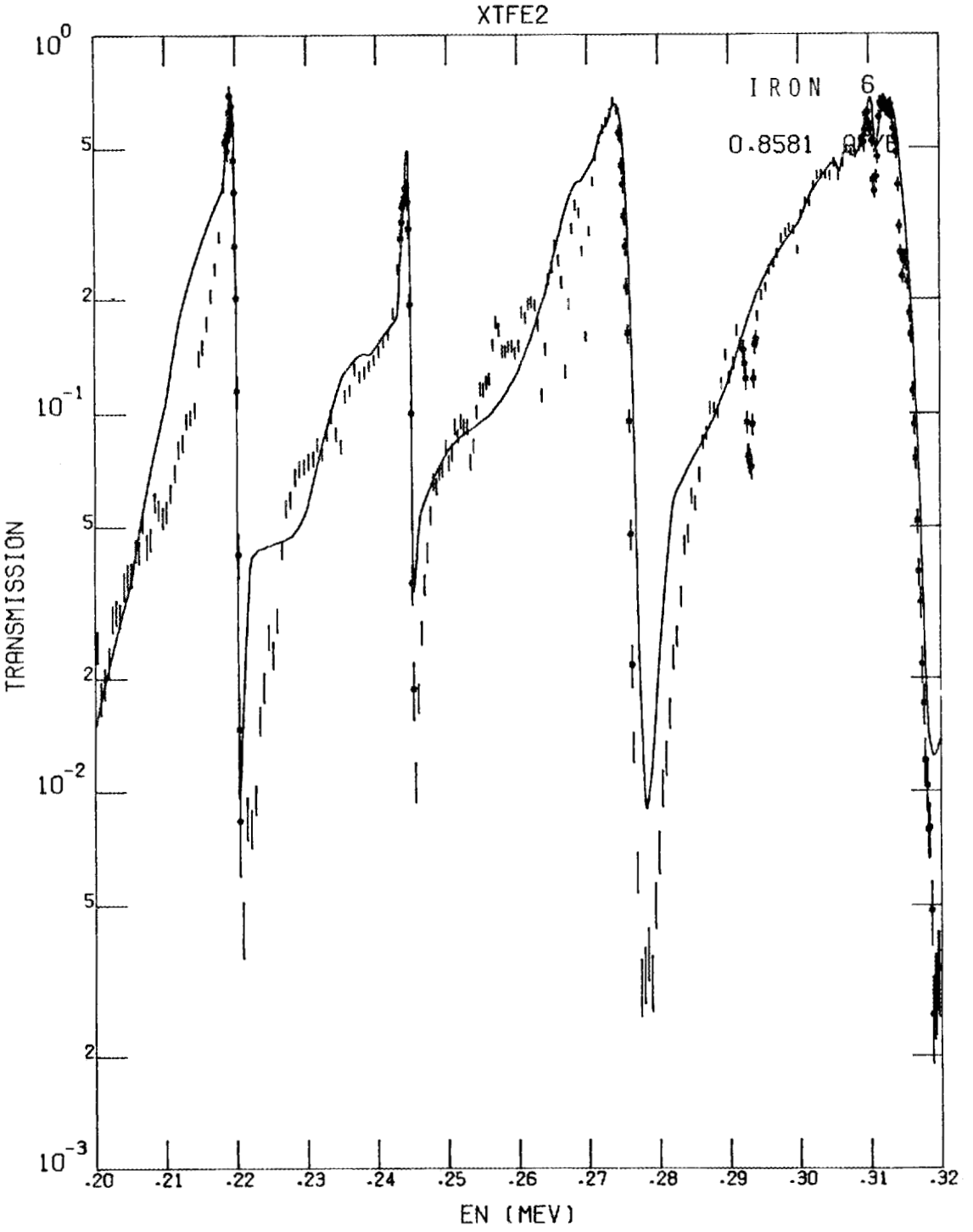
XTFE2
IRON 6
0.8581 GMCM
TRANSMISSION
EN (MEV)
10^0
5
2
10^{-1}
5
2
10^{-2}
5
2
10^{-3}
.20
.21
.22
.23
.24
.25
.26
.27
.28
.29
.30
.31
.32

Figure 50

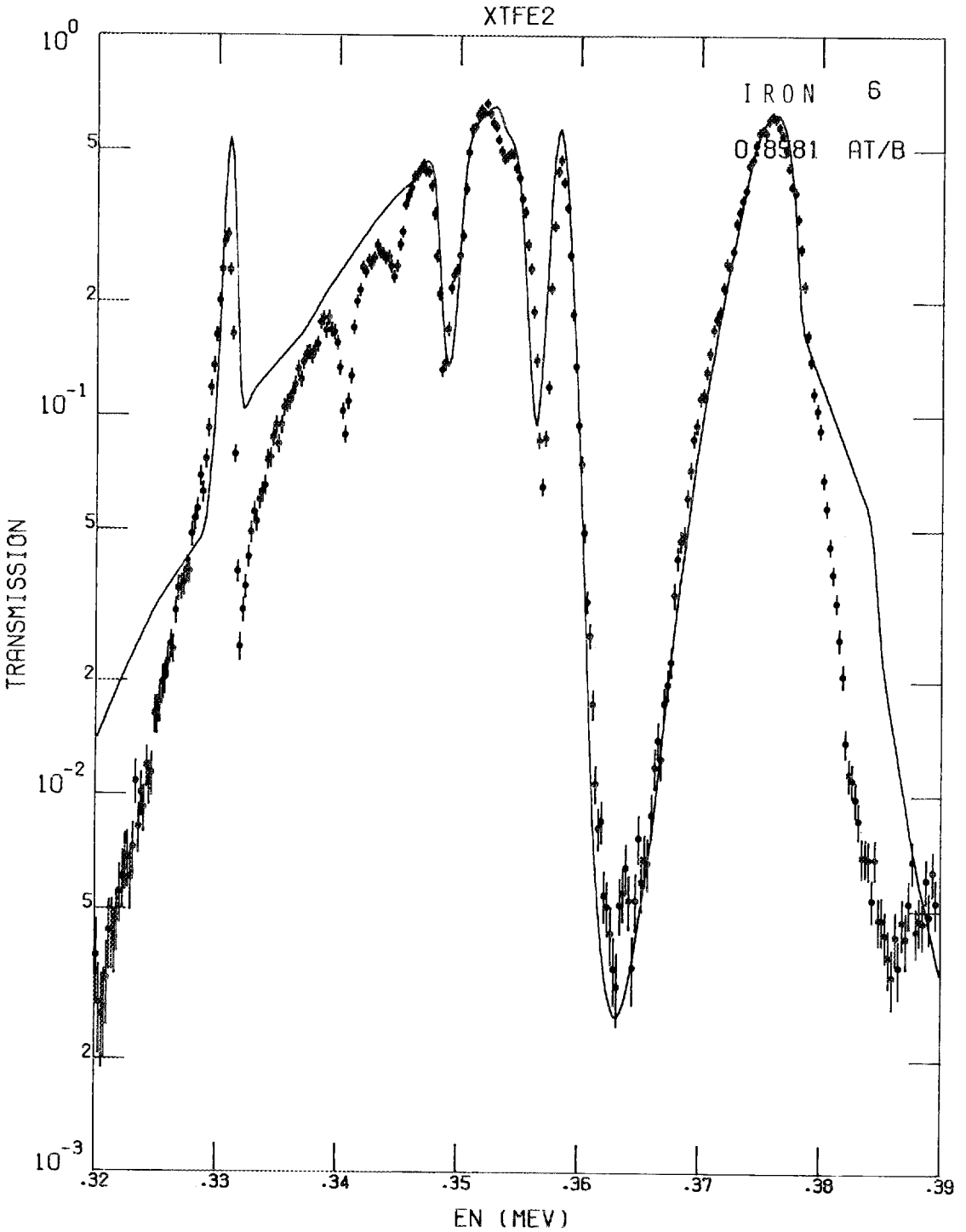
XTFE2
IRON 6
0.8581 AT/B
TRANSMISSION
EN (MEV)
10^0
5
2
10^{-1}
5
2
10^{-2}
5
2
10^{-3}
.32
.33
.34
.35
.36
.37
.38
.39

Figure 51

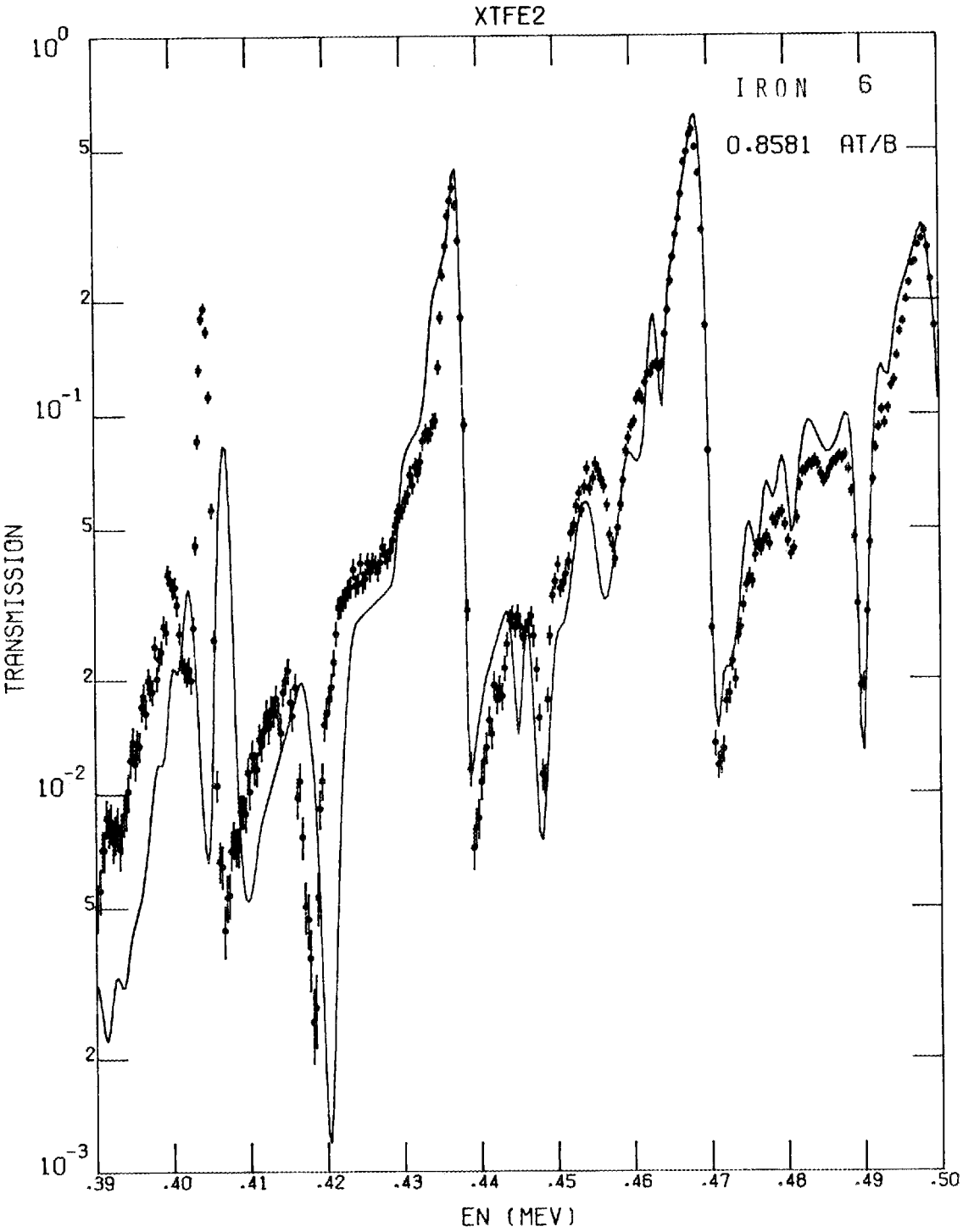
XTFE2
IRON 6
0.8581 AT/B
TRANSMISSION
EN (MEV)
10^0
5
2
10^{-1}
5
2
10^{-2}
5
2
10^{-3}
.39
.40
.41
.42
.43
.44
.45
.46
.47
.48
.49
.50

Figure 52

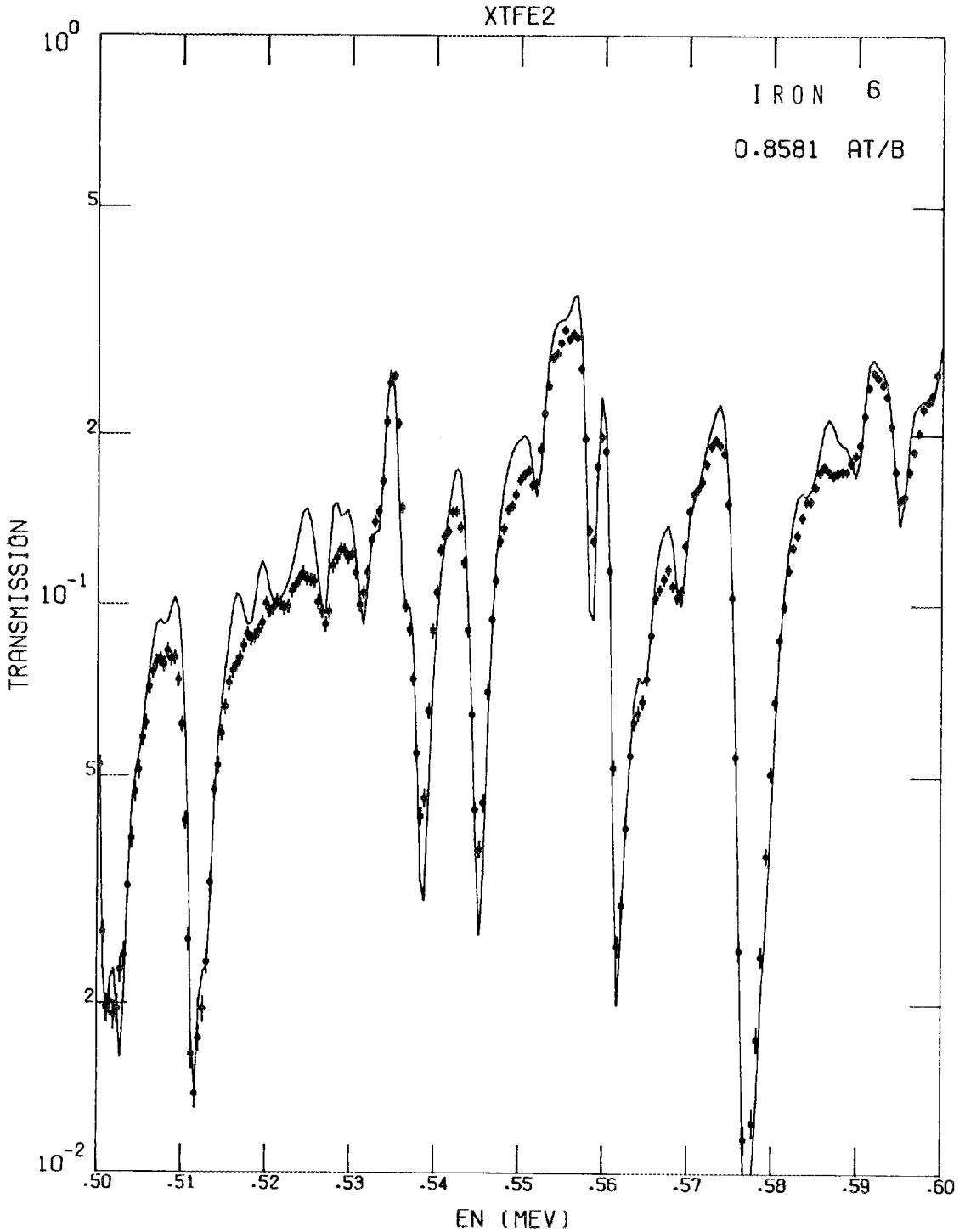
XTFE2
IRON 6
0.8581 AT/B
TRANSMISSION
EN (MEV)
10^0
5
2
10^{-1}
5
2
10^{-2}
.50
.51
.52
.53
.54
.55
.56
.57
.58
.59
.60

Figure 53

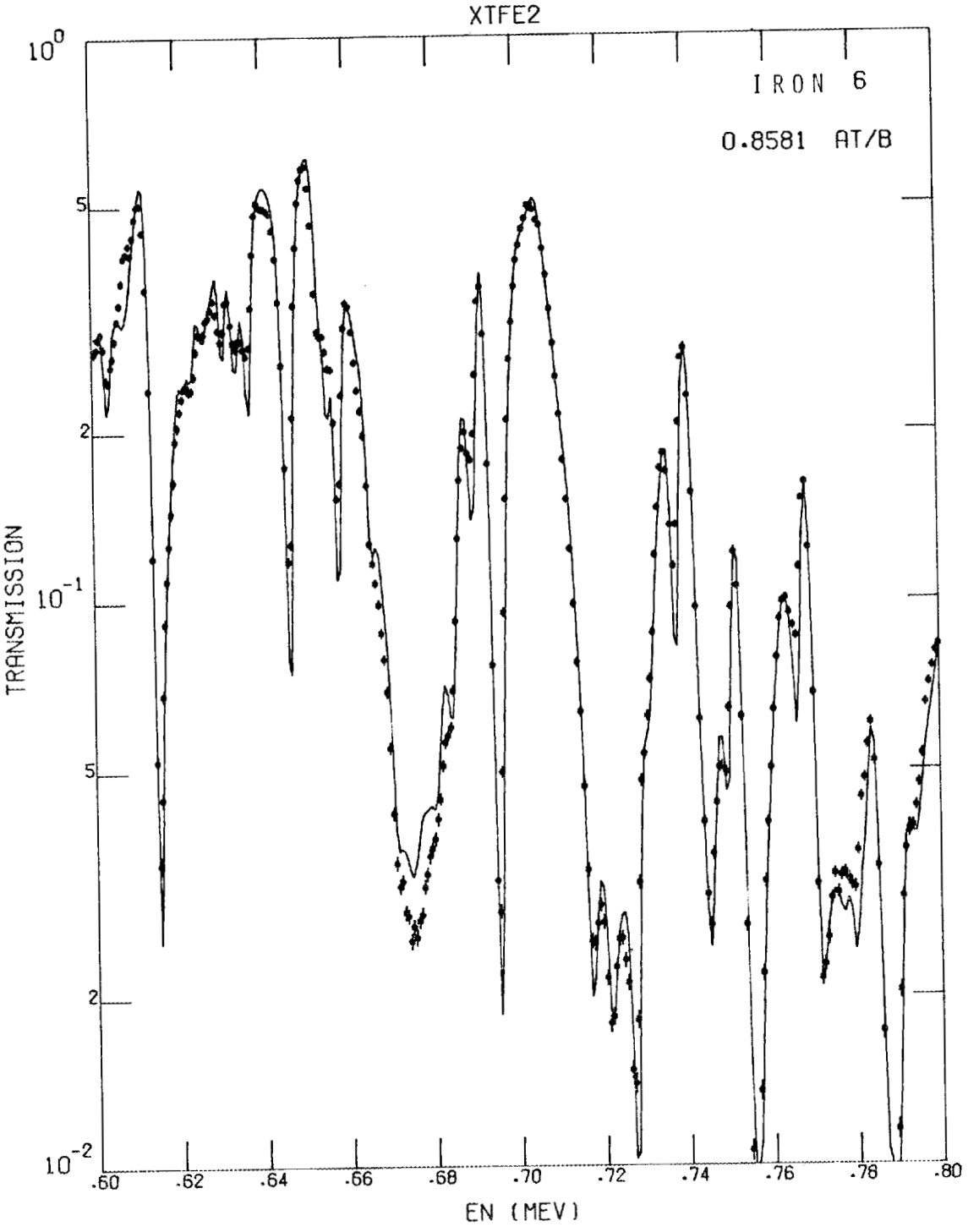
XTFE2
IRON 6
0.8581 AT/B
TRANSMISSION
EN (MEV)
10^0
5
2
10^{-1}
5
2
10^{-2}
.60
.62
.64
.66
.68
.70
.72
.74
.76
.78
.80

Figure 54

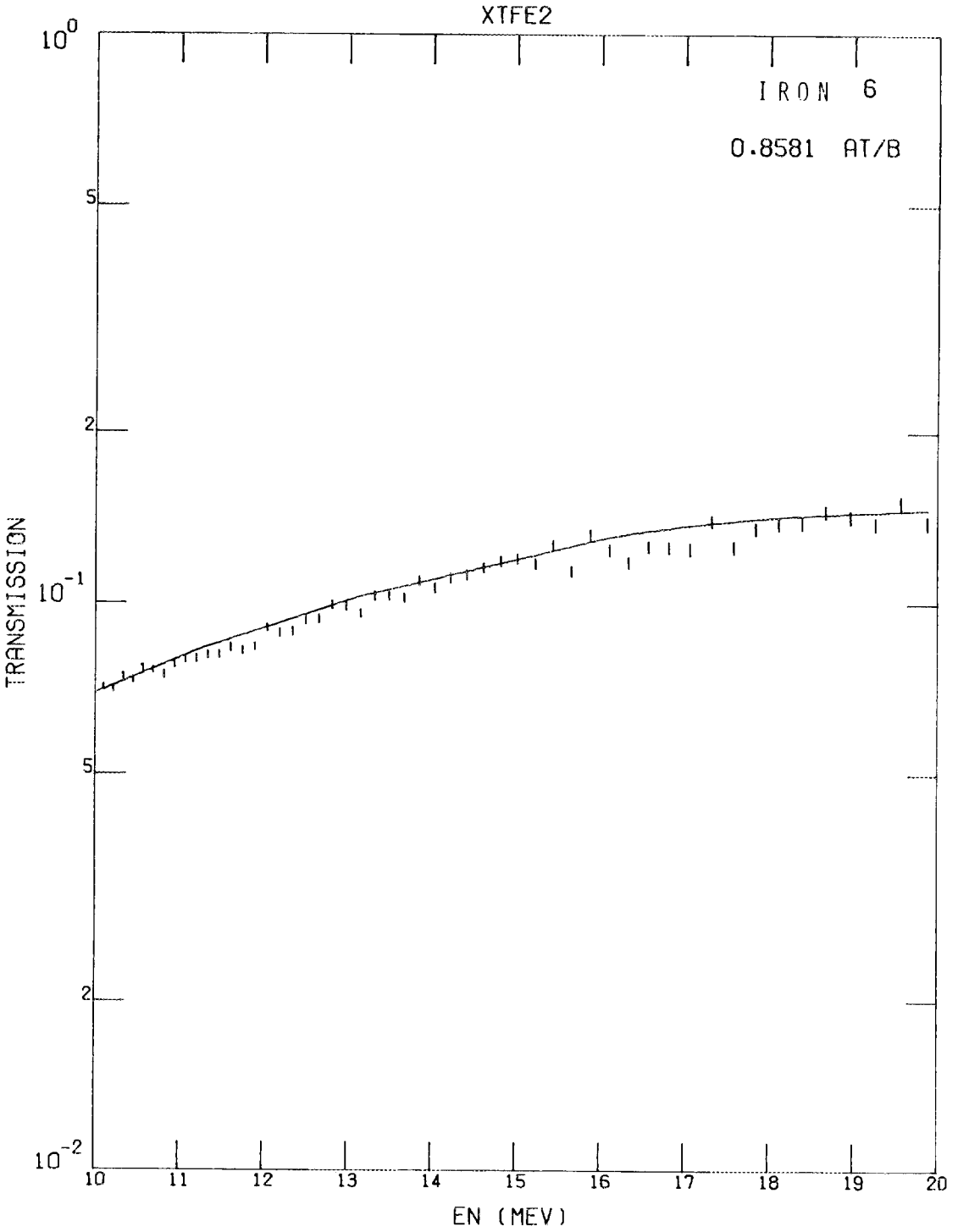
XTFE2
IRON 6
0.8581 AT/B
TRANSMISSION
EN (MEV)
10^0
5
2
10^-1
5
2
10^-2
10
11
12
13
14
15
16
17
18
19
20

Figure 55

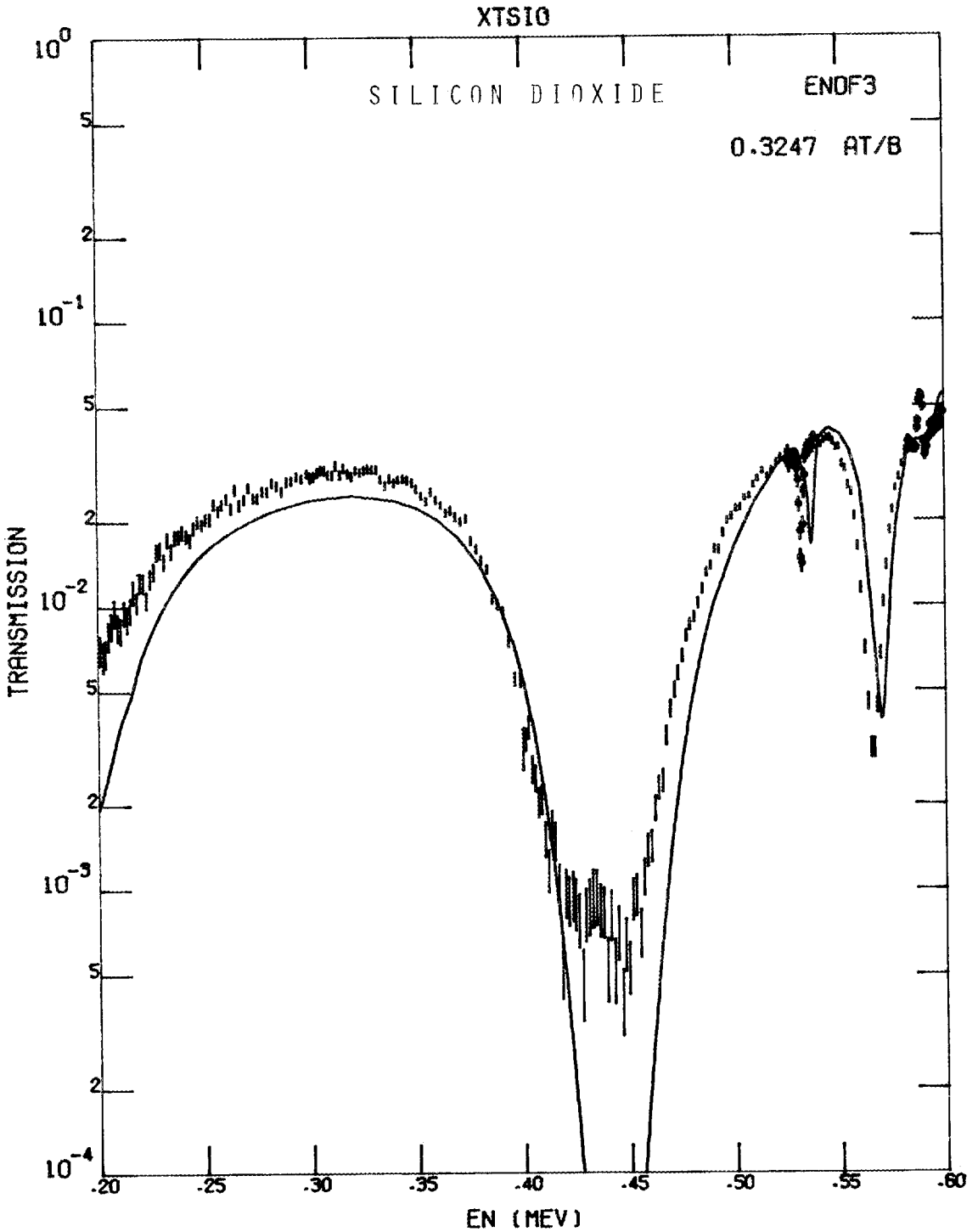
XTSIO
SILICON DIOXIDE
ENDF3
0.3247 AT/B
TRANSMISSION
EN (MEV)
10^0
10^{-1}
10^{-2}
10^{-3}
10^{-4}
.20
.25
.30
.35
.40
.45
.50
.55
.60

Figure 56

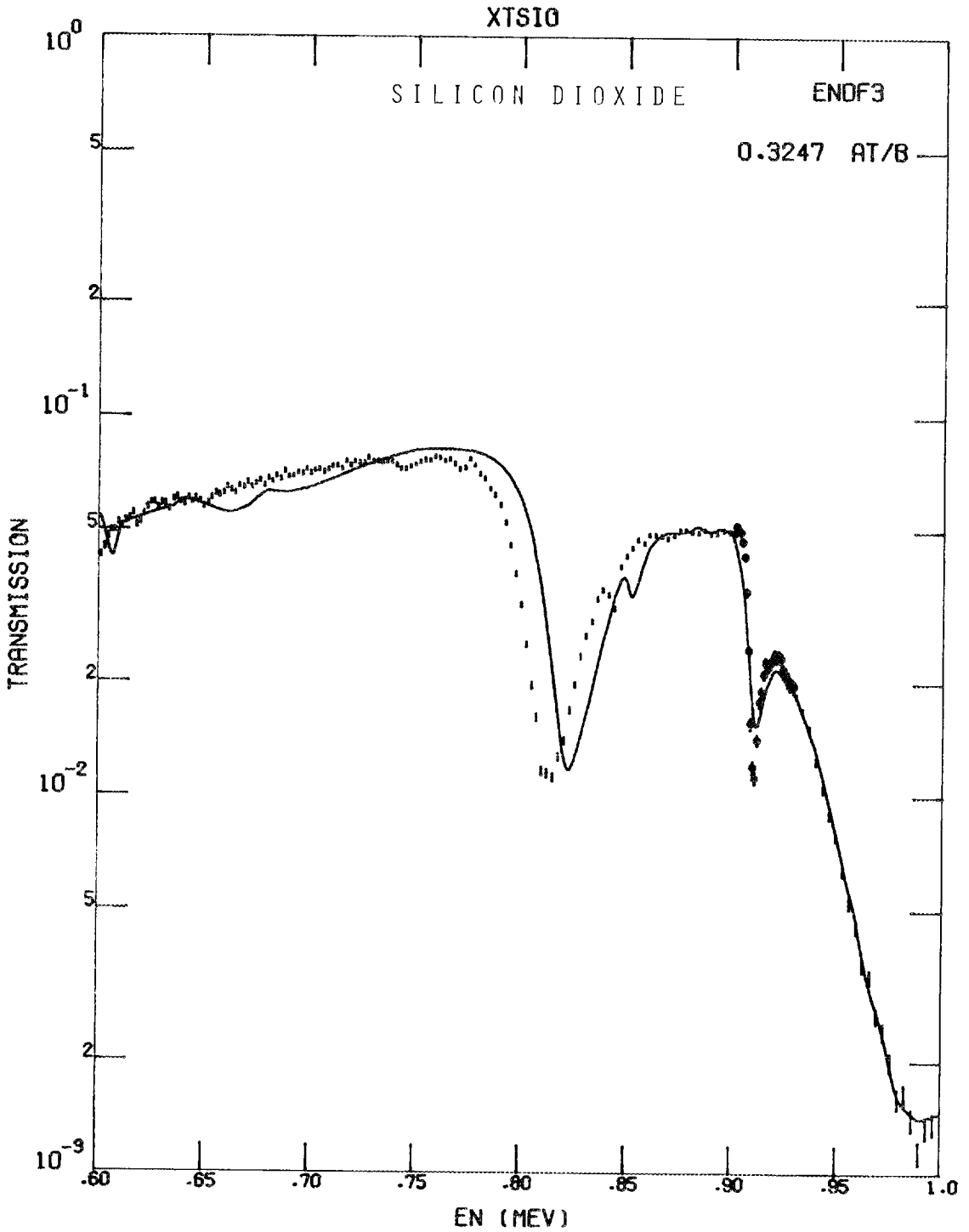
XTSIO
SILICON DIOXIDE
ENDF3
0.3247 AT/B
TRANSMISSION
EN (MEV)
10^0
5
2
10^-1
5
2
10^-2
5
2
10^-3
.60
.65
.70
.75
.80
.85
.90
.95
1.0

Figure 57

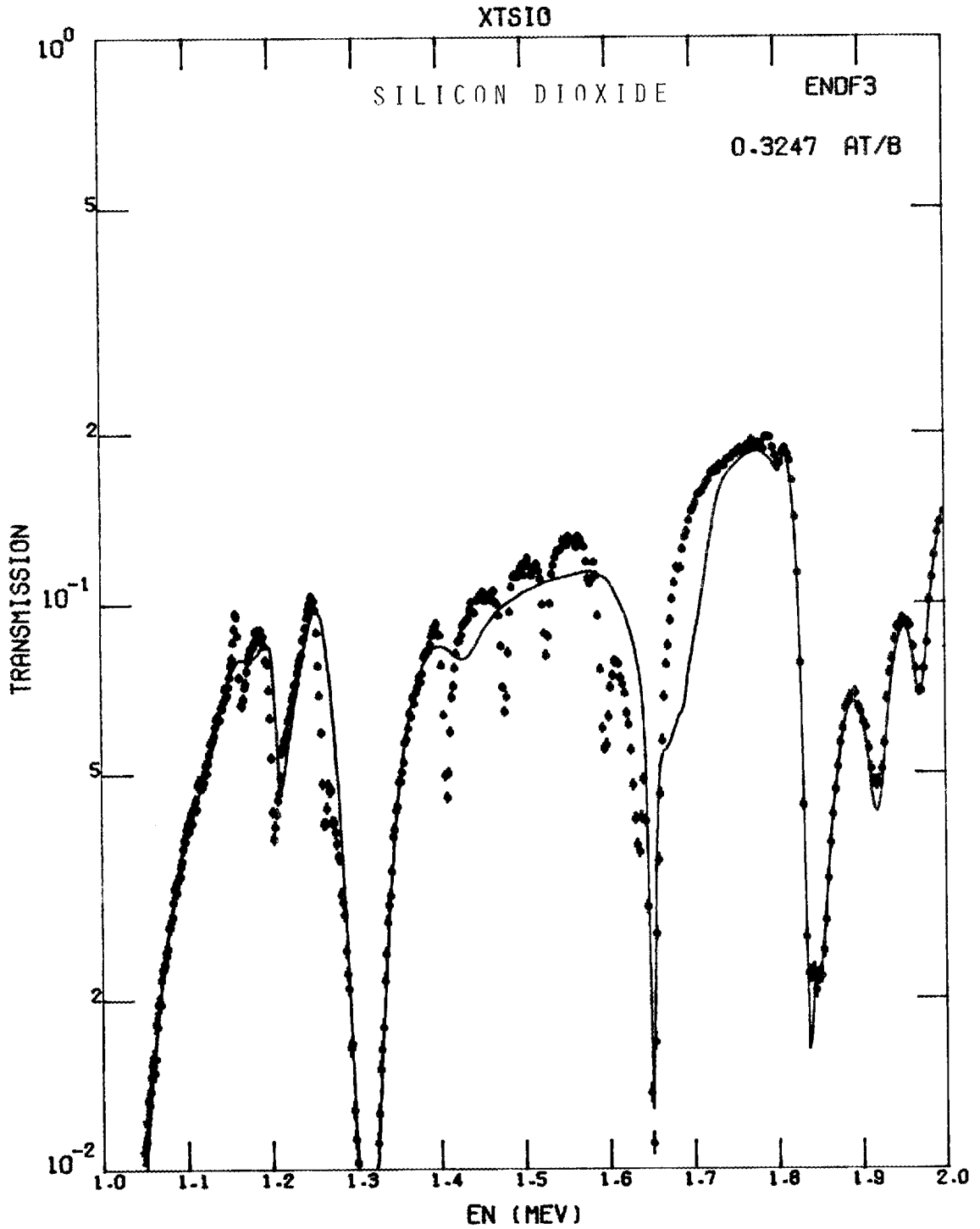
XTSIO
SILICON DIOXIDE
ENDF3
0.3247 AT/B
TRANSMISSION
EN (MEV)
10^0
5
2
10^-1
5
2
10^-2
1.0
1.1
1.2
1.3
1.4
1.5
1.6
1.7
1.8
1.9
2.0

Figure 58

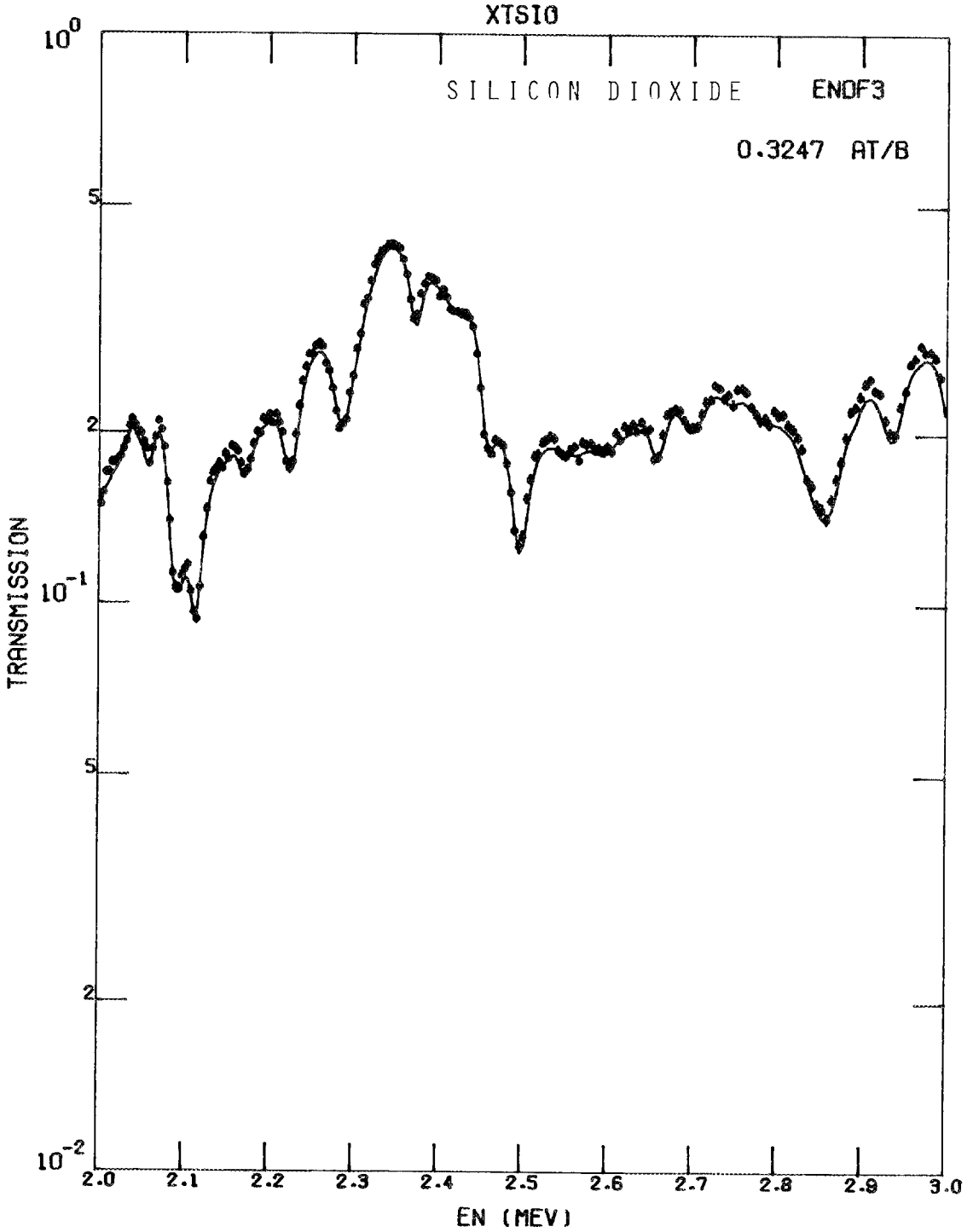
XTSIO
SILICON DIOXIDE
ENDF3
0.3247 AT/B
TRANSMISSION
EN (MEV)
10^0
5
2
10^{-1}
5
2
10^{-2}
2.0
2.1
2.2
2.3
2.4
2.5
2.6
2.7
2.8
2.9
3.0

Figure 59

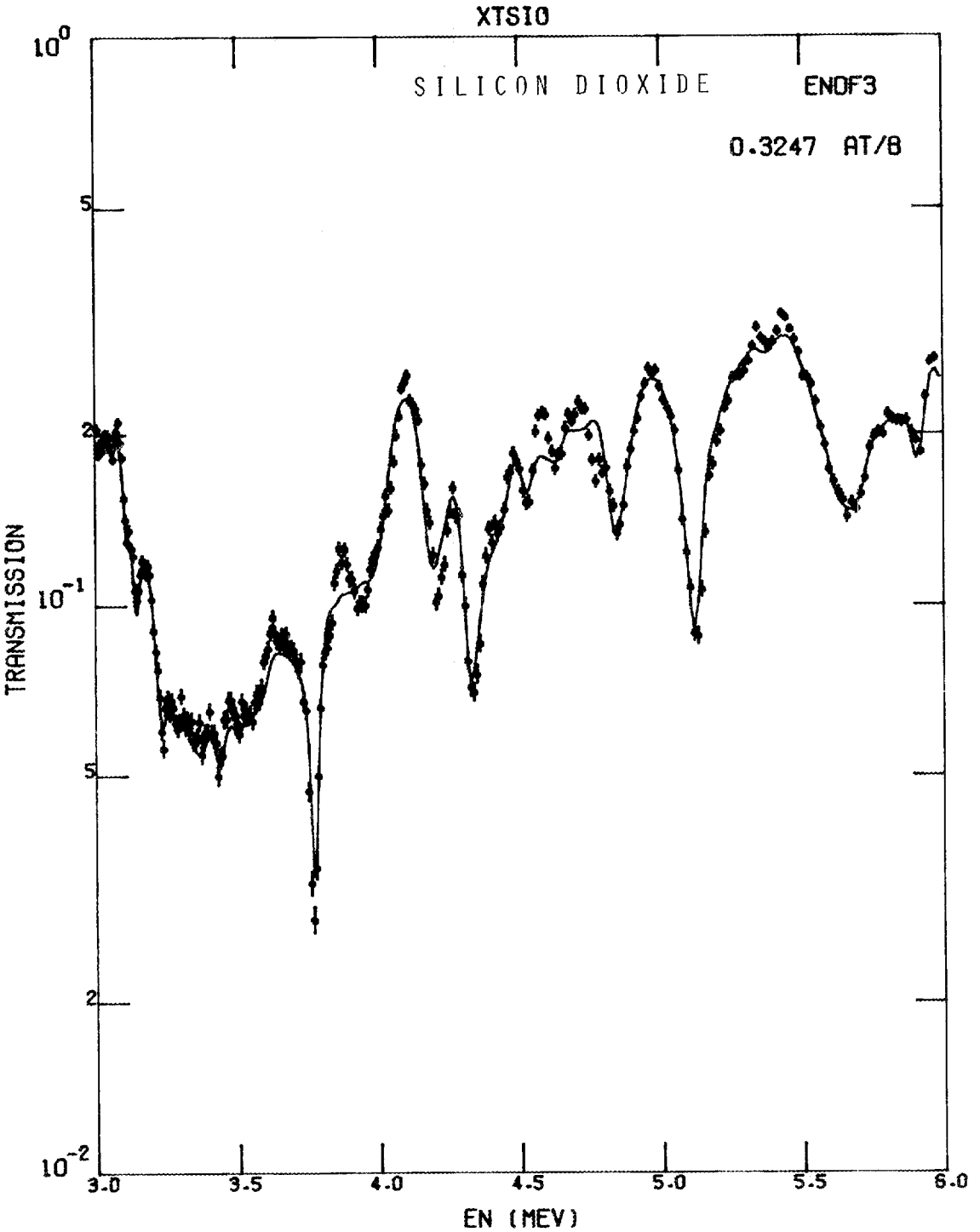
XTSIO
SILICON DIOXIDE
ENDF3
0.3247 AT/B
TRANSMISSION
EN (MEV)
10^0
5
2
10^-1
5
2
10^-2
3.0
3.5
4.0
4.5
5.0
5.5
6.0

Figure 60

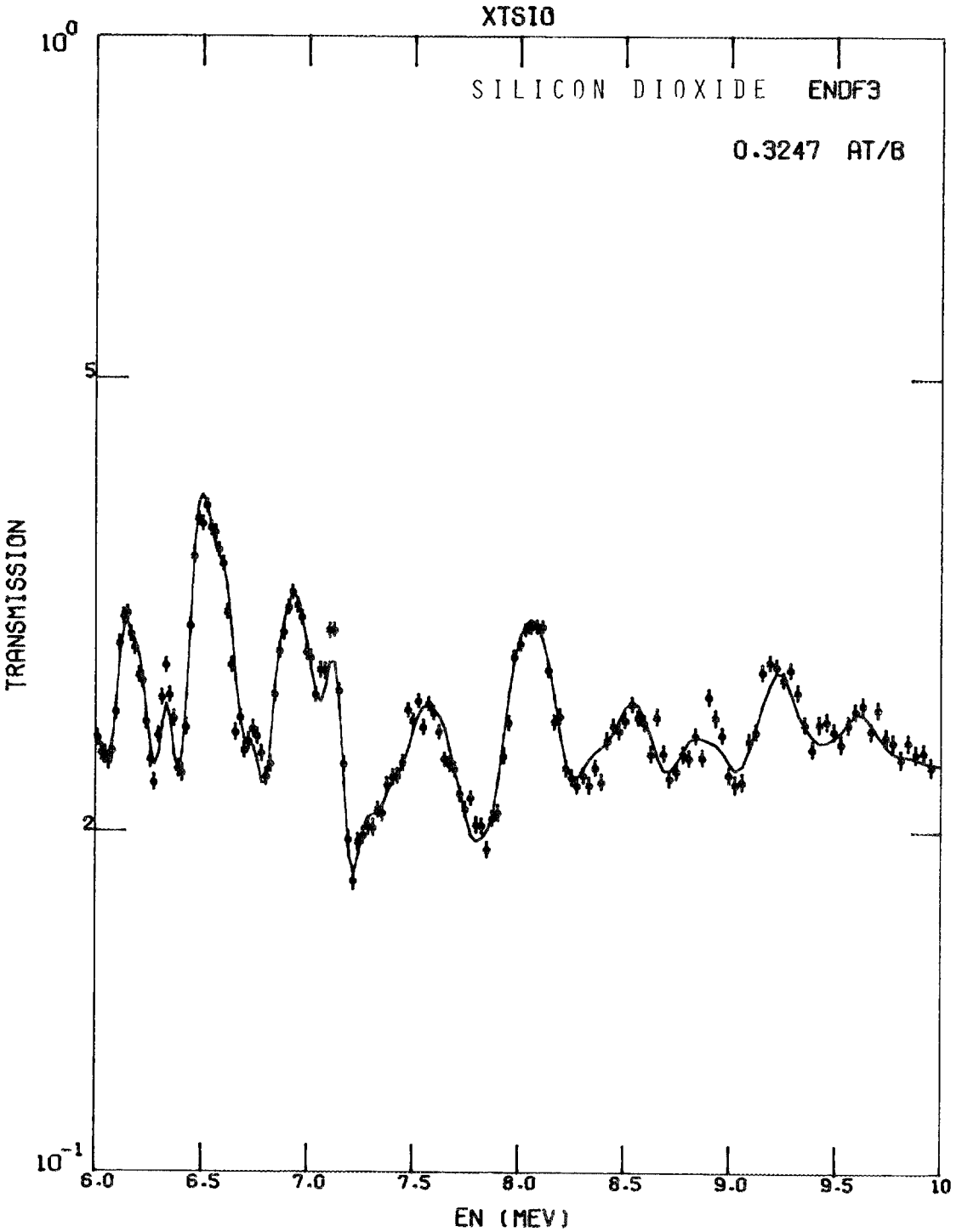
XTSIO
SILICON DIOXIDE ENDF3
0.3247 AT/B
TRANSMISSION
EN (MEV)
10^0
5
2
10^-1
6.0
6.5
7.0
7.5
8.0
8.5
9.0
9.5
10

Figure 61

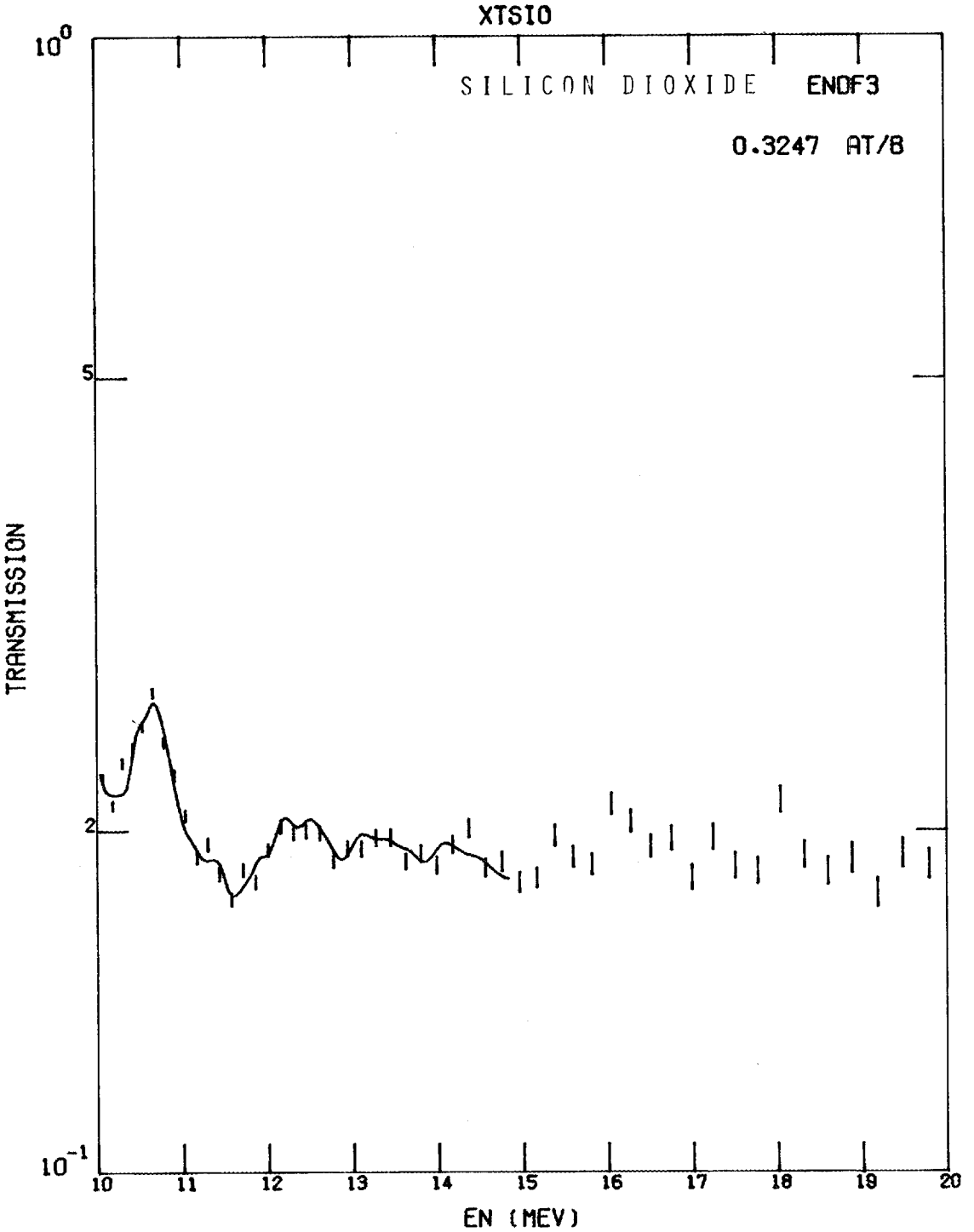
XTSIO
SILICON DIOXIDE ENDF3
0.3247 AT/B
TRANSMISSION
EN (MEV)
10^0
5
2
10^-1
10
11
12
13
14
15
16
17
18
19
20

Figure 62

ORNL-4823
UC-34 — Physics

INTERNAL DISTRIBUTION

1-3. Central Research Library
4. ORNL — Y-12 Technical Library Document Reference Section
5-54. Laboratory Records Department
55. Laboratory Records, ORNL R.C.
56. L. S. Abbott
57. R. G. Alsmiller, Jr.
58. A. R. Buhl
59. C. E. Clifford
60. F. L. Culler
61-65. J. K. Dickens
66. C. Y. Fu
67. W. O. Harms
68. R. F. Hibbs
69. W. E. Kinney
70-74. T. A. Love
75-76. F. C. Maienschein
77-81. G. L. Morgan
82. F. J. Muckenthaler
83. F. R. Mynatt
84. E. M. Oblow
85. R. W. Peelle
86. S. K. Penny
87-101. F. G. Perey
102-111. R. W. Roussin (RSIC)
112. M. J. Skinner
113. D. A. Sundberg
114. A. M. Weinberg
115. H. Feshbach (consultant)
116. P. F. Fox (consultant)
117. C. R. Mehl (consultant)
118. H. T. Motz (consultant)

EXTERNAL DISTRIBUTION

119. M. Drake, Gulf Radiation Technology, P.O. Box 608, San Diego, California 92112
120. Norman Francis, Knolls Atomic Power Laboratory, General Electric, Schenectady, New York 12309
121. Martin P. Fricke, Gulf Radiation Technology, P.O. Box 608, San Diego, California 92112
122. M. D. Goldberg, Brookhaven National Laboratory, Upton, L.I., New York 11973
123. H. Goldstein, Columbia University, 287 Engineering Terrace Bldg., 520 W. 120th St., New York, N.Y. 10027
124. W. H. Hannum, Division of Reactor Development and Technology, AEC, Washington, D.C. 20546
125. P. B. Hemmig, Division of Reactor Development and Technology, AEC, Washington, D.C. 20546
126. C. E. Hollandsworth, USA Nuclear Effects Lab., Aberdeen Proving Ground, Maryland
127. J. C. Hopkins, Los Alamos Scientific Laboratory, Los Alamos, New Mexico 87544
128. R. L. Howerton, Lawrence Radiation Laboratory, Livermore, California 94550
129. Kermit Laughon, AEC, Site Representative, ORNL
130. M. T. McEllistrem, University of Kentucky, Lexington, Kentucky 40506
131. Vic Orphan, Gulf Radiation Technology, P.O. Box 608, San Diego, California 92112
132. S. Pearlstein, Brookhaven National Laboratory, National Neutron Cross Section Center, Upton, L.I., New York 11973

133. A. B. Smith, Argonne National Laboratory, Argonne, Illinois 60440
134. Leona Stewart, Los Alamos Scientific Laboratory, Los Alamos, New Mexico 87544
135. J. A. Swartout, Union Carbide Corporation, New York, N.Y. 10017
136. W. E. Tucker, Texas Nuclear Corporation, 5805 Bullard Drive, Austin, Texas 78731
137. J. L. Weil, Physics Department, University of Kentucky, Lexington, Kentucky 40506
138. P. G. Young, Los Alamos Scientific Laboratory, Los Alamos, New Mexico 87544
139. Research and Technical Support Division, AEC, ORO
140. Patent Office, AEC, ORO

141-276. DNA Radiation Transport Distribution

277-411. National Neutron Cross Section Center, Brookhaven National Laboratory, Upton, L.I., New York 11973

412-639. Given distribution as shown in TID-4500 under Physics category (25 copies — NTIS)